Waterborne fluoropolymer dispersions for (super)hydrophobic coatings

Ana Belén López González

Chemical Engineering Group
University of the Basque Country UPV/EHU
Donostia-San Sebastián
(2016)

Contents

3. Highly hydrophobic coatings by blends of soft and hard latexes

4. Controlling film topography to enhance hydrophobicity

5. From fractal aggregation to superhydrophobic coatings

6. Incorporation of waterborne fluoropolymers in paint formulation

Chapter 1. Introduction and objective

1.1. Introduction

The development of hydrophobic and superhydrophobic materials has recently attracted a lot of attention due to the wide range of applications that these surfaces offer. Self-cleaning surfaces, anti-fouling materials, stain resistant textiles or antiicing coatings are just some examples that show the potential of these materials[1,2]. Additionally, the development of paints and coatings for outdoor use is another interesting field where durability, low dirt pick and water resistance is desired[3–5].

Hydrophobicity is commonly characterized by the water contact angle (θ), which is higher than 90º for hydrophobic surfaces and higher than 150º for superhydrophobic surfaces. The contact angle depends on both the nature of the material, which can be characterized by the water contact angle on a flat surface, and the texture of the surface[6–8]. The most hydrophobic polymers (fluoropolymers) have a contact angle on flat surfaces that rarely goes above 110^{0} [9,10]. Therefore, in order to increase the hydrophobicity of these systems, the introduction of surface roughness is needed[11].

Fluoropolymer coatings are useful for a wide variety of applications that range from houseware and medical articles to industrial coatings[12]. All these applications arise from the unique properties offered by these materials such as improved weatherability, corrosion resistance or easy to clean properties[13,14].

Environmental concerns have pushed coating and paint industries throughout the world to develop products with low toxicity levels. Water-based products are increasingly important because they substantially reduce the volatile organic compounds (VOC) levels and the hazardous air pollutants (HAP) emissions[15,16].

The production of (super)hydrophobic materials in water media would be particularly valuable and challenging at the same time since in order to produce stable dispersions in water, polymer particles should have a relatively hydrophilic surface.

In this work the different possibilities to obtain waterborne (super)hydrophobic coatings based on fluoropolymers will be studied.

1.2. Motivation and objective of the work

The motivation of the present work has its origin in the growing need for the development of hydrophobic and superhydrophobic coatings to be applied to large complex surfaces in high performance applications where excellent water repellency is required. There are many fields nowadays requesting materials to avoid the deposition of water or even ice formation and accumulation such as aeronautical devices, wind power generators and air conditioning equipments[17–19].

It would be particularly valuable to produce these materials in water media instead of solvent media in order to reduce VOCs. Emulsion polymerization constitutes an appropriate

technique to produce waterborne dispersions of polymer particles, than can be further incorporated into coating and paint formulation

Fluorinated polymers will be used because they provide a large number of additional benefits to the final coating[13,20]. Many formulations based on fluorinated polymers such as polytetrafluoroethylene or polyvinylidene fluoride have been already implemented in aqueous systems[21–28]. Additionally, fluoropolymer additives are widely used in different formulations that look for the increase in water and oil repellency, reduction in friction, scratching, surface tension, etc[14,29].

To prepare waterborne dispersions of these fluorinated materials, it is necessary to consider the hydrophobic nature of the fluorinated monomers. Fluorinated monomers are virtually insoluble in water. Therefore, their use in emulsion polymerization is restricted because in this process, mass transfer through the aqueous phase is necessary and the transport by collision[30] is not fast enough. Miniemulsion polymerization[31–33] is particularly well suited to polymerize water insoluble monomers in aqueous media, because transport through the aqueous phase is not needed as polymerization occurs in preformed droplets.

The main objective of this PhD Thesis is to produce waterborne (super)hydrophobic coatings from waterborne fluoropolymer dispersions. An important requirement is that the developed materials need to be applied to large surfaces by conventional coating methods such as brushing or spraying to make viable their commercial utilization.

The key aspects of this work include the synthesis of different water-based fluoropolymers and the attempts to fine-tune the film surface topography by several methods to increase hydrophobicity. Finally, the incorporation of the polymer dispersions in commercial paint formulations and the analysis of the properties of the final paints are also included.

1.3. Outline

Chapter 2 presents a general description of the fundamental aspects of hydrophobicity and superhydrophobicity together with a review of the most relevant techniques used to develop this kind of surfaces.

Chapter 3 reports on the formation of highly hydrophobic coatings from waterborne latexes able to form films at ambient temperature. The contact angle of film forming copolymers of 2-ethylhexyl acrylate (2EHA) and 1H, 1H, 2H, 2H-perfluorodecyl acrylate (PFDA) was limited to 114º because flat surfaces were obtained. Attempts to increase the roughness of the film using blends of film forming latexes with the latex of PFDA homopolymer (which is not film forming) were not successful under regular casting conditions because the PFDA particles accumulated at the film-substrate interface. Film formation engineering allowed modifying the morphology of the film obtaining a contact angle of 137º.

Chapter 4 shows that the challenge of producing cost effective and environmentally friendly, highly hydrophobic, cohesive and non-porous coatings applicable to large and irregular surfaces can be achieved by forming wrinkles on the surface of waterborne coatings

through fine tuning of the film forming conditions. The proof of concept was demonstrated by using waterborne dispersions of copolymers of PFDA and 2EHA, and using temperature and hardness of the copolymer as control variables during film formation. This allowed the formation of transparent films with a wrinkled surface that had a contact angle of 133º, which represents an increase of 20º with respect to the film cast under standard conditions.

In **Chapter 5** the production of superhydrophobic coatings from waterborne polymer dispersions is presented. For this purpose, a new strategy based on the fractal aggregation of the PFDA homopolymer and the open-time of the coatings was developed leading to films with water contact angles higher than 150º, low sliding angles and low contact angle hysteresis. Additionally, the mechanical strength of the films and the oleophobicity and icephobicity was studied.

The work presented in **Chapter 6** was carried out in Nuplex Resins (Bergen Op Zoom, The Netherlands) under the supervision of Dr. Javier Bohórquez. In this chapter, the synthesis and the incorporation of fluorinated polymer resins into paint formulations was studied. The potential benefits of the incorporation of fluorinated polymers into paints were analyzed by studying different properties such as gloss, contact angle or chemical resistance. Additionally, an approach to produce low VOCs paints is presented.

Finally, in **Chapter 7** the most relevant conclusions of this PhD Thesis are summarized.

1.4. References

(1) Kota, A. K.; Tuteja, A. Superoleophobic Surfaces. In *Advances in Fluorine-Containing Polymers*; **2012**; pp 171–185.

(2) Li, X.-M.; Reinhoudt, D.; Crego-Calama, M. What Do We Need for a Superhydrophobic Surface? A Review on the Recent Progress in the Preparation of Superhydrophobic Surfaces. *Chem.Soc.Rev* **2007**, *36*, 1350–1368.

(3) The Effect of Water Resistance on the Durability of Waterborne Coatings. *Paint & Coatings Industry*. **2003**.

(4) Vandezande, G. Improved Dirt Pickup Resistance Critical to Future Coating Innovation. *Paint & Coatings Industry*. **2007**.

(5) Vandezande, G. Improved Dirt Pickup Resistance Critical to Future Coating Innovation. *Paint & Coatings Industry*. **2008**.

(6) Wenzel, R. N. Resistance of Solid Surfaces to Wetting by Water. *Ind. Eng. Chem.* **1936**, *28*, 988–994.

(7) Cassie, A. B. D.; Baxter, S. Wettability of Porous Surfaces. *Trans. Faraday Soc.* **1944**, *40*, 546–551.

(8) Feng, L.; Li, S.; Li, Y.; Li, H.; Zhang, L.; Zhai, J.; Song, Y.; Liu, B.; Jiang, L.; Zhu, D. Super-Hydrophobic Surfaces: From Natural to Artificial. *Adv. Mater.* **2002**, *14*, 1857–1860.

(9) McKeen, L. W. *Fluorinated Coatings and Finishes Handbook*; **2006**.

(10) Drobny, J. G. *Technology of Fluoropolymers*; **2000**.

(11) Nosonovsky, M.; Bhushan, B. Hierarchical Roughness Makes Superhydrophobic States Stable. *Microelectron. Eng.* **2007**, *84*, 382–386.

(12) Barry, J. Fluoropolymers for Coating Applications. *JCT CoatingsTech* **2008**.

(13) Jones, B. Fluoropolymers for Coating Applications. *JCT CoatingsTech Mag.* **2008**.

(14) Ebnesajjad, S.; Morgan, R. Use of Fluorinated Additives in Coatings. In *Fluoropolymer Additives*; **2012**; pp 157–174.

(15) Thomas, G. P.; (2013, December 12). Waterborne Coatings - Methods, Benefits and Applications. Retrieved from: http://www.azom.com/article.aspx?ArticleID=8561.

(16) Fragata, F.; Almeida, E.; Santos, D.; De La Fuente, D.; Morcillo, M. Water-Borne versus Solvent-Borne Paints for Protection of Steel to Atmospheric Exposure. *Surf. Coatings Int. Part B Coatings Trans.* **2006**, *89*, 237–244.

(17) Authority, C. A. *Aircraft Icing Handbook*; **2000**.

(18) Parent, O.; Ilinca, A. Anti-Icing and de-Icing Techniques for Wind Turbines: Critical Review. *Cold Reg. Sci. Technol.* **2011**, *65*, 88–96.

(19) Sayward, J. M. *Seeking Low Ice Adhesion*; **1979**.

(20) Ebnesajjad, S.; Morgan, R. Introduction. In *Fluoropolymer Additives*; **2012**; pp 3–10.

(21) Bladel, H.; Felix, B.; Hintzer, K.; Lohr, G.; Mitterberger, W. D. Aqueous Dispersion of Fluoropolymers, Its Preparation and Use for Coatings, **1996**.

(22) Cardinal, A. J.; Edens, W. L.; W, V.; Van Dyk, J. W. Novel Tetrafluoroethylene Resins and Their Preparation, **1964**.

(23) Asakawa, A.; Unoki, M.; Hirono, T.; Takayanagi, T. Waterborne Fluoropolymers for Paint Use. *J. Fluor. Chem.* **2000**, *104*, 47–51.

(24) Iezzi, R. A.; Gaboury, S.; Wood, K. Acrylic-Fluoropolymer Mixtures and Their Use in Coatings. *Prog. Org. Coatings* **2000**, *40*, 55–60.

(25) Hartwimmer, R.; Kuhls, J. Copolymers of Tetrafluoroethylene and Process for Their Manufacture, **1981**.

(26) Concannon, T. P.; Vary, E. M. Fluoropolymer Blend Coating Compositions Containing Copolymers of Perfluorinated Polyvinyl Ether, **1981**.

(27) Gresham, W. F.; Vogelpohl, A. F.; Va, W. Aqueous Process for Making Improved Tetrafluoroethylene/fluoroalkyl Perfluorovinyl Ether Copolymers, **1972**.

(28) Kaulbach, R.; Mayer, L. Aqueous Emulsion Polymerization Process for Producing Fluoropolymers, **2006**.

(29) Ebnesajjad, S.; Morgan, R. *Fluorinated Additives for Plastics*; **2012**.

(30) Arzamendi, G.; Asua, J. M. Copolymer Composition Control during the Seeded Emulsion Copolymerization of Vinyl Acetate and Methyl Acrylate. *Makromol. Chem., Macromol. Symp.* **1990**, *35/36*, 249–268.

(31) Ugelstad, J.; El-Aasser, M. S.; Vanderhoff, J. W. Emulsion Polymerization: Initiation of Polymerization in Monomer Droplets. *J. Polym. Sci. B Polym. Lett. Ed.* **1973**, *11*, 503–513.

(32) Asua, J. M. Miniemulsion Polymerization. *Prog. Polym. Sci.* **2002**, *27*, 1283–1346.

(33) Asua, J. M. Challenges for Industrialization of Miniemulsion Polymerization. *Prog. Polym. Sci.* **2014**, *39*, 1797–1826.

Chapter 2. Hydrophobic and superhydrophobic coatings

2.1. Fundamental aspects of hydrophobicity and superhydrophobicity

As was explained in Chapter 1, hydrophobic and superhydrophobic surfaces are highly demanded because they present many useful properties such as antibiofouling, antisticking, anticorrosion, stain resistance and self cleanability[1,2]. In order to promote superhydrophobicity, two different factors should be considered: the hydrophobic nature of the material and the surface microstructure.

The hydrophobic nature of the materials is characterized by the wettability of their flat surfaces. When a water droplet rests on a flat surface, three different interfaces are created: solid-liquid, liquid-vapour and solid-vapour. Therefore, the balance between the corresponding interfacial forces ($\gamma_{sl}, \gamma_{lv}, \gamma_{sv}$) will determine whether the droplet will wet or not the surface. The spreading coefficient[3,4] is defined as the difference between the surface energy (per unit area) of the dry and wet substrate:

$$\mathbf{S = \gamma_{SV} - \gamma_{SL} - \gamma_{LV}} \qquad \textbf{(2.1)}$$

When S > 0, complete wetting of the surface occurs and the water droplet will spread on top of the surface. When S < 0, the wetting of the surface does not occur spontaneously and the droplet partially wets the substrate as illustrated in Figure 2.1. As it was described by Thomas Young[5] in 1805, the contact angle of a liquid drop on a solid surface (θ) is determined by the mechanical equilibrium of the drop under the action of the three interfacial tensions[6] (Equation 2.2).

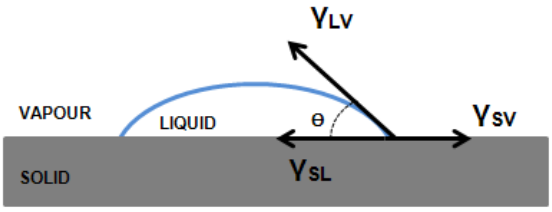

Figure 2.1. Water droplet on a flat surface

$$\gamma_{SV} = \gamma_{SL} + \gamma_{LV} \cdot \cos\theta \quad \textbf{(2.2)}$$

According to the contact angle value with water, surfaces can be defined as hydrophilic ($\theta < 90^{o}$), hydrophobic ($\theta > 90^{o}$) and superhydrophobic ($\theta > 150^{o}$).

Table 2.1 presents the surface tensions and the water contact angles of a representative list of polymers[7].

Table 2.1. Surface tension (γ_{SV}) and contact angle with water (θ) for various polymers[7].

Polymer name	***γ_{SV} (mN/m)***	***Θ (º)***
Polyvinyl alcohol (PVOH)	*37*	*51*
Polyvinyl acetate (PVA)	*35.3*	*60.6*
Nylon 6	*43.9*	*62.6*
Polyethylene oxide(PEO)/Polyethylene glycol(PEG)	*43*	*63*
Nylon 6,6	*42.2*	*68.3*
Polymethyl methacrylate (PMMA)	*37.5*	*70.9*
Nylon 12	*37.1*	*72.4*
Polyethylene terephthalate (PET)	*39*	*72.5*
Epoxies	*44.5*	*76.3*
Polyvinylidene chloride (PVDC)	*40.2*	*80*
Acrylonitrile butadiene styrene (ABS)	*38.5*	*80.9*
Polycarbonate (PC)	*44*	*82*
Polyvinyl fluoride (PVF)	*32.7*	*84.5*
Polyvinyl chloride (PVC)	*37.9*	*85.6*
Polystyrene (PS)	*34*	*87.4*
Polyvinylidene fluoride (PVDF)	*31.6*	*89*
Polytrifluoroethylene	*26.5*	*92*
Polybutadiene	*29.3*	*96*
Polyethylene (PE)	*31.6*	*96*
Polychlorotrifluoroethylene (PCTFE)	*30.8*	*99.3*
Polypropylene (PP)	*30.5*	*102.1*
Polydimethylsiloxane (PMDS)	*20.1*	*107.2*
Poly t-butyl methacrylate (PtBMA)	*18.1*	*108.1*
Fluorinated ethylene propylene (FEP)	*19.1*	*108.5*
Hexatriacontane	*20.6*	*108.5*
Paraffin	*24.8*	*108.9*
Polytetrafluoroethylene (PTFE)	*19.4*	*109.2*
Poly(hexafluoropropylene)	*16.9*	*112*
Polyisobutylene (PIB, butyl rubber)	*27*	*112.1*

It can be seen that low surface tension leads to high contact angles. Fluorine is very effective for lowering the surface free energy. It was reported by Zisman and coworkers[8] that the surface free energy decreased in the order $–CH_2$ > $–CH_3$ > $–CF_2$ > $–CF_2H$ > $-CF_3$ [9,10]. Therefore, the introduction of fluorine atoms into a polymer chain producing fluorinated polymers represents an important strategy to create low surface energy materials. Fluorine atom has unique characteristics that produce interesting properties in the fluorinated materials. It has small atomic radius and the biggest electronegativity among atoms. The C-F chemical bond is the strongest known single bond in organic chemistry leading to a great stability of these compounds. Additionally, polymers that contain C-F bonds exhibit excellent weather and chemical resistance, and also the small dipole moment of these compounds contributes to their oleophobicity and hydrophobicity, as well as their low surface tension, low refractive index, low friction coefficient and reduced adhesion to surfaces[11–14]. The values in Table 2.1 show that although low surface energy polymers as silicones and fluorinated polymers show hydrophobicity, they are far from providing superhydrophobicity, that can only be achieved increasing the surface roughness of intrinsically hydrophobic materials (materials with water contact angles greater than 90º).

2.1.1. Wetting of rough surfaces

The theory for the wetting of rough surfaces is well developed and two different situations are considered depending on the penetration of the liquid to the interior of the cavities of the rough surface.

a) Cassie-Baxter state:

In this case, which is illustrated in Figure 2.2, the liquid does not penetrate in the cavities of the rough surface and only wets the top of the asperities of the surface (a necessary condition for this to occur is that $\theta > 90^{o}$, where θ is the contact angle value on a flat surface).

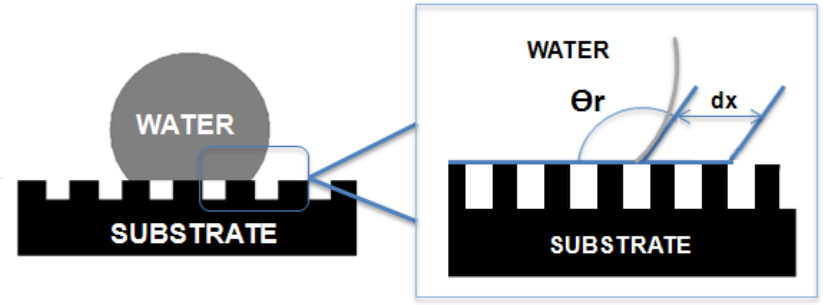

Figure 2.2. Cassie- Baxter state

The energy balance applied to the situation in which the water droplet moves a distance dx leads to the following expression[15].

$$\mathbf{dE} = \underbrace{\boldsymbol{\Phi_S} \cdot (\boldsymbol{\gamma_{SL}} - \boldsymbol{\gamma_{SV}}) \cdot \mathbf{dx}}_{\textit{Contribution for the creation of new solid–liquid interfaces}} + \underbrace{(\mathbf{1} - \boldsymbol{\Phi_S}) \cdot \boldsymbol{\gamma_{LV}} \cdot \mathbf{dx}}_{\textit{Contribution for the creation of new liquid–vapour interfaces}} - \underbrace{\boldsymbol{\gamma_{LV}} \cdot \mathbf{cos}(\mathbf{180} - \theta_r) \cdot \mathbf{dx}}_{\textit{Contribution for the reduction of the area of the droplet}} \quad \textbf{(2.3)}$$

Where Φ_S is the fraction of the horizontal surface of the substrate in contact with the liquid, and θ_r is the contact angle of the rough surface. Under equilibrium conditions (dE/dx) is equal to zero and combination of Equation 2.2 and Equation 2.3 yields:

$$\mathbf{cos}\,\theta_r = \boldsymbol{\Phi_S} \cdot \mathbf{cos}\theta + \boldsymbol{\Phi_S} - \mathbf{1} \quad \textbf{(2.4)}$$

Equation 2.4 is called Cassie's equation[16,17] and shows that when the liquid does not penetrate in the cavities, the contact angle of the rough surface is higher than in a flat surface and this difference increases as Φ_S decreases.

b) Wenzel state:

Wenzel[18] considered the case in which the liquid penetrates into the cavities of the rough surface (Figure 2.3).

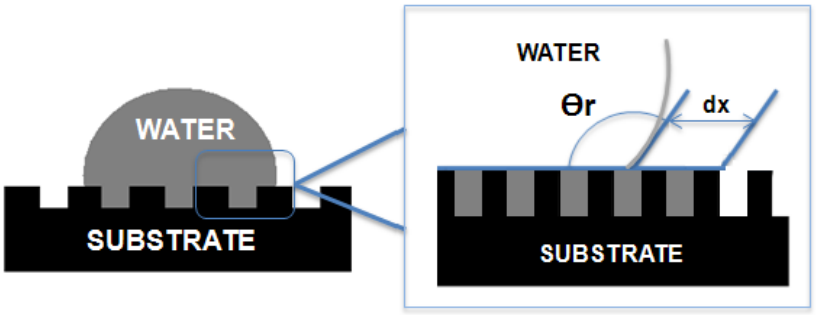

Figure 2.3. Wenzel state

The energy balance that arises from this situation is[15]:

$$\mathbf{dE} = \underbrace{\mathbf{r} \cdot (\boldsymbol{\gamma}_{\mathbf{SL}} - \boldsymbol{\gamma}_{\mathbf{SV}}) \cdot \mathbf{dx}}_{\textit{Contribution for the creation of new solid–liquid interfaces}} + \underbrace{\boldsymbol{\gamma}_{\mathbf{LV}} \cdot \cos\theta_{\mathbf{r}} \cdot \mathbf{dx}}_{\textit{Contribution for the reduction of the area of the droplet}} \qquad \textbf{(2.5)}$$

Under equilibrium, where (dE/dx) is zero, combination of Equation 2.2 and Equation 2.5 gives Wenzel's equation.

$$\cos\theta_{\mathbf{r}} = \mathbf{r} \cdot \cos\theta \qquad \textbf{(2.6)}$$

Where the term r, defined as the roughness factor, represents the ratio of the area of the real surface to the projected area in the horizontal plane, therefore, it will be always higher than 1. Because of the capillary forces, entry of fluid in the cavities of the surface will always occur when $\theta < 90º$. In this case, Equation 2.6 predicts $\theta_r < \theta$. For the cases where $\theta > 90º$, $\theta_r > \theta$ and θ_r increases with r[19].

In the previous discussion it has been shown that for $\theta > 90º$ both the Cassie's and the Wenzel's equation are available. In order to decide which one should be applicable, it is necessary to know if the liquid penetrate in the cavities. The liquid will not penetrate if $dE_{Cassie\text{-}Baxter} < dE_{Wenzel}$. Combination of Equations 2.3 and 2.5 lead to the condition for maintaining dry the cavities:

$$\cos\theta < \frac{\Phi_s - 1}{r - \Phi_s} \qquad \textbf{(2.7)}$$

Figure 2.4 illustrates the effect of Φ_S and r on the wetting of the cavities and the effect of the wetting on the contact angle of the rough surface. It can be seen that as r increases the wetting of the cavities is less likely and this results in a higher contact angle. The thermodynamic reason is that as r increases the energy needed to wet the cavities increases, and the Cassie's case becomes more favorable.

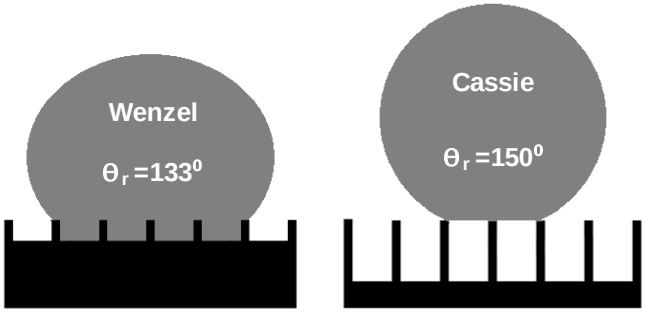

Φ_s = 0.2; r = 2

Φ_s = 0.2; r = 4

θ = 110º

$\cos\theta > \frac{\Phi_s - 1}{r - \Phi_s}$

$\cos\theta < \frac{\Phi_s - 1}{r - \Phi_s}$

Figure 2.4. Effect of $\boldsymbol{\Phi_s}$ and $\mathbf{r}$ on wetting of the cavities and on the contact angle.

Nature has overperformed the surface structures considered in the previous figures. Lotus leaves present some amazing properties. They have such superhydrophobicity that water droplets roll and slide over the surface and also, they collect the dirt located on top of it[20]. This superhydrophobicity is a consequence of the microstructure of these materials. As can be observed in Figure 2.5 they present a hierarchical structure built by wax tubules that are randomly oriented. The term 'hierarchical roughness' refers to the presence of roughness at different scales. The scanning electron micrographs of Figure 2.5 show a highly rough microstructure that present a large number of microbumps with an average peak to valley height of 13 μm, midwidth of 10 μm and peak radius of 3 μm. All over the surface and also, on the top of these microbumps, small nanobumps are present with an average peak to valley height of 780 nm, midwidth of 40 nm and peak radius of 150 nm[21].

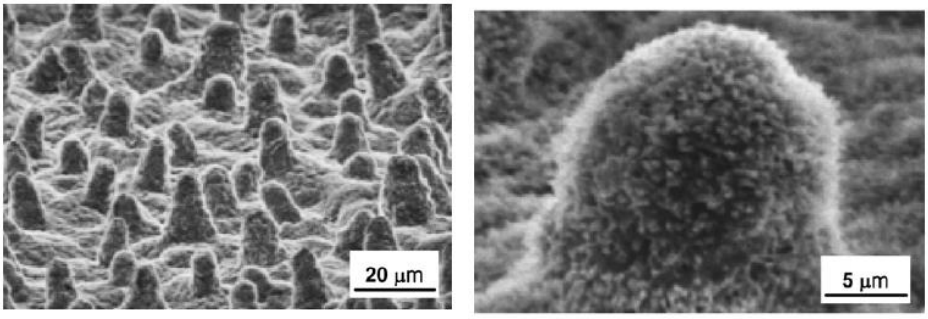

Figure 2.5. Scanning electron micrographs of the Lotus Leaf microstructure[21].

This hierarchical structure can be simplified in the scheme of Figure 2.6 where two scales of roughness are considered.

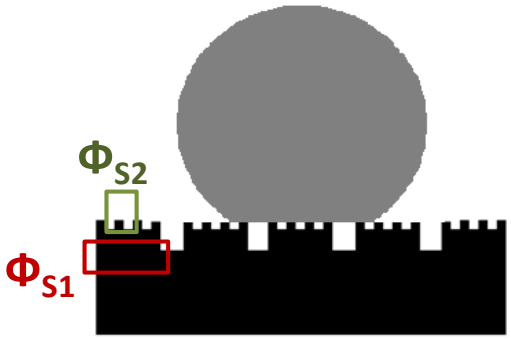

Figure 2.6. Water droplet on a surface with hierarchical roughness.

The fraction of solid-liquid contact surface is given by the product $\boldsymbol{\Phi_{s1} \cdot \Phi_{s2}}$. For this case, Cassie's equation becomes:

$$\boldsymbol{\cos\theta_r = -1 + \Phi_{s1} \cdot \Phi_{s2} \cdot (\cos\theta + 1)} \qquad \textbf{(2.8)}$$

The introduction of roughness at two different scales produces a significant increase in the final contact angle of the rough surface as shown below for the case of a material with $\theta = 110^{o}$.

One scale roughness	**Two scale roughness**
$\theta = 110^{o}$	$\theta = 110^{o}$
$\Phi_s = 0.25$	$\Phi_{s1} = 0.25$
$\theta_r = 146^{o}$	$\Phi_{s2} = 0.25$
	$\theta_r = 163^{o}$

2.1.2. Contact Angle Hysteresis (CAH) and Sliding Angle (SA)

When the Lotus leaf was discussed, it was mentioned that the water droplet easily slide over its surface. This property is characterized by means of the **Sliding Angle (SA)** and the **Contact Angle Hysteresis (CAH).**

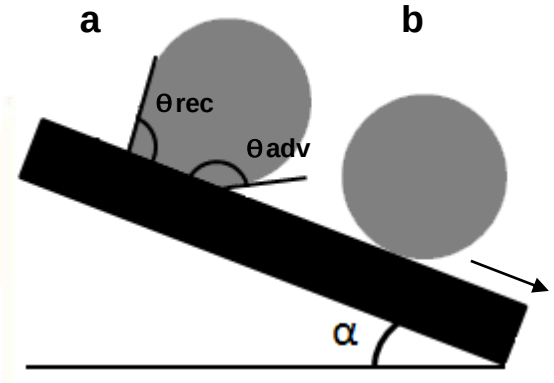

Figure 2.7. Contact Angle Hysteresis and Sliding Angle.

The sliding angle is the angle at which the liquid drop slides over the surface (α in Figure 2.7 for the droplet b). At tilting angles lower than the sliding angle, the droplet deforms by the action of the gravity and two contact angles can be measured. The contact angle hysteresis (CAH) is defined as the difference between the advancing (θ_{adv}) and the receding (θ_{rec}) contact angles, just before the sliding point (case a, Figure 2.7). These angles can be measured by placing a drop on the surface and varying the volume until the contact line moves or by tilting the substrate until the contact line begins to move[4,22]. The advancing contact angle is higher than the receding contact angle due to energy barriers to the droplet flow caused by the surface roughness or chemical heterogeneities[21]. Therefore, the lower the CAH, the easier the droplet will flow and roll off the surface. In general, superhydrophobic surfaces usually have CAH values lower than 10º.

It is worth pointing out that contact angle, CAH and SA respond to different characteristics of the surface. Gao and McCarthy[23] designed a clever experiment to demonstrate that contact angle is a function of the contact line where the three phases (liquid, vapour and solid) coexist, and not a function of the interfacial area between the solid and the liquid. To probe this concept, three types of two component surfaces were prepared by Gao and McCarthy[23], varying chemistry of the surface and topography. These surfaces are represented in Figure 2.8 where case (a) corresponds to a surface in which a hydrophilic spot is located inside a hydrophobic surface, in case (b), a rough hydrophobic region is located inside a flat hydrophobic field and in case (c), a flat hydrophobic spot is located inside a rough hydrophobic surface. The data from the experiments showed that the contact angle is determined by the interactions of the liquid and the solid at the three-phase contact line, the interfacial area within the contact perimeter being irrelevant as it is illustrated in Figure 2.8.

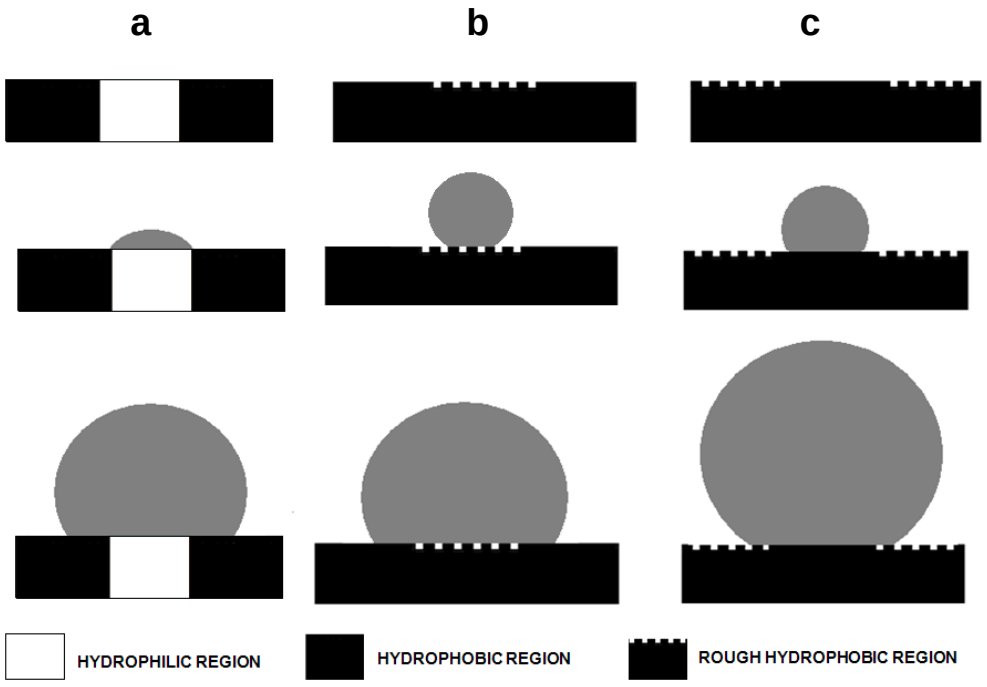

Figure 2.8. Surfaces with different wettabilities[23].

The sliding angle, which is defined as the critical angle where a water droplet with a certain weight begins to slide down the inclinated plane[24] is controlled by both the three-phase contact line and the interfacial area. This last influence can be understood by considering that for the droplet to slide, the gravity force (m·g·sinα) should overcome the adhesion energy between the droplet and the substrate. This energy is proportional to $\mathbf{r} \cdot (\boldsymbol{\gamma}_{\mathbf{sv}} - \boldsymbol{\gamma}_{\mathbf{sl}} - \boldsymbol{\gamma}_{\mathbf{lv}})$ when the cavities are wetted (Wenzel's regime) and to $\boldsymbol{\Phi}_{\mathbf{S}} \cdot (\boldsymbol{\gamma}_{\mathbf{sv}} - \boldsymbol{\gamma}_{\mathbf{sl}} - \boldsymbol{\gamma}_{\mathbf{lv}})$ when the cavities are not wetted (Cassie's regime). As $\mathbf{r} \gg \boldsymbol{\Phi}_{\mathbf{S}}$, the energy needed to remove the droplet is higher for Wenzel's case, namely higher sliding angles are expected for this case. The real situation is

more complex as in order to slide, the droplet has to cross the three-phase contact line. This consideration led Furmidge to develop an expression linking the contact angle hysteresis and the sliding angle[25].

$$\frac{m \cdot g \cdot \sin\alpha}{w} = \gamma_{lv} \cdot (\cos\theta_{rec} - \cos\theta_{adv}) \quad \textbf{(2.9)}$$

Where m and w are the mass and width of the droplet. As can be observed in the Equation 2.9, smaller values of contact angle hysteresis will result into smaller values of sliding angle[26].

2.2. Techniques for the preparation of rough surfaces

In the previous section it has been shown that very high contact angles, low contact angle hysteresis and low sliding angles can be achieved by avoiding the wetting of the cavities of the rough surface (Cassie's regime). For a given polymer, this requires a high value of roughness factor, r, therefore deep (and complex) cavities. If this condition is fulfilled, multiscale roughness may lead to superhydrophobicity (θ_r > 150º, CAH < 10º and very low sliding angles). Therefore, plenty of effort has been devoted to develop different techniques to produce this kind of surfaces. The most relevant procedures are summarized below.

Textiles and fibres

Textile technology is one of the most potential applications of these water repellent surfaces. It was firstly studied by Wenzel[27], stating that fibrous materials were very effective for water repellency. Indeed, many woven or non-woven cloths have been treated by immersion in different solutions to chemically increase the hydrophobicity of the system[28–32] or to introduce additional roughness to the initial structure[33]. Artificial fibers can be produced by the use of techniques such as electrospinning where the fiber size, composition and surface texture are varied[34]. Good control of this method yields excellent water repellent materials[35–37].

Lithographic techniques

Lithography constitutes a well established technique for the production of patterned surfaces and therefore, it is one of the most frequently used methods to produce superhydrophobic surfaces in academia. Its commercial implementation is limited by its high cost and the need of specific equipment. However, it has been very useful to understand wetting phenomena over the last decades. It allows the fabrication of surfaces where the solid-liquid contact area can be tuned, what allows users to create surfaces with different r and Φ_s values[4]. There are several lithographic techniques in which a certain design is transferred from a master onto a substrate, even in the nanometric scale, leading to nano-imprint lithography[38,39]. Photolithography is an alternative in which a photoactive polymer layer is irradiated through a patterned mask where either the exposed or the unexposed polymer layer is removed[40–42]. Although lithographic techniques have been mostly used to study the theories of wetting, they are also useful in other applications such as in the fabrication of electronic

devices or in the production of molds that will be used as templates for the fabrication of patterned surfaces[43].

Templating

Surfaces with microstructure can be produced by the use of templating techniques. A material is printed, pressed or grown in the voids of a template. After the template removal, the surface has the inverse of the template pattern which can be also used as a template to have a replicate of the original[44]. This technique is very reproducible and templates can be created in many different ways. Lithography is a procedure to produce well defined templates. Additionally, the production of anodic aluminum oxide (AAO) templates is widely used to produce nanopatterned surfaces[45,46]. The polymer is then infiltrated into the AAO template and later, the aluminum oxide is removed by dissolution leaving the polymer pillars. Other approaches with sacrificial templates to generate nanostructured surfaces can be done by producing polymeric films around nanoparticle arrays. The removal of the template leads to macroporous solids with highly rough microstructures[47]. Furthermore, natural superhydrophobic surfaces can be used directly as templates, obtaining replicas of some water repellent materials such as the Lotus leaves[48].

Phase separation

A multi-component mixture can phase separate due to changes in temperature or pressure. In such case, the different phases form a bicontinuous structure. If one of the components solidifies in this structure, the other can be removed leading to a 3D porous

network[49]. The size of the pores can be controlled by controlling the ratio between phases or the phase separation conditions together with the solidification conditions. This strategy is easy to produce and economically viable although the transparency and hardness of the materials produced generally decreases as the structures become larger. Phase separation was mainly used to produce filters and chromatography stationary phases, but many researchers have used this technique for the production of superhydrophobic surfaces out of a wide range polymers[50–53].

Crystal growth

The generation of rough surfaces by controlling the growth of crystals constitutes a versatile technique to create different microstructures such as nano-pillars, nano-fibers or needle-like structures. Size and shape of the crystals can be varied by changing different parameters such as the rate of cooling and solvent evaporation or addition. There are many examples in literature where rough superhydrophobic structures are created from different polymer systems[54–56] and also, with the use of different inorganic materials such as ZnO[57], carbon nanotubes[51,52] or SnO_2[60].

Diffusion-limited growth processes

The formation of surface roughness during the deposition of several layers on top of a certain substrate is often an undesired effect. Once the first protuberances are formed, they will gather more material on top of them than the surrounding areas. The growth of these structures will depend on the flux of material that arrives to the surface; therefore, the diffusion

of material[61] controls the size of the protuberances. Electrodeposition[62] and gas-phase deposition[63–65] are common techniques to produce such surfaces out of many different materials, from metals to polymers. The highly rough microstructure of these surfaces, make them quite fragile in some cases, and also the transparency is affected by the structures at different length scales. However, this technique is versatile and it allows the deposition of thin films on top of initially rough surfaces for further hydrophobisation.

Etching

This technique is often used for the creation of structured surfaces, out of directly hydrophobic substrates or by the combination of non-hydrophobic substrates and an additional hydrophobisation stage. Different etching techniques can be used including wet chemical etching of metals[66,67], plasma etching of polymers[68,69] or laser etching of inorganic materials[70,71].

Sol-gel processing

Sol-gel processing is a technique that has been widely used for the production of hydrophobic surfaces from different materials[72–75]. This technique is quite versatile in terms of application leading to different structures such as porours foams or sol-gel films. The morphology of the final surfaces can be controlled by varying the nature of the precursors used or the amount and size of particles incorporated[76–78].

Aggregation/assembly of particles

Colloidal particles can generate rough surfaces when they self assemble or they pack into closed arrays. This method, compared to the others, is applicable to larger surfaces and also more economically viable. Indeed, many industrial products such as paints are distributed in the form of particles in a binder to be used in large amounts[79]. To achieve more organized rough structures, it is possible to control the conditions of the aggregation[80,81] and also, the incorporation of different particle sizes[82] and morphologies[83] can be used to enhance the roughness of the system.

Wrinkling

Another way of producing rough surfaces is by wrinkling. Wrinkles are formed in two-layer composites due to the mismatch between the mechanical properties of the relatively hard upper layer and the soft elastic lower layer[84,85]. Mechanical stretching[86–89], swelling-evaporation[90–92], and templates[93,94] are commonly used methods.

Wrinkles can also be formed by creating the mechanical mismatch by chemical reactions. Wrinkling coatings have been produced from liquid-applied thermally cured acrylic-melamine and alkyd systems, from powder applied and thermally cured epoxy and polyesters systems as well as from UV-Cured acrylate systems[95]. Photoinitiated polymerization of furfuryl alcohol[96] has also been used to generate a wrinkled topography. However, these polymers are not hydrophobic ($\theta < 90°$) and for these systems Wenzel's equation predicts that roughness further reduces the contact angle. Hydrophobic wrinkles have been produced via reactive

silane infusion into a poly(2-hydroxyethyl methacrylate) film[97]. Superhydrophobicity has been achieved by nanoimprint lithography of the wrinkled surfaces[98]. However, these methods involve the use of solvents and are not suitable for large surfaces.

2.3. Challenges for the commercial production of superhydrophobic coatings

Coatings have a tremendous impact on economy as they reduce corrosion (the worldwide cost of corrosion has been estimated to be 3% of the world's GDP[99]) by limiting the transport of water containing corrosive ions to the substrate. A way of reducing this transport is to increase the hydrophobicity of the coating, if possible to the superhydrophobic level, but this requires control of the texture of the coating.

The methods discussed in Section 2.2 allow a quite good control of the roughness and hence superhydrophobic surfaces can be obtained. However, these methods are not well suited to produce commercial coatings because these coatings should: i) be easily applied to large and irregular (often rigid) surfaces, ii) form a cohesive non-porous and mechanical resistant film, iii) be cost effective, which is related to the possibility of high tonnage production, and iv) be environmentally friendly. Table 2.2 shows that none of the techniques described before able to produce highly hydrophobic and superhydrophobic coatings meet these conditions.

These four conditions are met by the waterborne coatings and this is the reason why these coatings are gaining share of the market to solvent-based ones, even in highly demanding applications as automotive coatings[100]. The global waterborne coatings market is estimated to reach $78 trillion by 2019[101]. However, the idea of highly hydrophobic waterborne coatings seems to be an oxymoron as in order to form a stable dispersion in water, the polymer particles should have a relatively hydrophilic surface.

Table 2.2. Conditions met by the techniques developed to produce (super)hydrophobic coatings.

	Easily applied to large and irregular rigid surfaces	***Cohesive nonporous mechanical resistant film***	***Cost effective***	***Environmentally friendly***	***(Super) hydrophobicity***
Lithography	*No*	*Yes*	*No*	*No*	*Yes*
Templating	*No*	*Yes*	*No*	*No*	*Yes*
Phase separation	*No*	*No*	*No*	*No*	*Yes*
Crystal growth	*No*	*Yes*	*No*	*No*	*Yes*
Etching	*No*	*Yes*	*No*	*No*	*Yes*
Colloidal particles coagulation	*Yes*	*No*	*Yes*	*??*	*Yes*
Wrinkles mechanical stretching	*No*	*Yes*	*No*	*??*	*Yes*
Wrinkles swelling-evaporation	*Yes*	*Yes*	*No*	*No*	*Yes*
Templated wrinkles	*No*	*Yes*	*No*	*No*	*Yes*
Wrinkles formed by reactions	*Sometimes*	*Yes*	*Sometimes*	*Perhaps sometimes*	*Sometimes*

Film formation from waterborne dispersed polymers is often described as a process involving three steps in series (Figure 2.9): i) water evaporation to form a close-packing of the polymer particles, ii) particle deformation to form a dodecahedral structure, and iii) interdiffusion and coalescence of the deformed polymer particles[102]. When the three steps occur, relatively flat films are formed, and therefore the contact angle is determined by the nature of both the polymer and the hydrophilic components of the latex formulation (surfactant and initiator).

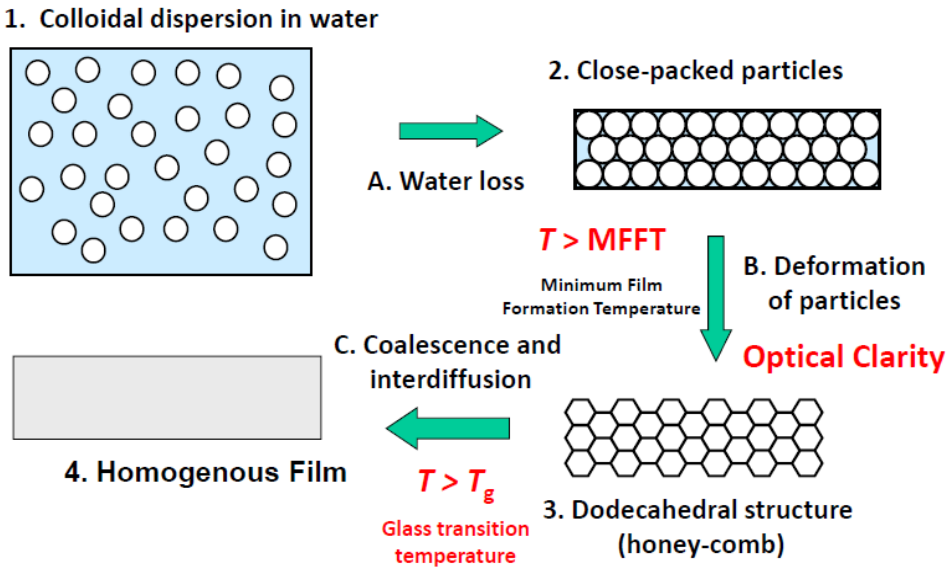

Figure 2.9. Stages of film formation.

When a waterborne dispersion of polymer particles is deposited onto a certain substrate, water evaporation will occur, and consequently, the particles will come into close contact forming a close-packed array of particles. This contact between particles will force particle deformation in order to fill the voids between them. In this point where no space

between particles is present, optical clarity in the film appears because light is not scattered anymore by the heterogeneities in the refractive index. This onset of optical clarity is defined as the Minimum Film Formation Temperature (MFFT). Once the particles are deformed, and at temperatures above the glass transition temperature of the polymer (Tg), interdiffusion of the polymer chains across the boundaries of the particles occurs leading to a continuous film[102].

Waterborne coatings can be easily applied to any type of surface, but for most common formulations the contact angle of the film rarely reaches the hydrophobic threshold. Thus, for styrene-acrylic systems, a contact angle of 72º was achieved[103]. Higher values have been achieved by including polydimethylsiloxane (PDMS) in hybrid polymer-polymer systems. Rodríguez et al.[104] synthesized silicone-(meth)acrylic latexes by miniemulsion polymerization finding that the amount of PDMS grafted to the (meth)acrylic chains, and not the overall amount of PDMS, was the main factor affecting film hydrophobicity. A value of θ = 100º was reported. PDMS has been also included in polyester waterborne dispersions reaching values of θ = 104º [105,106]. In spite of these improvements these contact angles are lower than those of the very hydrophobic polymers.

A large number of hydrophobic monomers have been polymerized using miniemulsion polymerization including lauryl methacrylate[107,108], isobornyl acrylate[109], stearyl acrylate[110,111] and fluorinated monomers[112]. In this last case, the latexes were not able to form films at ambient temperature. For fluorinated homopolymers, films were formed at 50ºC leading to θ = 130º. Smaller contact angles (θ = 105º) were obtained at temperatures above room temperature for copolymers of the fluorinated monomers and butyl methacrylate[112]. Fluorinated

surfmers (surfmers are surfactants containing a reactive double bond which allow them to be incorporated into the polymer with the main purpose of avoiding the drawbacks associated to surfactant migration[113]) were used in an attempt to increase the hydrophobicity of polystyrene latexes[114] but a very modest $\theta = 85^{o}$ was achieved, likely because the fluorinated chain of the polymer was oriented towards the interior of the particle and the hydrophilic moiety of the surfmer was at the surface of the particles giving them a rather hydrophilic character. This result indicates that, due to the presence of surfactants, the contact angle of films cast from fluorinated latexes may be lower than that of the neat fluoropolymer.

Superhydrophobic materials were developed by several authors from waterborne polymer dispersions incorporating silica nanoparticles[115–118]. Also superhydrophobic-superoleophilic filter paper was prepared for oil and water separation processes from fluorinated waterborne epoxy emulsions obtaining sticky surfaces with 152º of contact angle[119] and even superhydrophobic emulsions for cementitious composites in order to improve the freeze-thaw stability[120].

The production of (super)hydrophobic materials in water media may seem contradictory and challenging but at the same time particularly interesting in order to produce environmentally friendly systems that can be applied to large and complex surfaces at a competitive price.

2.4. References

(1) Li, X.-M.; Reinhoudt, D.; Crego-Calama, M. What Do We Need for a Superhydrophobic Surface? A Review on the Recent Progress in the Preparation of Superhydrophobic Surfaces. *Chem.Soc.Rev* **2007**, *36*, 1350–1368.

(2) Il'darkhanova, F. I.; Mironova, G. A.; Bogoslovsky, K. G.; Men'shikov, V. V.; Bykov, E. D. Development of Paint Coatings with Superhydrophobic Properties. *Prot. Met. Phys. Chem. Surfaces* **2012**, *48*, 796–802.

(3) De Gennes, P. G. Wetting: Statics and Dynamics. *Rev. Mod. Phys.* **1985**, *57*.

(4) Shirtcliffe, N. J.; McHale, G.; Atherton, S.; Newton, M. I. An Introduction to Superhydrophobicity. *Adv. Colloid Interface Sci.* **2010**, *161*, 124–138.

(5) Young, T. An Essay on the Cohesion of Fluids. *Phil. Trans. R. Soc. L.* **1805**, *95*, 65–87.

(6) Yuan, Y.; Lee, T. R. Contact Angle and Wetting Properties. In *Surface Science Techniques*; **2013**; pp 3–29.

(7) Diversified Enterprises. Critical Surface Tension and Contact Angle with Water for Various Polymers.

(8) Hare, E. F.; Shafrin, E. G.; Zisman, W. A. Properties of Films of Adsorbed Fluorinated Acids. *J. Phys. Chem.* **1954**, *58*, 236–239.

(9) Chaudhury, M. K. Interfacial Interaction between Low-Energy Surfaces. *Mater. Sci. Eng.* **1996**, *16*, 97–159.

(10) Kota, A. K.; Kwon, G.; Tuteja, A. The Design and Applications of Superomniphobic Surfaces. *NPG Asia Mater.* **2014**.

(11) Jones, B. Fluoropolymers for Coating Applications. *JCT CoatingsTech Mag.* **2008**.

(12) Nishino, T.; Meguro, M.; Nakamae, K.; Matsushita, M.; Ueda, Y. The Lowest Surface Free Energy Based on - CF3 Alignment. **1999**, *15*, 4321–4323.

(13) Pagliaro, M.; Ciriminna, R. New Fluorinated Functional Materials. *J. Mater. Chem.* **2005**, *15*, 4981–4991.

(14) Moreno-Mañas, M. Flúor, El Halógeno Redivivo. *An. la Real Soc. Española Química* **2005**.

(15) Bico, J.; Thiele, U.; Quéré, D. Wetting of Textured Surfaces. *Colloids Surfaces A Physicochem. Eng. Asp.* **2002**, *206*, 41–46.

(16) Cassie, A. B. D.; Baxter, S. Wettability of Porous Surfaces. *Trans. Faraday Soc.* **1944**, *40*, 546–551.

(17) Cassie, A. B. D. Contact Angles. *Discuss. Faraday Soc.* **1948**, *3*, 11–16.

(18) Wenzel, R.N. Surface Roughness and Contact Angle. *J.Phys.Chem.* **1949**, *53*, 1466–1467.

(19) Marmur, A. The Lotus Effect: Superhydrophobicity and Metastability. *Langmuir* **2004**, *20*, 3517–3519.

(20) Koch, K.; Bhushan, B.; Jung, Y. C.; Barthlott, W. Fabrication of Artificial Lotus Leaves and Significance of Hierarchical Structure for Superhydrophobicity and Low Adhesion. *Soft Matter* **2009**, *5*, 1386–1393.

(21) Nosonovsky, M.; Bhushan, B. Hierarchical Roughness Makes Superhydrophobic States Stable. *Microelectron. Eng.* **2007**, *84*, 382–386.

(22) Krasovitski, B.; Marmur, A. Drops Down the Hill: Theoretical Study of Limiting Contact Angles and the Hysteresis Range on a Tilted Plate. *Langmuir* **2005**, *21*, 3881–3885.

(23) Gao, L.; McCarthy, T. J. How Wenzel and Cassie Were Wrong. *Langmuir* **2007**, *23*, 3762–3765.

(24) Miwa, M.; Nakajima, A.; Fujishima, A.; Hashimoto, K.; Watanabe, T. Effects of the Surface Roughness on Sliding Angles of Water Droplets on Superhydrophobic Surfaces. *Langmuir* **2000**, *16*, 5754–5760.

(25) Furmidge, C. G. L. Studies at Phase Interfaces. I. The Sliding of Liquid Drops on Solid Surfaces and a Theory for Spray Retention. *J. Colloid Sci.* **1962**, *17*, 309–324.

(26) Feng, X.; Jiang, L. Design and Creation of Superwetting/Antiwetting Surfaces. *Adv. Mater.* **2006**, *18*, 3063–3078.

(27) Wenzel, R. N. Resistance of Solid Surfaces to Wetting by Water. *Ind. Eng. Chem.* **1936**, *28*, 988–994.

(28) Parker, D. Waterproofing Treatment of Materials. *US Pat.* **1945**, *2386259*.

(29) Gao, L.; McCarthy, T. J. “Artificial Lotus Leaf” Prepared Using a 1945 Patent and a Commercial Textile. *Langmuir* **2006**, *22*, 5998–6000.

(30) Zhang, J.; France, P.; Radomyselskiy, A.; Datta, S.; Zhao, J.; Van Ooij, W. Hydrophobic Cotton Fabric Coated by a Thin Nanoparticulate Plasma Film. *J. Appl. Polym. Sci.* **2003**, *88*, 1473–1481.

(31) Daoud, W. A.; Xin, J. H.; Tao, X. Superhydrophobic Silica Nanocomposite Coating by a Low-Temperature Process. *J. Am. Ceram. Soc.* **2004**, *87*, 1782–1784.

(32) Dai, S.; Zhang, D.; Shi, Q.; Han, X.; Wang, S.; Du, Z. Biomimetic Fabrication and Tunable Wetting Properties of Three-Dimensional Hierarchical ZnO Structures by Combining Soft Lithography Templated with Lotus Leaf and Hydrothermal Treatments. *Cryst. Eng. Comm* **2013**, *15*, 5417.

(33) Liu, Y.; Tang, J.; Wang, R.; Lu, H.; Li, L.; Kong, Y.; Qi, K.; Xin, J. H. Artificial Lotus Leaf Structures from Assembling Carbon Nanotubes and Their Applications in Hydrophobic Textiles. *J. Mater. Chem.* **2007**, *17*, 1071–1078.

(34) Srinivasan, G.; Reneker, D. H. Structure and Morphology of Small Diameter Electrospun Aramid Fibers. *Polym. Int.* **1995**, *36*, 195–201.

(35) Ma, M.; Gupta, M.; Li, Z.; Zhai, L.; Gleason, K. K.; Cohen, R. E.; Rubner, M. F.; Rutledge, G. C. Decorated Electrospun Fibers Exhibiting Superhydrophobicity. *Adv. Mater.* **2007**, *19*, 255–259.

(36) Zhu, M.; Zuo, W.; Yu, H.; Yang, W.; Chen, Y. Superhydrophobic Surface Directly Created by Electrospinning Based on Hydrophilic Material. *J. Mater. Sci.* **2006**, *41*, 3793–3797.

(37) Wang, X.; Ding, B.; Yu, J.; Wang, M. Engineering Biomimetic Superhydrophobic Surfaces of Electrospun Nanomaterials. *Nano Today* **2011**, *6*, 510–530.

(38) Pozzato, A.; Zilio, S. D.; Fois, G.; Vendramin, D.; Mistura, G.; Belotti, M.; Chen, Y.; Natali, M. Superhydrophobic Surfaces Fabricated by Nanoimprint Lithography. *Microelectron. Eng.* **2006**, *83*, 884–888.

(39) Shiu, J.-Y.; Kuo, C.-W.; Chen, P.; Mou, C.-Y. Fabrication of Tunable Superhydrophobic Surfaces by Nanosphere Lithography. *Chem. Mater.* **2004**, *16*, 561–564.

(40) Shirtcliffe, N. .; Aqil, S.; Evans, C.; McHale, G.; Newton, M. I.; Perry, C. C.; Roach, P. The Use of High Aspect Ratio Photoresist (SU-8) for Super-Hydrophobic Pattern Prototyping. *J. Micromechanics Microengineering* **2004**, *14*, 1384–1389.

(41) Öner, D.; McCarthy, T. J. Ultrahydrophobic Surfaces. Effects of Topography Length Scales on Wettability. *Langmuir* **2000**, *16*, 7777–7782.

(42) Zhu, L.; Feng, Y.; Ye, X.; Zhou, Z. Tuning Wettability and Getting Superhydrophobic Surface by Controlling Surface Roughness with Well-Designed Microstructures. *Sensors Actuators, A Phys.* **2006**, *130-131*, 595–600.

(43) El Mel, A. A.; Gautron, E.; Angleraud, B.; Granier, A.; Xu, W.; Choi, C. H.; Briston, K. J.; Inkson, B. J.; Tessier, P. Y. Fabrication of a Nickel Nanowire Mesh Electrode Suspended on Polymer Substrate. *Nanotechnology* **2012**, *23*, 275603.

(44) Roach, P.; Shirtcliffe, N. J.; Newton, M. I. Progress in Superhydrophobic Surface Development. *Soft Matter* **2008**, *4*, 224–240.

(45) Salsamendi, M.; Ballard, N.; Sanz, B.; Asua, J. M.; Mijangos, C. Polymerization Kinetics of a Fluorinated Monomer under Confinement in AAO Nanocavities. *RSC Adv.* **2015**, *5*, 19220–19228.

(46) Zhang, L.; Zhou, Z.; Cheng, B.; DeSimone, J. M.; Samulski, E. T. Superhydrophobic Behavior of a Perfluoropolyether Lotus-Leaf-like Topography. *Langmuir* **2006**, *22*, 8576–8580.

(47) Li, J.; Fu, J.; Cong, Y.; Wu, Y.; Xue, L.; Han, Y. Macroporous Fluoropolymeric Films Templated by Silica Colloidal Assembly: A Possible Route to Super-Hydrophobic Surfaces. *Appl. Surf. Sci.* **2006**, *252*, 2229–2234.

(48) Sun, M.; Luo, C.; Xu, L.; Ji, H.; Ouyang, Q.; Yu, D.; Chen, Y. Artificial Lotus Leaf by Nanocasting. *Langmuir* **2005**, *21*, 8978–8981.

(49) Martys, N. S.; Douglas, J. F. Critical Properties and Phase Separation in Lattice Boltzmann Fluid Mixtures. *Phys. Rev. E* **2001**, *63*, 1–18.

(50) Nakajima, A.; Abe, K.; Hashimoto, K.; Watanabe, T. Preparation of Hard Super-Hydrophobic Films with Visible Light Transmission. *Thin Solid Films* **2000**, *376*, 140–143.

(51) Nakajima, A.; Fujishima, A.; Hashimoto, K.; Watanabe, T. Preparation of Transparent Superhydrophobic Boehmite and Silica Films by Sublimation of Aluminum Acetylacetonate. *Adv. Mater.* **1999**, *11*, 1365–1368.

(52) Yamanaka, M.; Sada, K.; Miyata, M.; Hanabusa, K.; Nakano, K. Construction of Superhydrophobic Surfaces by Fibrous Aggregation of Perfluoroalkyl Chain-Containing Organogelators. *Chem. Commun.* **2006**, *21*, 2248–2250.

(53) Aruna, S. T.; Binsy, P.; Richard, E.; Basu, B. J. Properties of Phase Separation Method Synthesized Superhydrophobic Polystyrene Films. *Appl. Surf. Sci.* **2012**, *258*, 3202–3207.

(54) Shibuichi, S.; Onda, T.; Satoh, N.; Tsujii, K. Super Water-Repellent Surfaces Resulting from Fractal Structure. *J.Phys.Chem.* **1996**, *100*, 19512–19517.

(55) Zhang, J.; Li, J.; Han, Y. Superhydrophobic PTFE Surfaces by Extension. *Macromol. Rapid Commun.* **2004**, *25*, 1105–1108.

(56) Lu, X.; Zhang, C.; Han, Y. Low-Density Polyethylene Superhydrophobic Surface by Control of Its Crystallization Behavior. *Macromol. Rapid Commun.* **2004**, *25*, 1606–1610.

(57) Wu, X.; Zheng, L.; Wu, D. Fabrication of Superhydrophobic Surfaces from Microstructured ZnO-Based Surfaces via a Wet-Chemical Route. *Langmuir* **2005**, *21*, 2665–2667.

(58) Lau, K. K. S.; Bico, J.; Teo, K. B. K.; Chhowalla, M.; Amaratunga, G. A. J.; Milne, W. I.; McKinley, G. H.; Gleason, K. K. Superhydrophobic Carbon Nanotube Forests. *Nano Lett.* **2003**, *3*, 1701–1705.

(59) Liu, H.; Zhai, J.; Jiang, L. Wetting and Anti-Wetting on Aligned Carbon Nanotube Films. *Soft Matter* **2006**, *2*, 811–821.

(60) Chen, A.; Peng, X.; Koczkur, K.; Miller, B. Super-Hydrophobic Tin Oxide Nanoflowers. *Chem. Commun.* **2004**, *17*, 1964–1965.

(61) Brady, R. M.; Ball, R. C. Fractal Growth of Copper Electrodeposits. *Nature* **1984**, *309*, 225–229.

(62) Shirtcliffe, N. J.; McHale, G.; Newton, M. I.; Perry, C. C. Wetting and Wetting Transitions on Copper-Based Super-Hydrophobic Surfaces. *Langmuir* **2005**, *21*, 937–943.

(63) Satyaprasad, A.; Jain, V.; Nema, S. K. Deposition of Superhydrophobic Nanostructured Teflon-like Coating Using Expanding Plasma Arc. *Appl. Surf. Sci.* **2007**, *253*, 5462–5466.

(64) Shirtcliffe, N.; Thiemann, P.; Stratmann, M.; Grundmeier, G. Chemical Structure and Morphology of Thin, Organo-Silicon Plasma-Polymer Films as a Function of Process Parameters. *Surf. Coatings Technol.* **2001**, *142-144*, 1121–1128.

(65) Bonnar, M. P.; Burnside, B. M.; Little, A.; Reuben, R. L.; Wilson, J. I. B. Plasma Polymer Films for Dropwise Condensation of Steam. *Chem. Vap. Depos.* **1997**, *3*, 201–207.

(66) Guo, Z.; Zhou, F.; Hao, J.; Liu, W. Effects of System Parameters on Making Aluminum Alloy Lotus. *J. Colloid Interface Sci.* **2006**, *303*, 298–305.

(67) Han, M.; Park, Y.; Hyun, J.; Ahn, Y. Facile Method for Fabricating Superhydrophobic Surface on Magnesium. *Bull. Korean Chem. Soc.* **2010**, *31*, 1067–1069.

(68) Lacroix, L. M.; Lejeune, M.; Ceriotti, L.; Kormunda, M.; Meziani, T.; Colpo, P.; Rossi, F. Tuneable Rough Surfaces: A New Approach for Elaboration of Superhydrophobic Films. *Surf. Sci.* **2005**, *592*, 182–188.

(69) Chen, W.; Fadeev, A. Y.; Hsieh, M. C.; Didem, O.; Youngblood, J.; Mccarthy, T. Ultrahydrophobic and Ultralyophobic Surfaces: Some Comments and Examples. *Langmuir* **1999**, *15*, 3395–3399.

(70) Yoon, T. O.; Shin, H. J.; Jeoung, S. C.; Park, Y.-I. Formation of Superhydrophobic Poly(dimethysiloxane) by Ultrafast Laser-Induced Surface Modification. *Opt. Express* **2008**, *16*, 12715–12725.

(71) Baldacchini, T.; Carey, J. E.; Zhou, M.; Mazur, E. Superhydrophobic Surfaces Prepared by Microstructuring of Silicon Using a Femtosecond Laser. *Langmuir* **2006**, *22*, 4917–4919.

(72) Feng, X.; Feng, L.; Jin, M.; Zhai, J.; Jiang, L.; Zhu, D. Reversible Super-Hydrophobicity to Super-Hydrophilicity Transition of Aligned ZnO Nanorod Films. *J. Am. Chem. Soc.* **2004**, *126*, 62–63.

(73) Feng, X.; Zhai, J.; Jiang, L. The Fabrication and Switchable Superhydrophobicity of TiO2 Nanorod Films. *Angew. Chemie Int. Ed.* **2005**, *44*, 5115–5118.

(74) Hikita, M.; Tanaka, K.; Nakamura, T.; Kajiyama, T.; Takahara, A. Super-Liquid-Repellent Surfaces Prepared by Colloidal Silica Nanoparticles Covered with Fluoroalkyl Groups. *Langmuir* **2005**, *21*, 7299–7302.

(75) Ma, M.; Hill, R. M. Superhydrophobic Surfaces. *Curr. Opin. Colloid Interface Sci.* **2006**, *11*, 193–202.

(76) Schubert, U. New Materials by Sol-Gel Processing: Design at the Molecular Level. *J. Chem. Soc. Trans.* **1996**, 16, 3343–3348.

(77) Uhlmann, D. R.; Teowee, G. Sol-Gel Science and Technology : Current State and Future Prospects. *J. Sol-Gel Sci. Tecnol.* **1998**, *13*, 153–162.

(78) Pilotek, S.; Schmidt, H. K. Wettability of Microstructured Hydrophobic Sol-Gel Coatings. *J. Sol-Gel Sci. Technol.* **2003**, *26*, 789–792.

(79) Baumann, M.; Fritsche, K.-D.; Korbelarz, D.; Ludwig, S.; Poth, R. Self-Cleaning Paint Coating and a Method and Agent for Producing the Same, **2004**.

(80) Li, Y.; Huang, X. J.; Heo, S. H.; Li, C. C.; Choi, Y. K.; Cai, W. P.; Cho, S. O. Superhydrophobic Bionic Surfaces with Hierarchical Microsphere/SWCNT Composite Arrays. *Langmuir* **2007**, *23*, 2169–2174.

(81) Zhai, L.; Cebeci, F. C.; Cohen, R. E.; Rubner, M. F. Stable Superhydrophobic Coatings from Polyelectrolyte Multilayers. *Nano Lett.* **2004**, *4*, 1349–1353.

(82) Sun, C.; Ge, L. Q.; Gu, Z. Z. Fabrication of Super-Hydrophobic Film with Dual-Size Roughness by Silica Sphere Assembly. *Thin Solid Films* **2007**, *515*, 4686–4690.

(83) Ming, W.; Wu, D.; Van Benthem, R.; De With, G. Superhydrophobic Films from Raspberry-like Particles. *Nano Lett.* **2005**, *5*, 2298–2301.

(84) Genzer, J.; Groenewold, J. Soft Matter with Hard Skin: From Skin Wrinkles to Templating and Material Characterization. *Soft Matter* **2006**, *2*, 310–323.

(85) Yang, S.; Khare, K.; Lin, P.-C. Harnessing Surface Wrinkle Patterns in Soft Matter. *Adv. Funct. Mater.* **2010**, *20*, 2550–2564.

(86) Chung, J. Y.; Youngblood, J. P.; Stafford, C. M. Anisotropic Wetting on Tunable Micro-Wrinkled Surfaces. *Soft Matter* **2007**, *3*, 1163–1169.

(87) Efimenko, K.; Finlay, J.; Callow, M. E.; Callow, J. A.; Genzer, J. Development and Testing of Hierarchically Wrinkled Coatings for Marine Antifouling. *ACS Appl. Mater. Interfaces* **2009**, *1*, 1031–1040.

(88) Goel, P.; Kumar, S.; Sarkar, J.; Singh, J. P. Mechanical Strain Induced Tunable Anisotropic Wetting on Buckled PDMS Silver Nanorods Arrays. *ACS Appl. Mater. Interfaces* **2015**, *7*, 8419–8426.

(89) Lin, P.-C.; Yang, S. Mechanically Switchable Wetting on Wrinkled Elastomers with Dual-Scale Roughness. *Soft Matter* **2009**, *5*, 1011–1018.

(90) Tanaka, T.; Sun, S.-T.; Hirokawa, Y.; Katayama, S.; Kucera, J.; Hirose, Y.; Amiya, T. Mechanical Instability of Gels at the Phase Transition. *Nature* **1987**, *325*, 796–798.

(91) Chung, J. Y.; Nolte, A. J.; Stafford, C. M. Diffusion-Controlled, Self-Organized Growth of Symmetric Wrinkling Patterns. *Adv. Mater.* **2009**, *21*, 1358–1362.

(92) Liu, S.; Deng, R.; Li, W.; Zhu, J. Polymer Microparticles with Controllable Surface Textures Generated through Interfacial Instabilities of Emulsion Droplets. *Adv. Funct. Mater.* **2012**, *22*, 1692–1697.

(93) Chang, K. C.; Chuang, T-L.; Ji, W. F.; Chang, C. H.; Peng, Y. Y.; Shih, H.; Hsu, C. L.; Yeh, J. M.; Tang, W. C.; Su, Y. C.; UV-Curable Nanocasting Technique to Prepare Bioinspired Superhydrophobic Organic-Inorganic Composite Anticorrosion Coatings. *Express Polym. Lett.* **2015**, *9*, 143–153.

(94) Peng, C-W.; Chang, K-C.; Weng, C-J.; Lai, M-C.; Hsu, C-H.; Hsu, S-C.; Li, S-Y.; Wei, Y.; Yeh, J-M.; UV-Curable Nanocasting Technique to Prepare Bio-Mimetic Super-Hydrophobic Non-Fluorinated Polymeric Surfaces for Advanced Anticorrosive Coatings. *Polym. Chem.* **2013**, *4*, 926–932.

(95) Basu, S. K.; Scriven, L. E.; Francis, L. F.; McCormick, A. V. Mechanism of Wrinkle Formation in Curing Coatings. *Prog. Org. Coatings* **2005**, *53*, 1–16.

(96) Gaillard, J. G.; Hendrus, C.; Vogt, B. D. Tunable Wrinkle and Crease Surface Morphologies from Photoinitiated Polymerization of Furfuryl Alcohol. *Langmuir* **2013**, *29*, 15083–15089.

(97) Li, Y.; Peterson, J. J.; Jhaveri, S. B.; Carter, K. R. Patterned Polymer Films Via Reactive Silane Infusion Induced Wrinkling. *Langmuir* **2013**, *29*, 4632–4639.

(98) Li, Y.; Dai, S.; John, J.; Carter, K. R. Superhydrophobic Surfaces from Hierarchically Structured Wrinkled Polymers. *ACS Appl. Mater. Interfaces* **2013**, *5*, 11066–11073.

(99) Hays, G. F.(2016, April). Now is the time. Retrieved from: http://corrosion.org/.

(100) (2016, January). Retrieved from: http://www.futuremarketinsights.com/reports/waterborne-automobile-coating-market.

(101) (2016, January). Retrieved from: http://www.marketsandmarkets.com/PressReleases/waterborne-waterbased-coatings.asp.

(102) Keddie, J. L.; Routh, A. F. *Fundamentals of Latex Film Formation: Processes and Properties*; **2010**.

(103) Bassett, D. R. Hydrophobic Coatings from Emulsion Polymers. *J. Coatings Technol.* **2001**, *73*, 43–55.

(104) Rodríguez, R.; de las Heras Alarcón, C.; Ekanayake, P.; Mcdonald, P. J.; Keddie, J. L.; Barandiaran, M. J.; Asua, J. M. Correlation of Silicone Incorporation into Hybrid Acrylic Coatings with the Resulting Hydrophobic and Thermal Properties. *Macromolecules* **2008**, *41*, 8537–8546.

(105) Verma, G.; Dhoke, S. K.; Khanna, A. S. Polyester Based-Siloxane Modified Waterborne Anticorrosive Hydrophobic Coating on Copper. *Surf. Coatings Technol.* **2012**, *212*, 101–108.

(106) Verma, G.; Swain, S.; Khanna, A. S. Hydrophobic Self-Cleaning Coating Based on Siloxane Modified Waterborne Polyester. *Int. J. Sci. Eng. Technol.* **2013**, *2*, 192–200.

(107) Yildiz, U.; Landfester, K.; Antonietti, M. The Fabrication of Very Small Miniemulsion Latexes from N-Stearoylglutamate and Lauryl Methacrylate: Evidence for Droplet Budding. *Macromol. Chem. Phys.* **2003**, *204*, 1966–1970.

(108) Tauer, K.; Ali, A. M. I.; Yildiz, U.; Sedlak, M. On the Role of Hydrophilicity and Hydrophobicity in Aqueous Heterophase Polymerization. *Polymer* **2005**, *46*, 1003–1015.

(109) Back, A. J.; Schork, F. J. Emulsion and Miniemulsion Polymerization of Isolbornyl Acrylate. *J. App. Polym. Sci.* **2007**, *103*, 819–833.

(110) Mehravar, E.; Leiza, J. R.; Asua, J. M. Synthesis and Characterization of Comb-like Acrylic-Based Polymer Latexes Containing Nano-Sized Crystallizable Domains. *Polymer* **2016**, *84*, 167–177.

(111) Agirre, A.; de las Heras-Alarcón, C.; Wang, T.; Keddie, J. L.; Asua, J. M. Waterborne, Semicrystalline, Pressure-Sensitive Adhesives with Temperature-Responsiveness and Optimum Properties. *ACS Appl. Mater. Interfaces* **2010**, *2*, 443–451.

(112) Landfester, K.; Rothe, R.; Antonietti, M. Convenient Synthesis of Fluorinated Latexes and Core - Shell Structures by Miniemulsion Polymerization. *Macromolecules* **2002**, *35*, 1658–1662.

(113) Asua, J. M.; Schoonbrood, H. A. S. Reactive Surfactants in Heterophase Polymerization. *Acta Polym.* **1998**, *49*, 671–686.

(114) Pich, A.; Datta, S.; Musyanovych, A.; Adler, H. J. P.; Engelbrecht, L. Polymeric Particles Prepared with Fluorinated Surfmer. *Polymer* **2005**, *46*, 1323–1330.

(115) Motornov, M.; Sheparovych, R.; Lupitskyy, R.; MacWilliams, E.; Minko, S. Superhydrophobic Surfaces Generated from Water-Borne Dispersions of Hierarchically Assembled Nanoparticles Coated with a Reversibly Switchable Shell. *Adv. Mater.* **2008**, *20*, 200–205.

(116) Qu, A.; Wen, X.; Pi, P.; Cheng, J.; Yang, Z. Preparation of Hybrid Film with Superhydrophobic Surfaces Based on Irregularly Structure by Emulsion Polymerization. *Appl. Surf. Sci.* **2007**, *253*, 9430–9434.

(117) Deng, X.; Mammen, L.; Zhao, Y.; Lellig, P.; Müllen, K.; Li, C.; Butt, H. J.; Vollmer, D. Transparent, Thermally Stable and Mechanically Robust Superhydrophobic Surfaces Made from Porous Silica Capsules. *Adv. Mater.* **2011**, *23*, 2962–2965.

(118) Wen, X. F.; Wang, K.; Pi, P. H.; Yang, J. X.; Cai, Z. Q.; Zhang, L. J.; Qian, Y.; Yang, Z. R.; Zheng, D. F.; Cheng, J. Organic-Inorganic Hybrid Superhydrophobic Surfaces Using Methyltriethoxysilane and Tetraethoxysilane Sol-Gel Derived Materials in Emulsion. *Appl. Surf. Sci.* **2011**, *258*, 991–998.

(119) Huang, X.; Wen, X.; Cheng, J.; Yang, Z. Sticky Superhydrophobic Filter Paper Developed by Dip-Coating of Fluorinated Waterborne Epoxy Emulsion. *Appl. Surf. Sci.* **2012**, *258*, 8739–8746.

(120) Muzenski, S. W.; Flores-Vivian, I.; Sobolev, K. The Development of Hydrophobic and Superhydrophobic Cementitious Composites. *Proc. 4th Int. Conf. Durab. Concr. Struct.* **2014**.

Chapter 3. Highly hydrophobic coatings by blends of soft and hard latexes

3.1. Introduction

As it has been explained in Chapters 1 and 2, hydrophobic or water repellent surfaces are highly demanded because they present many useful properties such as antibiofouling, antisticking, anticorrosion, stain resistance and self cleanability[1,2]. The most convenient way to provide with these properties to widely different products is by means of a polymer coating; ideally, a waterborne coating that avoids the environmental impact of the solventborne coatings.

Film formation from waterborne dispersions involves three steps. i) water evaporation, ii) particle deformation, and iii) particle coalescence and polymer interpenetration[3], and the result of these processes is a film with a rather flat surface. Rougher surfaces can be obtained using hard particles, but then a mechanically weak film with many pores is obtained.

This work aims at producing highly hydrophobic coatings from waterborne latexes able to form films at ambient temperature. Film forming latexes were synthesized by miniemulsion copolymerization of a fluorinated monomer and a soft acrylic monomer. These films showed a relatively high contact angle (114º) but further increase was precluded by the relatively flat surface of the film. Attempts to increase the roughness of the film using blends of film-forming latexes with latex of the fluorinated homopolymer (which is not film forming) were not successful under regular conditions because the fluorinated homopolymer particles

accumulated at the film-substrate interface. Film formation engineering allowed to modify the morphology of the film obtaining a contact angle of 137º.

3.2. Experimental

3.2.1. Materials

1H, 1H, 2H, 2H-perfluorodecyl acrylate (PFDA) supplied by Interchim and 2-ethylhexyl acrylate (2EHA) supplied by Quimidroga were used as monomers. Dowfax 2A1 (alkyl diphenyloxide disulfonate); (anionic) from Dow Chemical and Capstone FS-30 (non ionic) from DuPont were used as surfactants. 2,2-azobisisobutyronitrile (AIBN) from Aldrich was used as oil soluble initiator for the polymerizations. All these compounds were used as received. Double deionized water (DDI) was used as continuous medium in the polymerizations.

3.2.2. Miniemulsion polymerization

40% solids content miniemulsions were prepared and further polymerized in a batch process. The organic phase was prepared dissolving the AIBN in the monomer mixture (PFDA in the homopolymerization and PFDA and 2EHA in the copolymerizations). The aqueous phase contained the surfactant. The organic phase was gently added to the aqueous phase and mixed under magnetic stirring for fifteen minutes. The coarse miniemulsion was sonified for 10 min (70% amplitude, 50% duty cycle) in a Branson Sonifier 450. The miniemulsion stability was checked by the use of a Turbiscan LAb^{expert} equipment where the backscattered light signal of

the dispersions is recorded as a function of time. The bigger the change of the backscattering over time, the less stable the miniemulsion.

The reactions were carried out in batch in a 250 ml glass-jacketed reactor equipped with a reflux condenser, N_2 inlet, and a stainless steel turbine stirrer working at 200 rpm. The system was led to react during four hours at 70ºC. The polymerizations carried out are summarized in Table 3.1.

Two latexes were produced by copolymerization of PFDA and 2EHA in different proportions. In addition, two PFDA homopolymer hard latexes were synthesized using different types and concentrations of surfactants. The goal of these experiments was to have widely different particle sizes because it was expected that the topography of the surface of the films cast from blends of film forming and hard latexes would be influenced by the size of the hard latex.

Table 3.1. Formulation for the latexes synthesized

LATEX	ORGANIC PHASE		AQUEOUS PHASE		$d_{droplet}$ (nm)	$d_{particle}$ (nm)
	MONOMER RATIO[a] (wt/wt)	INITIATOR [b]	EMULSIFIER [b]	WATER		
1	PFDA/2EHA (100/0)	AIBN 1 wt%	CAPSTONE FS-30 4 wt%	≈60 wt%	≈ 750	≈ 750
2	PFDA/2EHA (100/0)	AIBN 1 wt%	DOWFAX 2A-1 1 wt%		181	200
3	PFDA/2EHA (90/10)	AIBN 1 wt%	DOWFAX 2A-1 1 wt%		154	169
4	PFDA/2EHA (82/18)	AIBN 1 wt%	DOWFAX 2A-1 1 wt%		169	177

[a]Monomer represents 40% of the total weight of the formulation.

[b]based on the total weight of monomer

3.2.3. Characterization

The droplet and particle size were measured by Dynamic Light Scattering (Zetasizer Nano Z, Malvern Instruments). Scanning Electron Microscopy was used for the large particle sizes.

Monomer conversion was determined gravimetrically. The final latexes were dried at 23ºC and 55% humidity and their thermal transitions were analyzed by Differential Scanning Calorimetry (DSC, Q1000, TA Instruments). The heating rate used was 10ºC/min over a temperature range from -80 to 120ºC under nitrogen atmosphere.

Water contact angles were measured in a OCA 20 Instrument (Dataphysics). Films from the different latexes were cast on glass substrates and then dried for two days at 23ºC and 55% relative humidity. In order to mimic the removal of the migrated surfactant by rain, films were immersed in water for 24 hours and dried again for another two days. The measurement of the contact angle was done by placing 10 µl droplets of distilled water on the surface of the films. The values given are an average of twenty measurements per film. The appearance of the films was evaluated visually and by SEM microscopy.

3.3. Results and discussion

Table 3.1 presents the latexes synthesized. It can be seen that for all the cases, the particle size was very similar to the droplet size, which indicated an efficient nucleation of stable droplets. Droplet nucleation was favored by the use of an oil soluble initiator, which mainly produced radicals in the droplets. However, this alone does not guarantee an efficient droplet nucleation because AIBN partitions between the monomer droplets and the aqueous phase and hence radicals can also be generated in this phase. In addition, initiator radicals produced in the droplets can desorb to the aqueous phase[4]. These radicals can initiate polymerization in the aqueous phase leading to the formation of new particles by homogeneous nucleation. In the present case, the water insolubility of the monomers precluded this process.

Figure 3.1 presents the evolution of the light backscattered from the miniemulsions over four hours. Because the stability of the miniemulsions decreases as temperature increases, the

measurements were carried out at the maximum temperature of the equipment (60ºC) in order to be as close as possible to the polymerization temperature (70ºC). It can be seen that the PFDA miniemulsions were stable for the whole period of time (no change in backscattered light) whereas the miniemulsions containing 2EHA showed some degradation that was more accused for the miniemulsion containing the highest amount of 2EHA. This was due to the higher water solubility of the 2EHA. With these results in mind, it may be surprising that droplet degradation/coalescence was avoided in the polymerization of the miniemulsions containing 2EHA. The reason was that polymerization was very fast (Figure 3.2) and the droplets did not have time to degrade. The fast polymerization was due to the high propagation rate of the acrylates[5].

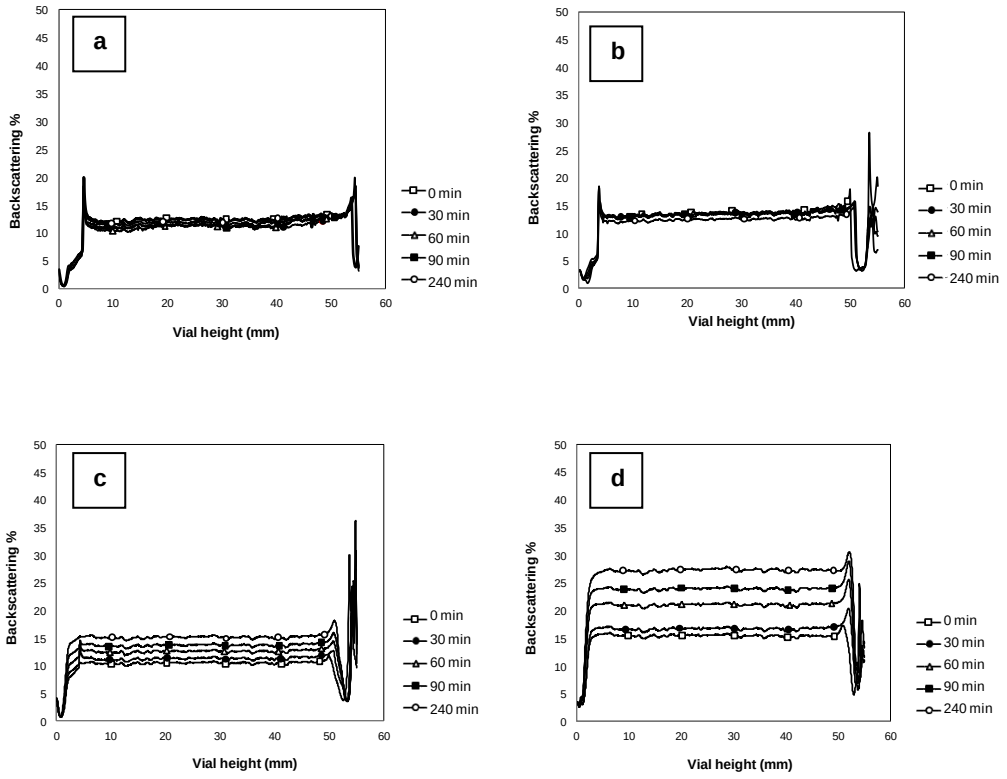

Figure 3.1. Evolution of the light backscattering profiles at 60ºC for the miniemulsions: a) PFDA homopolymer with Capstone FS-30, b) PFDA homopolymer with Dowfax 2A1, c) 90/10 (PFDA/2EHA) copolymer, d) 82/18 (PFDA/2EHA) copolymer. In the abscissa, 0 is the bottom of the miniemulsion and the top is close to 50.

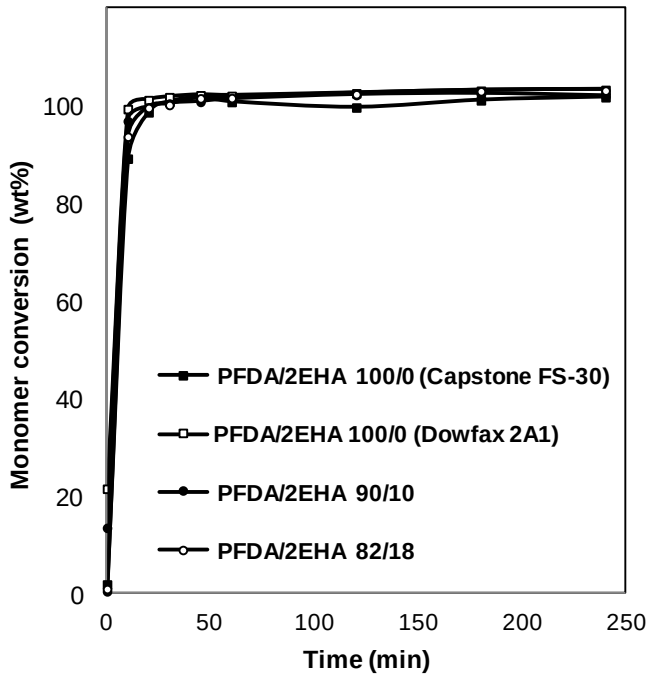

Figure 3.2. Evolution of the conversion for the different reactions.

Figure 3.3 presents the DSC thermograms of the polymers synthesized. The represented homopolymer corresponds to the one from Latex 2, although no difference was found with respect to the one from Latex 1. It can be observed that the homopolymer is crystalline showing a big melting peak at a temperature close to 75ºC. Increasing the percentage of 2EHA incorporated in the copolymer, the melting temperature and the crystallinity decreased. This affected film formation. Latexes 1 and 2 (homopolymer) and Latex

3 (90/10) were too hard to form coherent films at ambient temperature, but Latex 4 (82/18) yielded a good and transparent film (Figure 3.4).

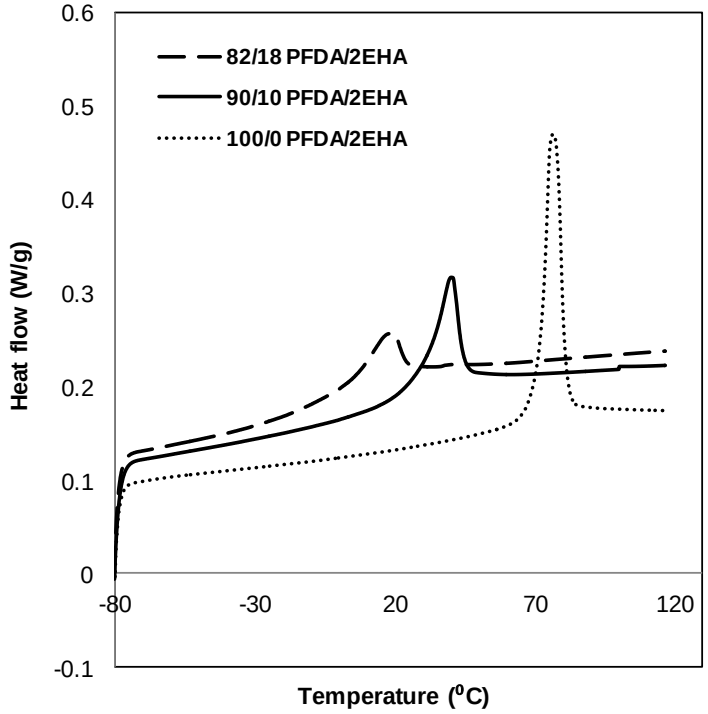

Figure 3.3. DSC thermograms for the different polymers. (Exo Down)

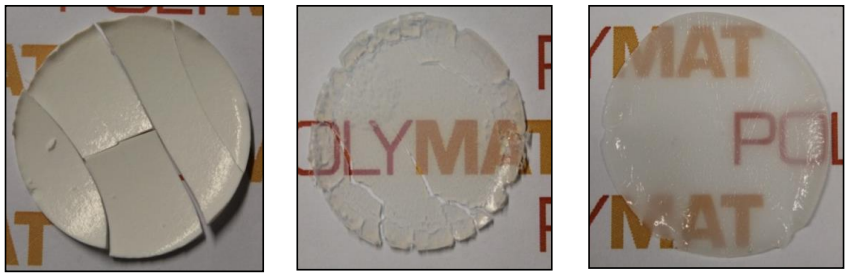

Latex 2 (PFDA/2EHA 100/0) **Latex 3 (PFDA/2EHA 90/10)** **Latex 4 (PFDA/2EHA 82/18)**

Figure 3.4. Films formed from the homopolymer and the different copolymers**.**

Figure 3.5 presents the effect of the polymer composition on the water contact angle. It can be seen that contact angles higher than 114º were obtained in all the cases and that the contact angle increased with the PFDA content, reaching 134º for the Latex 2 (small particle size homopolymer of PFDA). However, PFDA contents higher than 82 wt% were too hard to form films at ambient temperature.

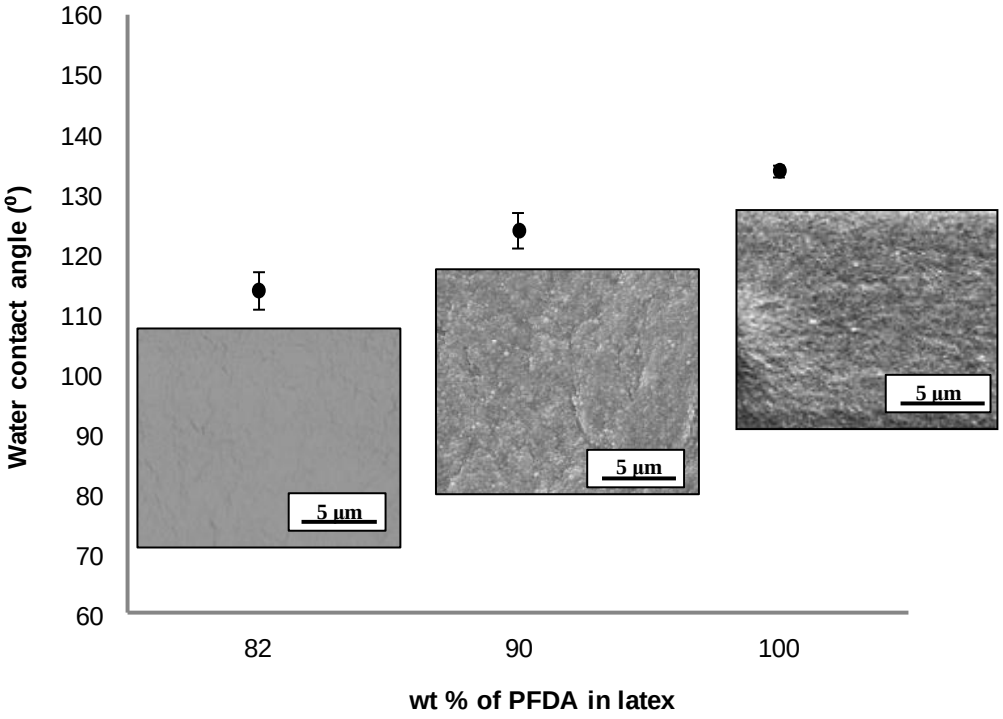

Figure 3.5. Effect of the PFDA content on the contact angle (the PFDA homopolymer is Latex 2).

The contact angle value of the flat homopolymer was also determined by preparing a film of Latex 2 at 90ºC, well above its melting temperature. A value of 111º was measured; therefore the fact that the observed contact angles were higher than the value for a flat surface of the homopolymer indicates that surface topography contributed to increase the contact angles. Actually the surface roughness can be observed in the SEM images of Figure 3.5. Comparison between these images shows that roughness increased with the PFDA content,

due to the fact that particles became harder, and hence they did not deform during film formation. The drawback is that the mechanical properties of the films deteriorated. This means that using film forming latexes produced by copolymerization of PFDA and 2EHA, the maximum contact angle is limited to a value of about 114°.

Blends of soft and hard latexes have shown to be beneficial in many applications including zero VOC coatings[6], coatings with improved mechanical properties[7,8] and adhesives with both temperature responsiveness and optimum properties[9]. This last article is particularly interesting for the present work because it shows a latex blend that led to a good film with a rough surface.

This prompted us to explore the possibility of improving the hydrophobicity of the films obtained from waterborne polymer dispersions by using latex blends of the film forming Latex 4 (82/18) and Latexes 1 and 2 (PFDA homopolymer).

The films cast from blends of Latex 4 (82/18) and Latex 2 (PFDA with the smaller particle size) showed contact angles that were similar to those of the copolymer (Table 3.2), which indicated that the surface of the film was covered by the copolymer. This was confirmed by the SEM images of the surface of the film (Figure 3.6, top). Further analysis of the films showed that the hard particles accumulated at the film-substrate interface, indicating sedimentation of the more dense homopolymer particles. This led to higher contact angles at the film-substrate interfaces (Figure 3.2). Latex 1 was not used at this stage because a stronger sedimentation was expected for larger PFDA particles.

Table 3.2. Water contact angles for blends of Latex 2 (PFDA) and Latex 4 (82/18) in different ratios at the air-film and film-substrate interfaces. These films had 1250 µm of wet thickness.

Latex 4/ Latex 2	*Θ water air-film interface (º)*	*Θ water film-substrate interface (º)*
0/100	*134±1*	*134±1*
50/50	*117±3*	*129±2*
60/40	*110±2*	*121±8*
70/30	*112±3*	*121±2*
100/0	*114±3*	*114±3*

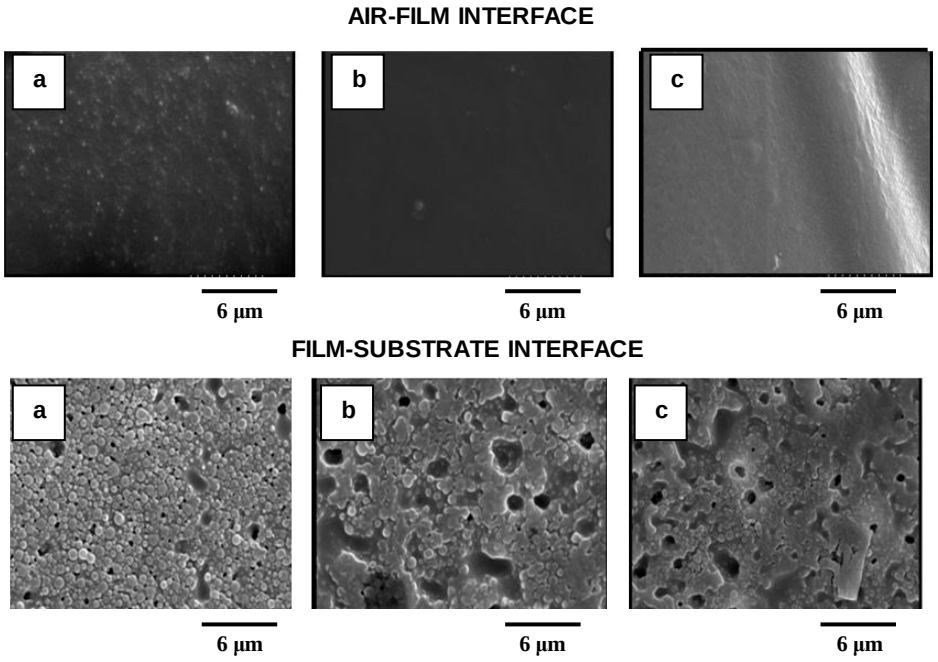

Figure 3.6. SEM images for the air-film interface and film-substrate interface for different blending ratios: a) Latex 4/Latex 2: 50/50; b) Latex 4/Latex 2: 60/40; c) Latex 4/Latex 2: 70/30.

Several strategies were adopted to avoid or at least minimize the effect of the sedimentation and to take advantage of gravity. These strategies include: i) to use thinner films; ii) reverting the orientation of the film to use gravity to bring the PFDA particles to the air-film interface; iii) increasing the viscosity of the blend and the density of the softer latex; and iv) applying the PFDA homopolymer latex onto a primer of the softer latex during the open time of this latex.

3.3.1. Use a thinner film

The effect of sedimentation can be reduced by preparing thinner films, because as these films dry faster, the denser particles have less time to sediment.

50/50 and 20/80 wt/wt blends of Latexes 1 (large particle size PFDA homopolymer) and 4 (82/18 2EHA/PFDA copolymer) were used to cast 90 μm wet thick films that were dried at 23^0C and 55% relative humidity. Figure 3.7 presents the SEM images of the air-film interfaces of the dried films and the corresponding contact angles. Comparison of the results obtained with the 50/50 blend with those in Figure 3.6,a show that reducing the film wet thickness from 1250 μm to 90 μm substantially increased the amount of PFDA particles at the air-film interface leading to a higher contact angle (123º±8). For the 20/80 blend, the thickness of the film did not have any significant effect on the distribution of the hard PFDA particles and on the contact angle.

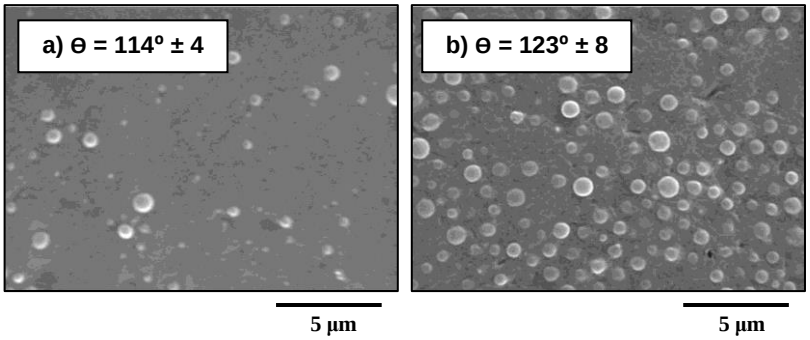

Figure 3.7. PFDA distribution and contact angles for the 90 µm wet thick films of blends of Latexes 1 and 4. a) Latex1/Latex 4 = 20/80 wt/wt; b) Latex1/Latex 4 = 50/50 wt/wt.

3.3.2. Reverting the orientation of the film during drying

A simple way of bringing the denser and bigger PFDA particles to the air-film interface is to dry the film upside down. 50/50 and 20/80 wt/wt blends of the Latexes 1 and 4 were prepared, 90 µm wet films were cast on a glass substrate and turned upside down while drying at 23ºC and 55% relative humidity. Figure 3.8 shows the SEM images of the air-film interface and the contact angles. It can be seen that drying upside down did not have any effect for the 20/80 blend, but for the 50/50 blend the contact angle increased from 123º to 130º. This effect would likely be stronger in thicker films.

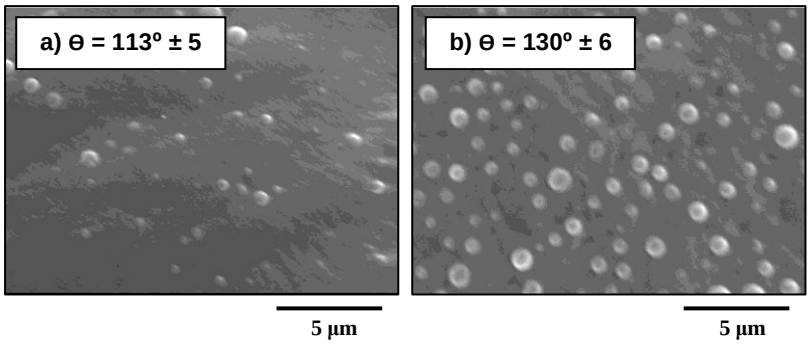

Figure 3.8. Effect of drying upside down on PFDA distribution and contact angle for the 90 µm wet films of blends of Latexes 1 and 4. a) Latex1/Latex 4 = 20/80 wt/wt; b) Latex1/Latex 4 = 50/50 wt/wt.

3.3.3. Increasing the viscosity of the dispersion and the density of the softer latex

This was achieved by using a high solids (60 wt%) poly(vinylidene chloride) (p(VDC)) latex supplied by Solvay (particle diameter = 185 nm). The high solids increased the viscosity and the p(VDC) has a density of 1.69 kg/L, which is closer to the PFDA homopolymer density (1.91 kg/L) than that of the 82/18 copolymer (1.56 kg/L). The p(VDC) latex was blended with Latexes 1 and 2 (PFDA homopolymers) in a 50/50 weight ratio (dry basis) and 90 µm wet films were cast at 23ºC and 55% relative humidity.

Figure 3.9 shows the SEM images of the air-film and film-substrate interfaces. These images show that for the case of the blend with the small particle size PFDA homopolymer, no

proof of sedimentation can be observed in the film-substrate interface. On the other hand, for the case of the large PFDA homopolymer particles, sedimentation is only partially prevented likely due to the fact that these particles were larger and therefore they sedimented faster. This uneven distribution of the hydrophobic particles affected the contact angle at the air-film interface that was 133º±1 for the small PFDA particles and 120º±2 for the large ones. These values are remarkably high having in mind that the contact angle of the p(VDC) is only 68º±1.

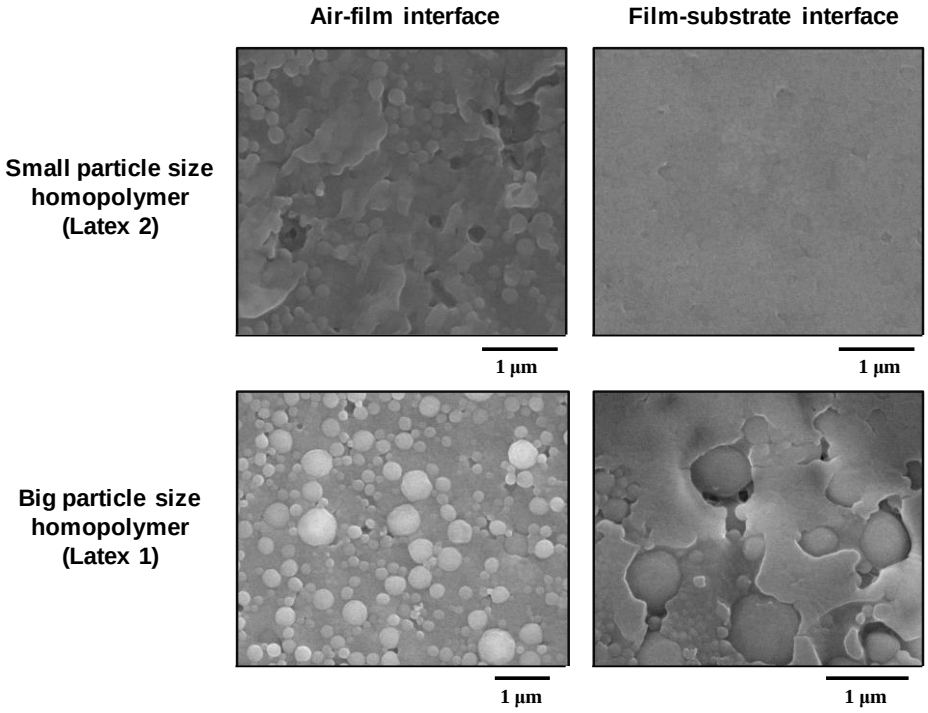

Figure 3.9. SEM images of the air-film (left) and film-substrate (right) interfaces of the films cast from 50/50 wt/wt (dry basis) of latexes 1 and 2 (PFDA homopolymers) with the p(VDC) latex.

3.3.4. Application of the PFDA latex onto a primer of soft latex

In the previous section, it has been shown that blends of the PFDA and p(VDC) latexes can provide very high contact angles. However, when high weatherability is required, fluorinated polymers are preferred. As it is discussed above, the maximum contact angle achieved with blends of PFDA and PFDA-2EHA was 130º using upside down drying. However, this type of drying is difficult to implement in practice. Therefore, the fraction of PFDA at the air-film interface was increased by using a coating procedure that takes advantage of the open time of the waterborne coatings. Open time is the time available to rework a wet coating after its initial application[10]. This means that during this time, the layer of drying latex can be mixed with another latex that is applied on top of this layer. This opens the possibility of increasing the contact angle of a coating by casting a layer of hydrophobic particles on top of a primer. In order to proof the concept, the films were cast in a spin-coater. First, a primer was formed by spin-coating. This primer was Latex 4 (82/18 copolymer) that was spin-coated at 500 rpm during 30 seconds. Then, an equal amount of Latex 1 (large particle size PFDA latex) was added on top of the primer and spin coated at 1500 rpm for 60 seconds. The composite film was allowed to dry at 23ºC and 55% relative humidity obtaining a cohesive film. Figure 3.10 (left) shows that this coating technique led to an air-film interface completely covered by PFDA particles. The texture of the surface allowed reaching a contact angle of 133º (well above that of the flat PFDA).

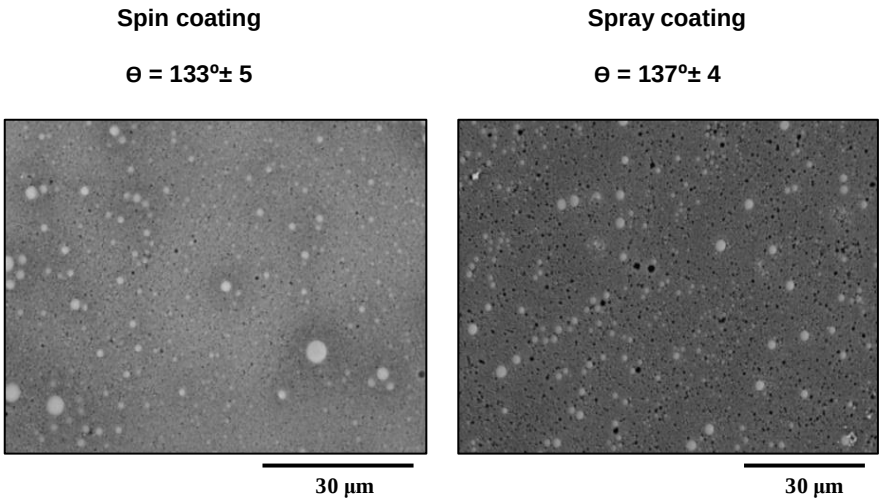

Figure 3.10. SEM images and water contact angles of the films obtained by means of the double coating strategy.

Once the proof of concept was demonstrated, the idea was applied to a coating strategy better suited to coat large and complex surfaces. In this strategy, the 82/18 latex (Latex 4) was cast and let to dry for three minutes at 23ºC and 55% relative humidity. Then, the large particle size PFDA latex (Latex 1) was sprayed on top of the partially dried film (2-3 mg polymer/cm^2 in 15 seconds), and then, completely dried at 23ºC and 55% relative humidity. Figure 3.10 (right) shows that the air-film interface was completely covered by PFDA particles, which led to a contact angle of 137º±4.

3.4. Conclusions

This work aims at producing highly hydrophobic coatings (water contact angles greater than 130º) from waterborne latexes able to form films at ambient temperature. These are conflicting requirements because these contact angles can only be achieved by means of textured surfaces and polymers able to form film at ambient temperature yield flat surfaces. Film-forming latexes prepared by miniemulsion copolymerization of 2-ethylhexyl acrylate (2EHA) and 1H, 1H, 2H, 2H- perfluorodecyl acrylate (PFDA) yielded a contact angle of 114º. Higher contact angles were obtained with formulations richer in PFDA, but films of poor quality were obtained at room temperature.

Blending of these latexes with a latex of PFDA homopolymer (which is not film forming at room temperature) did not show any improvement in the case of thick films because the denser PFDA particles sedimented. Sedimentation was reduced by using thinner films and higher contact angles were observed (θ = 123º). In an attempt to take advantage of gravity, films were dried upside down and a contact angle of 130º was achieved because PFDA particles sedimented at the air-film interface. However, this type of drying is difficult to implement in practice. Higher contact angles (θ = 133º) were obtained reducing sedimentation by using a film forming 60 wt% solids content latex of poly(vinylidene chloride) that increase both the viscosity of the blend and the density of the soft polymer. A dual coating strategy which is not limited in terms of density of the polymers and takes advantage of the open time of the waterborne coatings was developed. In this strategy, a film forming dispersion is cast first

and during its open time, a latex of hard hydrophobic particles is cast on top of it using spray coating. A contact angle of 137º was obtained using this strategy.

3.5. References

(1) Li, X.-M.; Reinhoudt, D.; Crego-Calama, M. What Do We Need for a Superhydrophobic Surface? A Review on the Recent Progress in the Preparation of Superhydrophobic Surfaces. *Chem.Soc.Rev* **2007**, *36*, 1350–1368.

(2) Il'darkhanova, F. I.; Mironova, G. A.; Bogoslovsky, K. G.; Men'shikov, V. V.; Bykov, E. D. Development of Paint Coatings with Superhydrophobic Properties. *Prot. Met. Phys. Chem. Surfaces* **2012**, *48*, 796–802.

(3) Keddie, J. L.; Routh, A. F. *Fundamentals of Latex Film Formation: Processes and Properties*; **2010**.

(4) Autran, C.; de la Cal, J. C.; Asua, J. M. (Mini)emulsion Polymerization Kinetics Using Oil-Soluble Initiators. *Macromolecules* **2007**, *40*, 6233–6238.

(5) Asua, J. M.; Beuermaann, S.; Buback, M.; Castignolles, P.; Charleux, B.; Gilbert, R.; Hutchinson, R. A.; Leiza, J. R.; Nikitin, A. N.; Vairon, J.-P.; van Herk, A. M.; Critically Evaluated Rate Coefficients for Free-Radical Polymerization. Propagation Rate Coefficient for Butyl Acrylate. *Macromol. Chem. Phys.* **2004**, *205*, 2151–2160.

(6) Winnik, M. A.; Feng, J. Latex Blends: An Approach to Zero VOC Coatings. *J. coatings Technol.* **1996**, *68*, 39–50.

(7) Colombini, D.; Hassander, H.; Karlsson, O. J.; Maurer, F. H. J. Effects of Thermal Annealing on the Viscoelastic Properties and Morphology of Bimodal Hard/soft Latex Blends. *J. Polym. Sci. Part B Polym. Phys.* **2005**, *43*, 2289–2306.

(8) Qin, F.; Li, M.; Li, X. Y.; Wang, H. Q. Stability and Mechanical Properties of Hard/Soft Latex Blends. *Appl. Mech. Mater.* **2015**, *731*, 483–487.

(9) Agirre, A.; de las Heras-Alarcón, C.; Wang, T.; Keddie, J. L.; Asua, J. M. Waterborne, Semicrystalline, Pressure-Sensitive Adhesives with Temperature-Responsiveness and Optimum Properties. *ACS Appl. Mater. Interfaces* **2010**, *2*, 443–451.

(10) Overbeek, A.; Bückmann, F.; Martin, E.; Steenwinkel, P.; Annable, T. New Generation Decorative Paint Technology. *Prog. Org. Coatings* **2003**, *48*, 125–139.

Chapter 4. Controlling film topography to enhance hydrophobicity

4.1. Introduction

Among the different methods to produce (super)hydrophobic coatings presented in Chapter 2, wrinkling was one of the potential techniques to produce hydrophobic surfaces. In this chapter a wrinkling strategy to produce easy to apply, cost effective, environmentally friendly, good quality (super)hydrophobic coatings is presented.

Chapter 3 showed that the formation of a cohesive non-porous and mechanical resistant film with a rough surface from waterborne polymer dispersions is very challenging. Nevertheless, film formation engineering allowed modifying the morphology of the film obtaining a contact angle of 137º.

This chapter presents a solution for this problem by promoting the formation of wrinkles during film formation. This was achieved by taking advantage of the phenomenon of skin formation that can occur during the first part of the water evaporation[1]. It is shown that controlling the conditions for film formation; a polymer skin can be formed at the film-air interface before the interior of the film becomes dry. As a consequence, a mechanical mismatch between the surface of the film and its interior is created and wrinkles can be formed. The wrinkled film presented a water contact angle substantially higher than that of the film obtained under standard conditions.

4.2. Experimental

4.2.1. Materials

1H, 1H, 2H, 2H-perfluorodecyl acrylate (PFDA) supplied by Interchim and 2-ethylhexyl acrylate (2EHA) supplied by Quimidroga were used as monomers. Dowfax 2A1 (alkyl diphenyloxide disulfonate) from Dow Chemical was used as anionic surfactant for the miniemulsion stabilization. 2,2-azobisisobutyronitrile (AIBN) from Aldrich was used as oil soluble initiator for the polymerizations. All these compounds were used as received. Double deionized water (DDI) was used as continuous medium in the polymerizations.

4.2.2. Miniemulsion polymerization

40% solids content miniemulsions were prepared and polymerized in a batch process. The organic phase was prepared dissolving the AIBN in the monomer mixture (1 wt% based on monomers). The aqueous phase contained the surfactant (1 wt% based on monomers). The organic phase was gently added to the aqueous phase and mixed under magnetic stirring for fifteen minutes. The coarse miniemulsion was sonified for ten minutes (70% amplitude, 50% duty cycle) in a Branson Sonifier 450.

The reactions were carried out in batch in a 250 ml glass-jacketed reactor equipped with a reflux condenser, N_2 inlet, and a stainless steel turbine stirrer working at 200 rpm. The

system was led to react during four hours at 70ºC. The polymerizations carried out are summarized in Table 4.1.

Table 4.1. Properties of the latexes synthesized

MONOMER RATIO (wt/wt)	***d particle (nm)***	**Tm (ºC)**	**Xc[a]**
PFDA/2EHA (100/0)	*200*	*76*	*100*
PFDA/2EHA (90/10)	*169*	*40*	*61*
PFDA/2EHA (82/18)	*177*	*17*	*29*
PFDA/2EHA (80/20)	*209*	*13*	*18*
PFDA/2EHA (75/25)	*187*	*6*	*5*

[a] Referred to the homopolymer

4.2.3. Characterization

The droplet and particle diameter (Z-average) was measured by Dynamic Light Scattering (Zetasizer Nano Z, Malvern Instruments). The values given are the average of two measurements. Monomer conversion was determined gravimetrically reaching in all the cases 100%.

The final latexes were dried at 23ºC and 55% relative humidity and their thermal transitions were analyzed by Differential Scanning Calorimetry (DSC, Q1000, TA Instruments). The heating rate used was 10ºC/min over a temperature range from -80 to 120ºC under nitrogen atmosphere. The crystallinity of the polymers, Xc, was calculated by dividing the calorimetric heat of fusion (ΔHf) of each polymer by the ΔHf for the fluorinated homopolymer.

Films were cast onto glass substrates and dried at 23ºC and 90ºC and 55% relative humidity in both cases. In order to mimic the removal of the surfactant that migrates to the surface of the film by rain, the films were rinsed with water and dried again at 23ºC and 55% relative humidity.

Water contact angles were measured in an OCA 20 Instrument (DataPhysics). The measurement was carried out by placing 10 µl droplets of distilled water on the surface of the films. The given values are an average of ten measurements per film.

The surface of the film was analyzed by Scanning Electron Microscopy in a Hitachi TM3030 Scanning Electron Microscope.

4.3. Results and discussion

Table 4.1 summarizes the properties of the latexes. Before the polymerization, the miniemulsion stability was checked at 60ºC. Figure 4.1 presents the evolution of the light backscattered from the miniemulsions over four hours.

It can be observed that the PFDA miniemulsion was stable for the whole period of time (no change in backscattered light) whereas those miniemulsions containing the highest amounts of 2EHA showed some degradation. As was explained in Chapter 3, this was due to the higher water solubility of the 2EHA. However, droplets did not have time to degrade in the reactor since the polymerization was very fast (Figure 4.2) due to the high propagation rate of the acrylates[2].

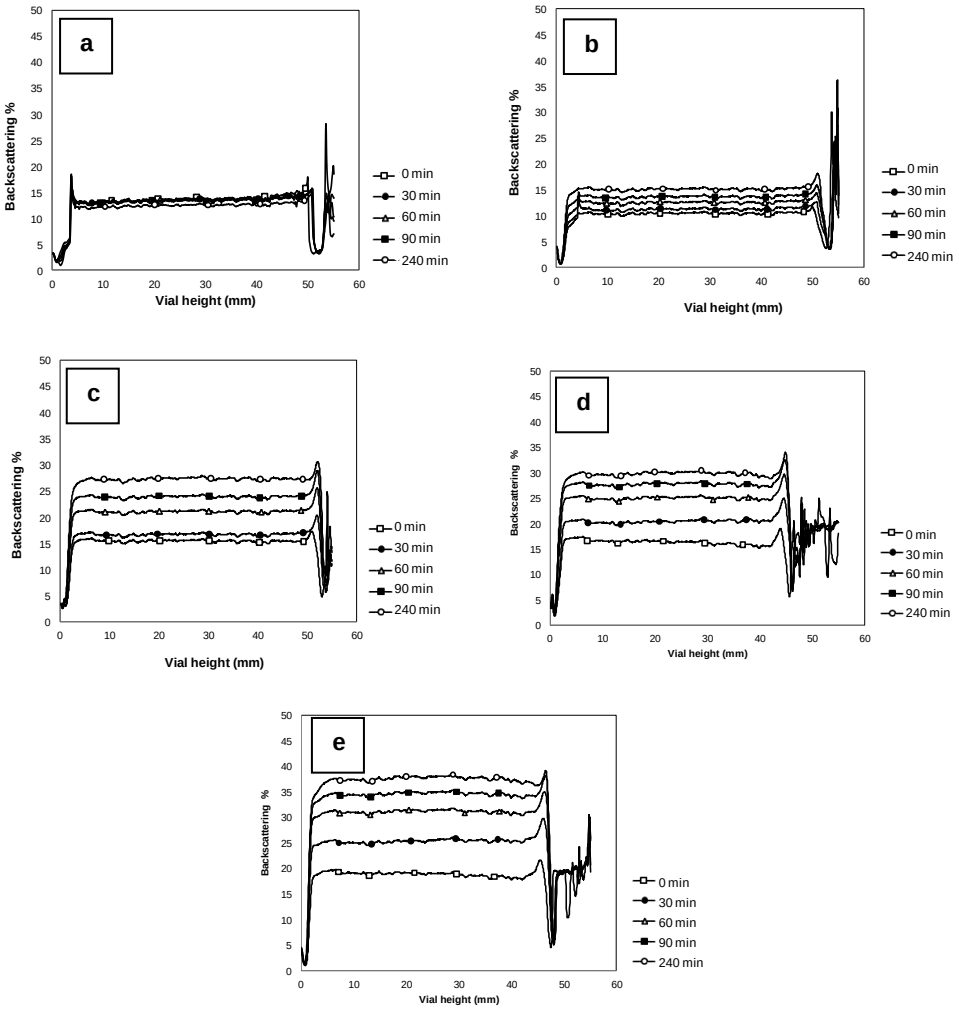

Figure 4.1. Evolution of the light backscattering profiles at 60ºC for the miniemulsions: a) PFDA homopolymer, b) 90/10 (PFDA/2EHA) copolymer, c) 82/18 (PFDA/2EHA) copolymer, d) 80/20 (PFDA/2EHA) copolymer, e) 75/25 (PFDA/2EHA) copolymer. In the abscissa, 0 is the bottom of the miniemulsion and the top is close to 50.

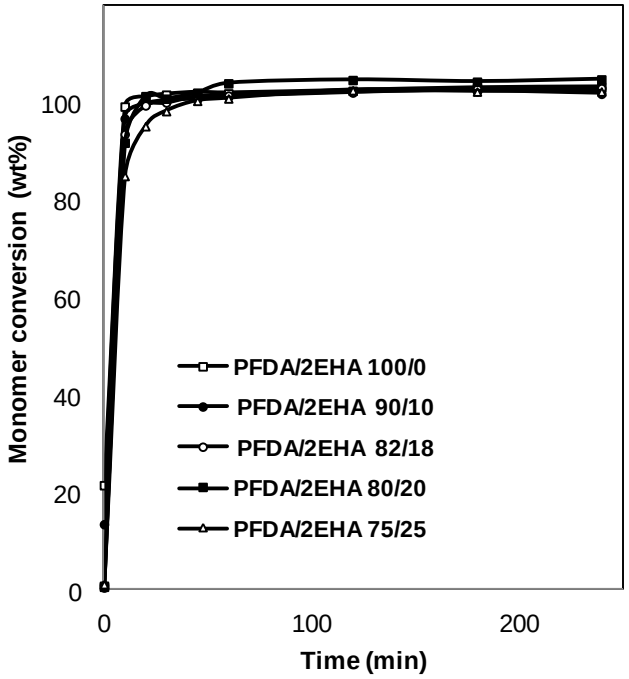

Figure 4.2. Evolution of the conversion for the different reactions.

The thermal transitions of the polymers were analyzed and the DSC thermograms are presented in Figure 4.3. All of them presented some crystallinity (Xc) with melting temperatures (Tm) that decreased with the 2EHA content.

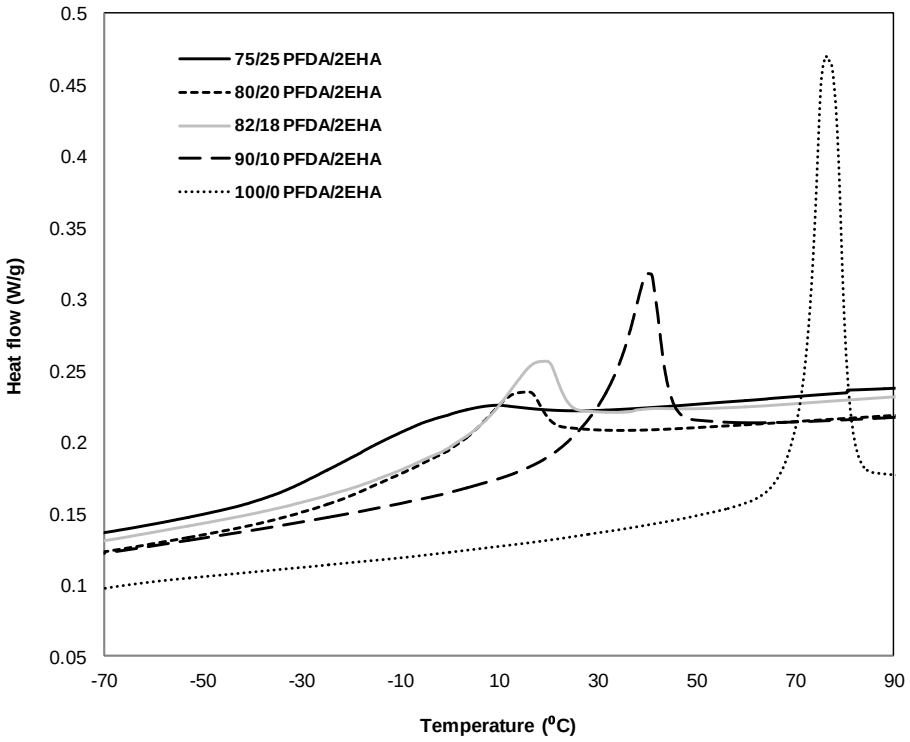

Figure 4.3. DSC thermograms of the polymers synthesized. (Exo Down)

The Tgs of the amorphous part of the polymers could not be determined from the data in Figure 4.3. The big the melting peaks that are obtained in these systems make the observation of the Tg transitions very complicated. Therefore, a different approach was used. A completely amorphous copolymer of PFDA and PFHA (1H,1H,2H,2H-perfluorohexyl acrylate) in a 75/25 wt/wt ratio was synthesized and its Tg measured (Tg ≈ -2ºC). Then, the Tg of poly(PFHA) was determined from the DSC of its homopolymer (Tg ≈ -26ºC). Finally, the Tg of poly(PFDA) was determined from these data using the Fox equation[3,4] (Equation 4.1) where x

represents the weight fraction of each component in the mixture. Figure 4.4 represents the DSC thermograms for the PFHA homopolymer and for the PFDA/PFHA amorphous copolymer.

$$\frac{1}{T_g} = \frac{x_1}{T_{g,1}} + \frac{x_2}{T_{g,2}} \quad \textbf{(4.1)}$$

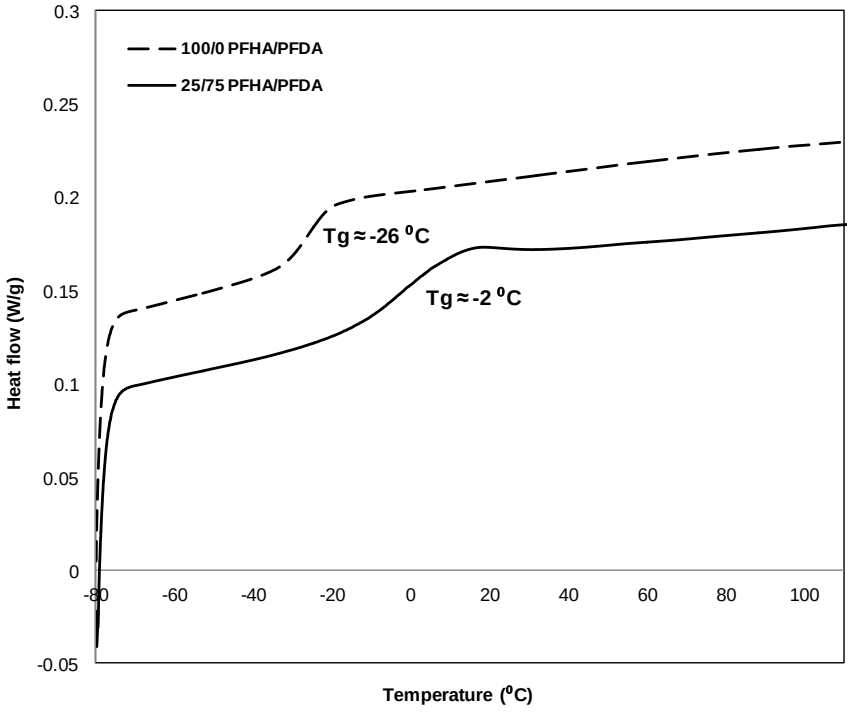

Figure 4.4. DSC thermograms of the PFDA/PFHA copolymer (75/25 wt/wt) and the PFHA homopolymer. (Exo Down)

The Tg of the poly(PFDA) was estimated to be 7ºC. As the Tg of 2EHA is -50 ºC[5] , the Tg of the amorphous PFDA-2EHA copolymers was for all of them lower than the casting

temperature. Therefore for this system particle deformation and interdiffusion was controlled by the Tm.

Film formation was theoretically analyzed by Routh and Russell[6]. They predicted that the regimes for the deformation mechanisms of the polymer particles depend on the relative rates of water evaporation, particle collapse and diffusion rate of the particles within the wet film. When the water evaporation rate is faster than the rate of diffusion of the particles in the wet film, the particles are trapped by the receding water front and accumulate at the air-film interface. For relatively hard polymers, i.e. polymers with a Tg/Tm in the order or higher than the casting temperature, the particles accumulated at the interface will not collapse and form a porous structure that allows evaporation of the rest of water. However, for softer polymer particles, the particles may collapse forming a continuous polymer film (skin) at the air-film interface. According to Routh and Russell[6] this occurs when the rate for particle collapse is of the order or higher than the evaporation rate. Therefore, in order to form skin, the rate of evaporation should be faster than the rate of particle diffusion and similar or slower than the rate of particle coalescence.

There are several ways in which these rates can be modified. Thus, the rate of diffusion of the particles can be increased by decreasing the particle size, the solids content and the viscosity of the continuous medium. Water evaporation can be accelerated by increasing the temperature and decreasing the relative humidity. The rate of particle coalescence increases as the size of the particles and the Tg/Tm of the polymer decreases as well as when the temperature increases. Among all these possibilities, in this work, the casting temperature and the Tg/Tm of the copolymer were chosen as variables to demonstrate the proof of concept.

Films were cast at 23ºC and 90ºC using 55% relative humidity. On the other hand, the Tg/Tm of the copolymer was controlled by means of its composition, which was varied from PFDA/2EHA = 75/25 wt/wt to 100/0 wt/wt (Table 4.1).

Figure 4.5 presents the films obtained at 23ºC. It can be seen that coherent and transparent films were formed for latexes containing 2EHA contents higher than 18 wt%. However, as was discussed in Chapter 3 (Figures 3.4 and 3.5), latexes with 2EHA contents lower than 18 wt% were too hard to form films at ambient temperature and therefore for the PFDA homopolymer and the 90/10 copolymer the crystalline domains of PFDA hindered the formation of a good film and a porous weak film was obtained. The whiteness of the film is a fingerprint of the presence of pores that resulted from the lack of particle deformation and coalescence during film formation as it can be observed in the SEM image of the PFDA homopolymer (Figure 4.5). The contact angles of the films are given in Figure 4.6. It can be seen that the higher contact angles corresponded to the films cast from the PFDA homopolymer because of the higher hydrophobicity of the polymer and the roughness of the porous structure of the film caused by the hard particles that did not deform at the casting temperature. Contact angle decreased increasing the 2EHA content until 18 wt%, because the polymer was more hydrophilic and the film less rough. Surprisingly, the films prepared with higher amounts of 2EHA led to an increase in the contact angle. The presence of wrinkles in the 75/25 and the 80/20 films was the reason for the higher contact angle as compared with the 82/18 film. The formation of these wrinkles is discussed below.

PFDA/2EHA(wt/wt)	FILMS CAST AT 23°C, 55% RELATIVE HUMIDITY
75/25	
80/20	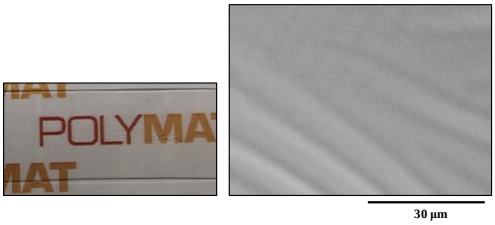
82/18	
90/10	
100/0	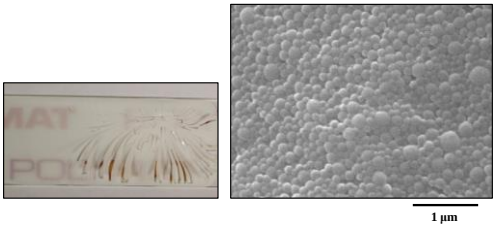

Figure 4.5. Films cast at 23ºC and 55% relative humidity

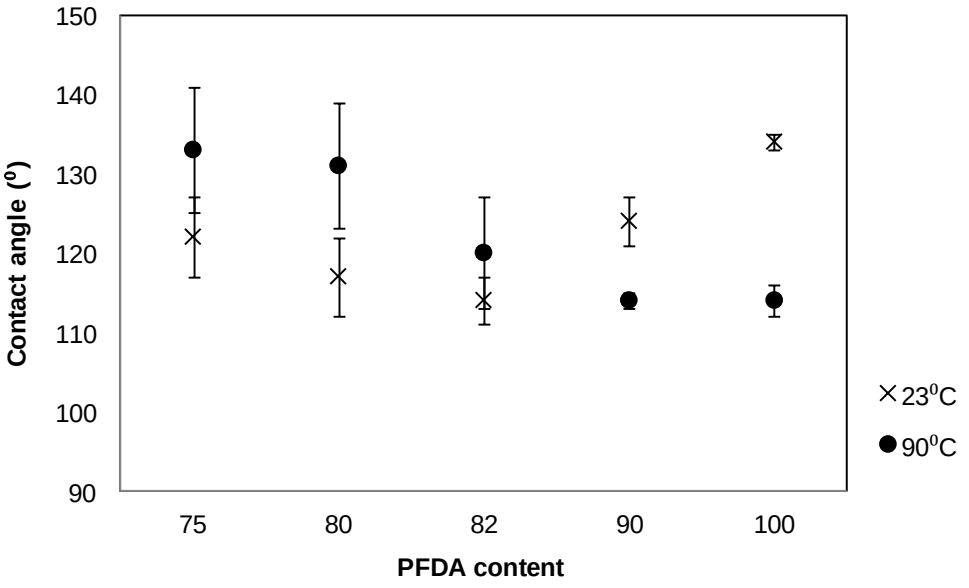

Figure 4.6. Effect of the copolymer composition and casting conditions on the contact angle.

Figure 4.7 presents the SEM micrographs and pictures of the films obtained at 90ºC. In all cases, coherent films were obtained because the casting temperature was higher than the melting temperature of the polymers. It can be seen that polymer composition strongly affected the topography of the film surface. Wrinkled surfaces were obtained for the 82/18, 80/20 and 75/25 latexes, whereas flat surfaces were produced with higher PFDA contents. The peak to valley distance for the 75/25 latex was 1.5-2 μm as estimated from the SEM images of the cracks generated in the film when it was detached from a glass substrate by using liquid nitrogen (Figure 4.8).

PFDA/2EHA (wt/wt)	FILMS CAST AT 90°C, 55% RELATIVE HUMIDITY
75/25	
80/20	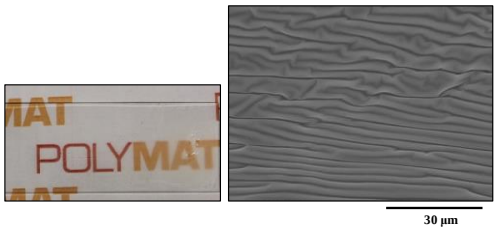
82/18	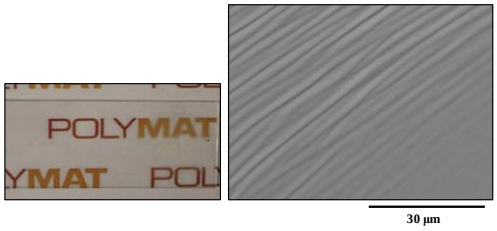
90/10	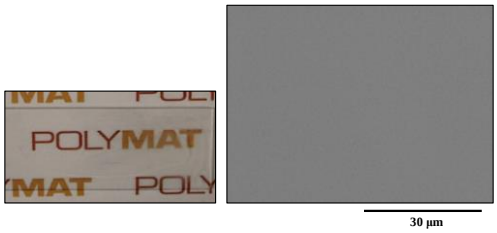
100/0	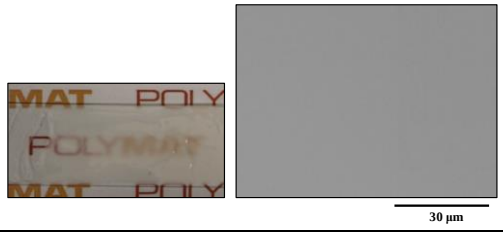

Figure 4.7. Films cast at 90ºC and 55% relative humidity.

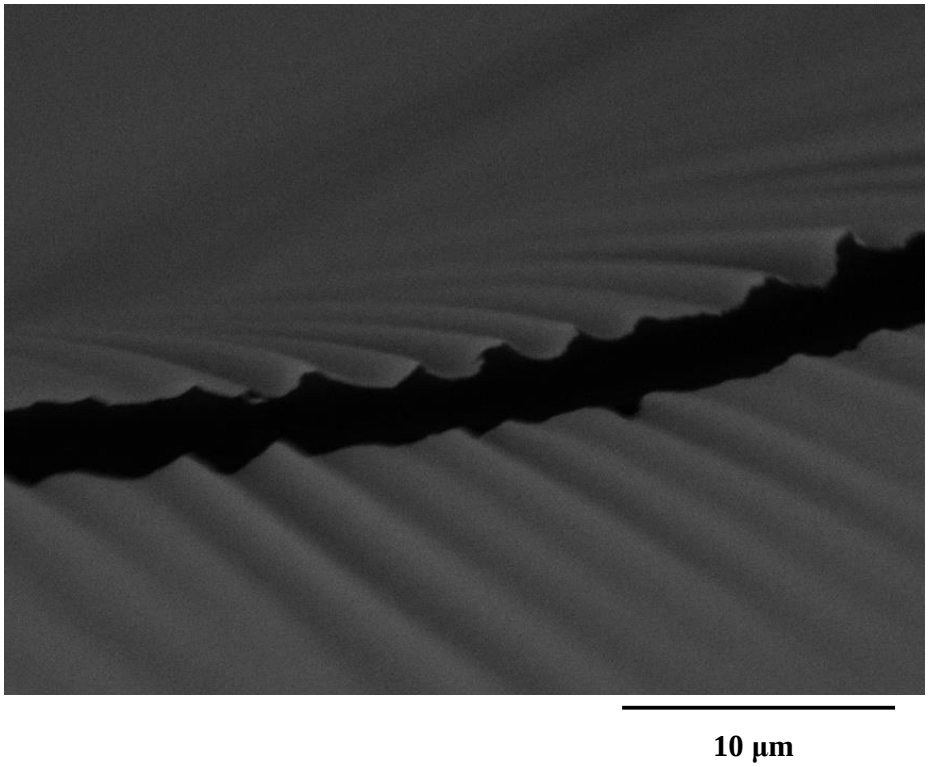

Figure 4.8. SEM micrograph of a crack generated in the 75/25 film cast at 90ºC and 55% relative humidity, when it was detached from a glass substrate by using liquid nitrogen.

The reason for these results is as follows. In all cases, at the beginning of the film formation process, the rate of evaporation was faster than the rate of diffusion of the polymer particles, and therefore polymer particles concentrated at the water-air interface. For the softer polymers, the rate of particle coalescence was similar or faster than the rate of evaporation and particle coalescence formed a polymer skin on top of the drying film. This led to the formation

of a bilayer structure: a soft polymer film on top of an aqueous dispersion of polymer particles. The mismatch between the mechanical properties of the two layers combined with the decrease in volume of the lower layer caused by the evaporation of water resulted in the formation of wrinkles at the film surface. Harder polymer particles (i.e. particles with a higher PFDA content) did not deform rapidly and hence they were not able to form a skin at the surface of the drying film before the majority of the water evaporates. Consequently there was no formation of the bilayer structure and rather flat films were formed through capillary, receding water front or moist sintering particle deformation mechanisms[6]. Figure 4.6 shows that for the latexes cast at 90^0C, the water contact angle was maximum for the latexes that led to wrinkled films even though they had the lowest fluoropolymer content (75 wt% and 80 wt% of PFDA). Thus, the 75/25 latex dried at 90ºC reached a contact angle of 133º.

4.4. Conclusions

This chapter deals with the challenge of producing in a cost effective and environmentally friendly manner highly hydrophobic, cohesive and non-porous coatings applicable to large and irregular surfaces. It is shown that this goal can be achieved by manipulating the film formation process in order to fine tune the texture of the surface of waterborne coatings. Waterborne dispersions of copolymers of 1H, 1H, 2H, 2H-perfluorodecyl acrylate and 2-ethylhexyl acrylate were chosen as a case study. The Tg of the copolymer can be easily tuned by modifying the monomer ratio. In Chapter 3, it was observed that the film forming copolymer PFDA/2EHA of 82/18 composition presented a contact angle of 114º when

the film was cast at 23ºC. In order to increase this value, roughness of the surface of the films cast from these dispersions was enhanced by creating wrinkles, which are naturally formed during film formation when the following conditions are met: 1) the rate of water evaporation is high enough to make the velocity of the receding water front faster than the rate of diffusion of the polymer particles in the wet film, and 2) the rate of coalescence of the particles is similar or faster than the rate of evaporation. Under these conditions, a polymer skin is formed at the film-air interface before the interior of the film becomes dry. The mechanical mismatch between the surface of the film and its interior leads to the formation of wrinkles when the film dries. Among the different ways in which these rates can be modified, in this work, temperature and hardness of the polymer were chosen to demonstrate the proof of concept. This allowed the formation of transparent films with a wrinkled surface that had a contact angle of 133º, which is a substantial increase with respect to the film cast under standard conditions.

4.5. References

(1) Keddie, J. L.; Routh, A. F. *Fundamentals of Latex Film Formation: Processes and Properties*; **2010**.

(2) Asua, J. M.; Beuermaann, S.; Buback, M.; Castignolles, P.; Charleux, B.; Gilbert, R.; Hutchinson, R. A.; Leiza, J. R.; Nikitin, A. N.; Vairon, J.-P.; van Herk, A. M.; Critically Evaluated Rate Coefficients for Free-Radical Polymerization. Propagation Rate Coefficient for Butyl Acrylate. *Macromol. Chem. Phys.* **2004**, *205*, 2151–2160.

(3) Fox, T. G. The Influence of Diluent and of Copolymer Composition on the Glass Temperature of a Polymer System. *Bull. Am. Phys. Soc.* **1956**, *1*, 123.

(4) Brostow, W.; Chiu, R.; Kalogeras, I. M.; Vassilikou-Dova, A. Prediction of Glass Transition Temperatures: Binary Blends and Copolymers. *Mater. Lett.* **2008**, *62*, 3152–3155.

(5) Brandrup, J.; Immergut, E. H.; Grulke, E. A. Polymer Handbook; **1999**; pp VI – 200.

(6) Routh, A. F.; Russel, W. B. Deformation Mechanisms during Latex Film Formation: Experimental Evidence. *Ind. Eng. Chem. Res.* **2001**, *40*, 4302–4308.

Chapter 5. From fractal aggregation to superhydrophobic coatings

5.1. Introduction

In Chapters 3 and 4, the topography of the surface of the films cast from waterborne polymer dispersions was modified by forming wrinkles and by taking advantage of the open time during film formation. However, the maximum water contact angle for wrinkled films was 133º. In the open-time strategy, a film forming latex is cast first and during the open time of this film, a hard and hydrophobic latex is applied. This second latex blends with the first one, but its polymer particles concentrate near the surface of the film leading to a rough surface mainly covered by the hard and hydrophobic particles of the second latex. By using a second latex of large fluoropolymer particles (750 nm) the contact angle obtained was 137º. This strategy has the advantage that can be applied at ambient temperature, but the topography of the film surface was not enough to provide superhydrophobicity.

A way to increase the roughness of the final film would be to have a dispersion of colloidal fractals as second latex. The term fractal, first coined by Mandelbrot[1], refers to objects that exhibit self-similarity over an infinite range of length scales[2]. However, for real fractals self-similarity is restricted to a limited number of scales. Fractal surfaces have huge values of the roughness factor, r (ratio of the real area to the projected area), and hence lead to superhydrophobic surfaces[3,4].

Colloidal fractals can be produced by aggregation of primary particles. The field has been recently reviewed[5]. Fractals are characterized by the fractal dimension of the aggregates, df, that varies from df=1 (linear aggregates) to 3 (spherical aggregates). The aggregation

mechanism strongly affects the fractal dimension. Open clusters are formed through the so-called diffusion limited cluster aggregation mechanism (DLCA) which occurs when each contact between particles leads to aggregation, namely there is no repulsion. For stabilized colloids, several contacts are needed before aggregation occurs. This mechanism is called reaction-limited cluster aggregation (RLCA) and leads to relatively compact clusters. It has been reported that df increases with the stability of the colloid[6] and the initial concentration of primary particles (initially occupied volume fraction, $\emptyset_0$)[7]. On the other hand, df decreases with the size of the primary particles[8] and the polydispersity of the primary particles[9].

In the present case, the fractal aggregates should meet several conflicting requirements.

- Mechanical strength as they are intended to form the surface of the coating. Therefore, relatively compact aggregates should be aimed.
- High solids content to minimize the amount of water added to the film. The solids content is limited by the high viscosity of the fractal aggregates.
- Made out of a hydrophobic polymer. This leads to miniemulsion polymerization, which yields to broad particle size distributions, which tend to form open aggregates.

Often fractal aggregates are formed by destabilization of previously formed colloidal dispersions[10–16]. For the case of polymer dispersions this involves two stages: polymerization and destabilization. In this chapter, formation of fractal aggregates during the miniemulsion polymerization was attempted because this substantially reduces cost and operation time. In order to achieve this goal, the miniemulsion polymerization should be carried out near the

stability limit and this is expected to yield large and polydispersed latexes that according to previous works[8,9] may lead to open and therefore, weak aggregates. This effect was compensated increasing the solids content. Additionally, the incorporation of this polymer latex in a dual coating strategy taking advantage of the open-time of waterborne coatings was explored in an attempt to achieve the formation of mechanically strong superhydrophobic coatings from waterborne polymer dispersions.

5.2. Experimental

5.2.1. Materials

In this work, 1H, 1H, 2H, 2H-perfluorodecyl acrylate (PFDA) supplied by Interchim was used as monomer. Disponil AFX 4060 (modified ethoxylated fattyalcohol) from BASF was used as surfactant (non ionic). The polymeric ionic liquid poly(1-vinyl-3-ethylimidazolium bromide) (Poly(ViEtIm^{+}Br^{-})[17], Mw of 20000 g/mol) was also used as stabilizer. As initiators, the redox pair composed by tert-butyl hydroperoxide (TBHP, Aldrich) and FF7 (Brüggemann Chemical, Heilbronn) and the oil soluble thermal initiator AIBN were used.

5.2.2. Synthesis of the waterborne dispersions

For the open-time strategy, both a film forming and a fractal aggregated hard latex are needed. A film forming latex was synthesized using the formulation given in Table 5.1 (Latex 1). Latex 1 was a methyl methacrylate/ butyl acrylate/ methacrylic acid (MMA/BA/MAA) copolymer produced by seeded semicontinuous emulsion polymerization[18]. The seed was

synthesized by semicontinuous emulsion polymerization using the formulation in Table 5.2. An anionic surfactant (Dowfax 2A1) was used.

Table 5.1. Formulation used to synthesize Latex 1 (dp=318 nm, S.C.=61.2%)

Component	***Initial charge (g)***	***Stream 1 (g)***
Seed	*19.83*	---
MMA	*1*	*175.74*
BA	*1*	*175.74*
MAA	---	*3.57*
Water	*135.504*	*80.466* [a]
KPS	*1.79*	---
Dowfax 2A1 [b]	---	*5.36*

[a] added water + water coming from the surfactant solution

[b] active matter

Table 5.2. Formulation for the seed latex (dp=64 nm, S.C. = 14.8%)

Component	***Initial charge (g)***	***Stream 1 (g)***
MMA	---	*44.55*
BA	---	*44.55*
MAA	---	*0.9*
Water [a]	*507.1*	---
KPS	*0.45*	---
$NaHCO_3$	*0.14*	---
Ammonia [b]	*0.9*	---
Dowfax 2A1 [c]	*0.9*	---

[a] added water + water coming from the surfactant solution

[b] 25% aqueous solution

[c] active matter

The fractal aggregated hard latex was a PFDA homopolymer synthesized by batch miniemulsion polymerization. Different homopolymers were synthesized by changing the emulsifiers and initiators (Table 5.3). A non ionic surfactant (Disponil AFX 4060) which is less sensitive to water than the ionic ones was used. In addition, a polymeric ionic liquid (PIL) poly(1-vinyl-3-ethylimidazolium bromide) with a Mw ≈ 20000 g/mol was also used. Initiators yielding non-charged radicals (AIBN and TBHP/FF7) were used. AIBN is a thermal initiator that forms radicals in pairs within the droplets/particles and its efficiency is limited by the frequent termination between these radicals[19]. TBHP/FF7 forms tert-butoxyl radicals in the aqueous phase that as they are hydrophobic enter rapidly in the polymer particles. The concentration of the surfactants was varied to achieve aggregation of the polymer particles, but to avoid complete coagulation. The type of initiator was varied in an attempt to influence polymerization rate, which through the polymer content affects the stickiness of the polymer particles and hence the aggregation. The formulations for the different reactions are presented in Table 5.3.

The miniemulsions were sonified for 10 min (70% amplitude, 50% duty cycle) in a Branson Sonifier 450. In reaction E, where the redox pair TBHP/FF7 was used, the FF7 was incorporated to the aqueous phase and the TBHP was dissolved in water and fed to the reactor during the first hour of reaction. In the cases in which AIBN was used, the oil soluble initiator was dissolved in the fluorinated monomer.

The miniemulsion polymerizations were carried out in a 250 ml glass-jacketed reactor equipped with a reflux condenser, N_2 inlet, and a stainless steel turbine stirrer. Although the size of the aggregates is determined by the aggregation and breakage processes that are strongly affected by agitation[5], it was decided to maintain constant the agitation rate at 200 rpm

and control the aggregation through the surfactant and initiator systems. The systems were allowed to react during four hours at 40 ºC (TBHP/FF7) or 70 ºC (AIBN).

Table 5.3. Formulations used to obtain the fractal aggregated hard PFDA latex.

	Component	***A (wt %)***	***B (wt %)***	***C (wt %)***	***D (wt %)***	***E (wt %)***
Organic phase	*PFDA*	*20 wt %*	*20 wt %*	*20 wt %*	*20 wt %*	*20 wt %*
	AIBN [a]	*1 wt %*	*1 wt %*	*1 wt %*	*1 wt %*	----
Water phase	*Disponil AFX 4060* [a,b]	*1 wt %*	*0.8 wt %*	*0.5 wt %*	*0.5 wt %*	*0.5 wt %*
	PIL [a]	*0.5 wt %*	*0.5 wt %*	*0.5 wt %*	----	----
	FF7/TBHP [a]	----	----	----	----	*1.1 wt %/1.1 wt %*
	Water	*≈80 wt %*	*≈80 wt %*	*≈80 wt %*	*≈80 wt %*	*≈80 wt %* [c]

[a] based on the total weight of monomer

[b] active matter

[c] total amount of water including miniemulsion preparation and TBHP feeding.

5.2.3. Characterization

Scanning Electron Microscopy was used to characterize the size of the aggregates.

Monomer conversion was determined gravimetrically. Thermal transitions were analyzed by Differential Scanning Calorimetry (DSC, Q1000, TA Instruments). The heating rate used was 10 ºC /min over a temperature range from -20 to 120 ºC under nitrogen atmosphere.

Static water contact angles, contact angle hysteresis and sliding angles were measured in an OCA 20 Instrument (Dataphysics) equipped with an electronic tilting base. Films from the latexes were cast on glass substrates and dried under different conditions. In order to mimic the removal of the migrated surfactant by rain, films were immersed in water for 24 hours and dried again for two days. The measurement of the contact angle was done by placing 10 µl droplets of distilled water on the surface of the films. The values given are an average of twenty measurements per film. In order to measure the sliding angle, 10 µl droplets were placed on the film surfaces and the equipment was tilted gradually at a rate of 0.6 º/sec until the water droplet slides down the inclined plane. The contact angle hysteresis (CAH) is the difference between the advancing (θ_{adv}) and the receding (θ_{rec}) contact angles. Considering the case of a sessile drop, θ_{adv} was measured when additional liquid is added to the existing droplet, and θ_{rec}, when liquid was removed from the droplet. Experimentally, a 10 µl water droplet was initially placed on top of the films and then by pumping 5 extra µl into and out the water droplet the advancing and receding contact angles were measured. The oleophobicity of the films was also evaluated by measuring the contact angles of olive oil and hexadecane.

The appearance of the films was evaluated visually and by SEM microscopy. The roughness profiles of the films were extracted from the height images of the AFM micrographs of the samples. The software Nanoscope Analysis allows the characterization of roughness and the calculation of the Image RMS (also known as Rq) which is the root mean square average of height deviations taken from the mean image data plane as calculated with Equation 5.1. In this equation, Zi represents the height deviation from the mean to the i point and N is the number of data points. The roughness profiles presented represent one line of the AFM micrograph that is considered representative for the whole image while the RMS value is calculated for the whole area of the micrograph.

$$\mathbf{RMS} = \sqrt{\frac{(\mathbf{Z_i})^2}{\mathbf{N}}} \qquad \textbf{(5.1)}$$

To evaluate the drying kinetics of the films, the weight of the water loss during the drying was recorded. For this purpose, 120 μm wet thick films were casted onto a glass substrate (17 x 10 cm) and placed on a digital balance. The weight loss was recorded during the first hour of drying.

An optical technique based on Multispeckle Diffusing-Wave spectroscopy (MS-DWS) was used to study the film formation[20–22]. This technique is implemented into an Horus apparatus[23] which measures the fluctuation of the intensity of the light scattered by the mobility of the particles in the sample. The scattered light is detected by a video camera that displays an interference image, also called speckle image. The changes that the sample undergoes during film formation produces temporal fluctuations in the scattered light and therefore in the speckle image. The deformation speed of the speckle pattern due to the motion of scatterers

(particles, droplets, etc.) in the sample is defined as the speckle rate[24]. As the film progressively forms, the motion of the particles slows down due to an increase in film viscosity and consequently, the speckle deformation speed (speckle rate) decreases. Successive speckle images are acquired over time in order to quantify the deformation speed of the speckle patterns as a function of time. With this technique, the different steps of the film formation process: water evaporation, particle ordering, particle deformation and diffusion and coalescence can be observed and correlated to the time of drying. It is considered that the open time corresponds to the first two steps: water evaporation and particle ordering. 120 µm films were casted onto a glass substrate and the variation of the speckle rate was recorded as a function of the time. The measurements were carried out at 23ºC and 55% relative humidity.

The mechanical strength of the films was checked by means of a scrub resistance test performed in a washability equipment (Braive Instruments) as explained in Section 5.3.1 of this chapter. The experiments were performed using completely dry brushes and in the absence of any liquid media. The brushes pass over the surface several cycles. Each cycle comprises two passes over the surface.

The potential use of the films as icephobic coatings was studied through different experiments. Ice adhesion strength was characterized using a TA.HD plus texture analyzer equipment (Stable Micro Systems) in which an ice block was separated from the substrate by using a peel mode experiment. The effect of water vapour condensation on the surface of the film was studied by measuring the contact angle at different surface temperatures. Additionally, ice formation and accumulation was also studied by introducing samples of the films in the

freezer and pouring supercooled water onto the samples. These experiments are discussed in detail in Section 5.3.3 of this chapter.

5.3. Results and discussion

Figure 5.1 presents the SEM images of the films cast with PFDA latexes synthesized with AIBN and different concentrations of surfactant according to the formulations in Table 5.3. It can be seen that less aggregated polymer particles were obtained with 1 wt% of Disponil AFX 4060 and 0.5 wt% of PIL and that aggregates were formed when the concentration of Disponil was decreased to 0.5 wt% (maintaining 0.5 wt% of PIL). Massive coagulation occurred when only 0.5 wt% of Disponil was used. In order to assess if these levels of aggregation were enough to achieve superhydrophobicity, the water contact angles were measured. The data are reported in Figure 5.1 where it can be seen that the contact angle increases with aggregation, but the maximum contact angle achieved (142º) was below the threshold of superhydrophobicity. This indicated that the fractal aggregates were not large enough.

The coagulation observed when only 0.5 wt% of Disponil was used, led to a material formed by fused particles, suggesting that the aggregation occurred when the particles were soft, namely when they contained a substantial amount of monomer.

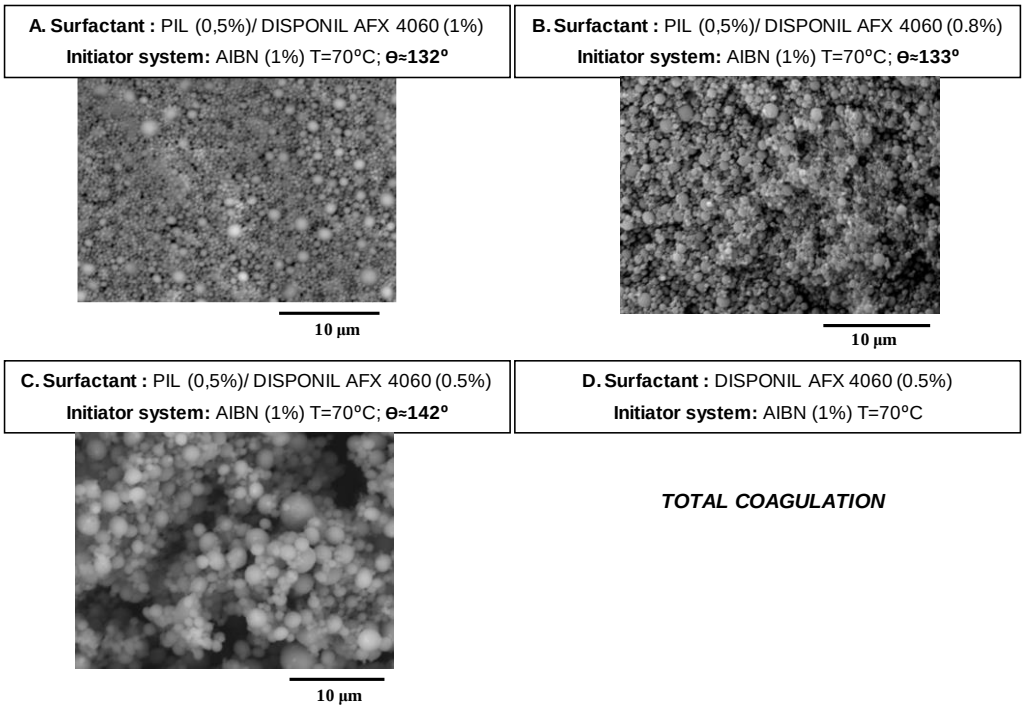

Figure 5.1. Effect of the surfactant system on the films cast from the PFDA latexes synthesized using AIBN as initiator.

Let us assume that for the highly hydrophobic monomer that was used, most of the droplets were nucleated and no mass transfer between droplets/particles occurred. Under these circumstances we can imagine that the system is ruled by the interplay between the kinetics of aggregation and the kinetics of polymerization. For a given aggregation kinetics, low polymerization rates will lead to coagulation of fused particles, whereas for faster polymerization rates the formation of fractal aggregates of hard particles is expected.

In order to check this idea, Run E (Table 5.3) was carried out using 0.5 wt% of Disponil and a redox initiator to accelerate the reaction. A highly viscous dispersion with no

macroscopic coagulum was obtained. Figure 5.2 compares the viscosity of this latex with that of a regular latex of higher solids content (40 wt% solids PFDA/2EHA copolymer, Latex 4, Chapter 3). It can be seen that even though Latex E had only 20 wt% of solids content, its viscosity was more than one order of magnitude higher than that of the regular latex with 40 wt% solids content. This strongly suggests that Latex E was a colloidal fractal. This is clearly shown in Figure 5.3 a, where the SEM image of the aggregated fractals is presented. It can be seen that relatively compact fractal aggregates formed by a broad distribution of large particles were obtained. This indicates that the solids content used (20 wt%, very high for the values usually employed to form colloidal fractals (< 10 wt%[5])) compensated the effect of the particle size distribution.

Figure 5.3 b presents a SEM image of the surface of the film cast from Latex E. Comparison with Figure 5.1 shows that the surface was rougher. This resulted in a water contact angle ($\Theta > 150^{o}$) which was in the superhydrophobic range.

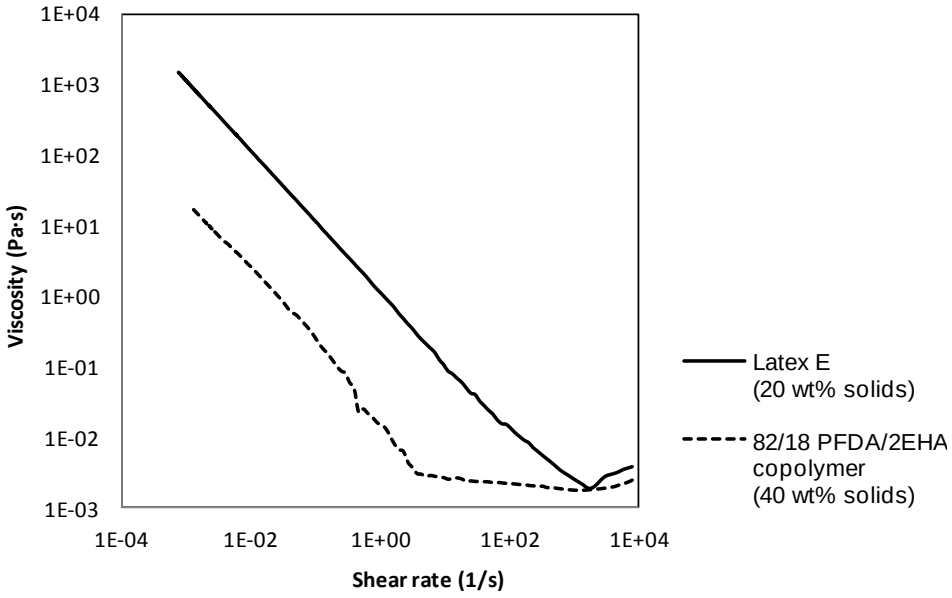

Figure 5.2. Viscosity as a function of the shear rate for latex E (20 wt% solids) and for a 82/18 PFDA/2EHA copolymer (40 wt% solids).

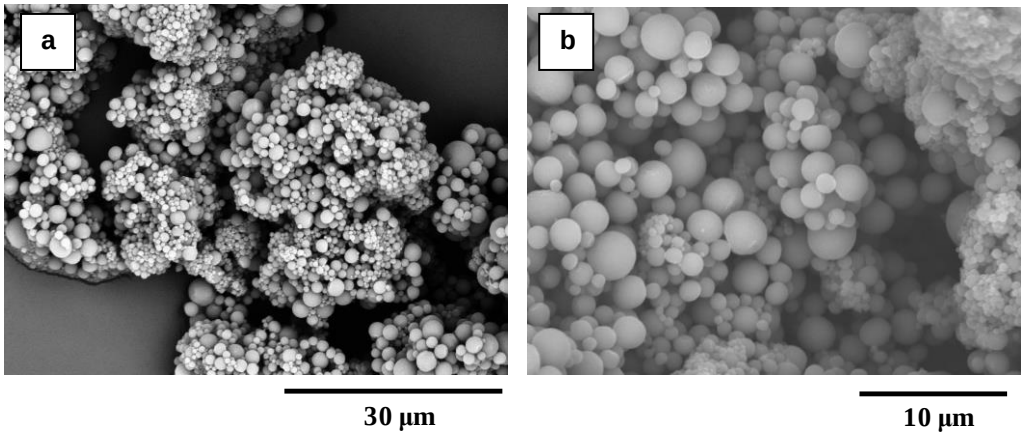

Figure 5.3. SEM images of a) the fractal aggregates and b) the film of Latex E.

When cast at ambient temperature, Latex E alone formed a porous film which was not useful for coatings. Although the main purpose of the synthesis of this latex was to use it as second stage of the open-time strategy, and it has the required characteristics for that usage, one wonders if the film can be consolidated by casting the latex at a temperature above the Tg/Tm of the polymer. The DSC thermogram presented in Figure 5.4 shows that the polymer is crystalline with a melting peak at 75-80ºC. Therefore, films were cast from Latex E between 77 and 85ºC.

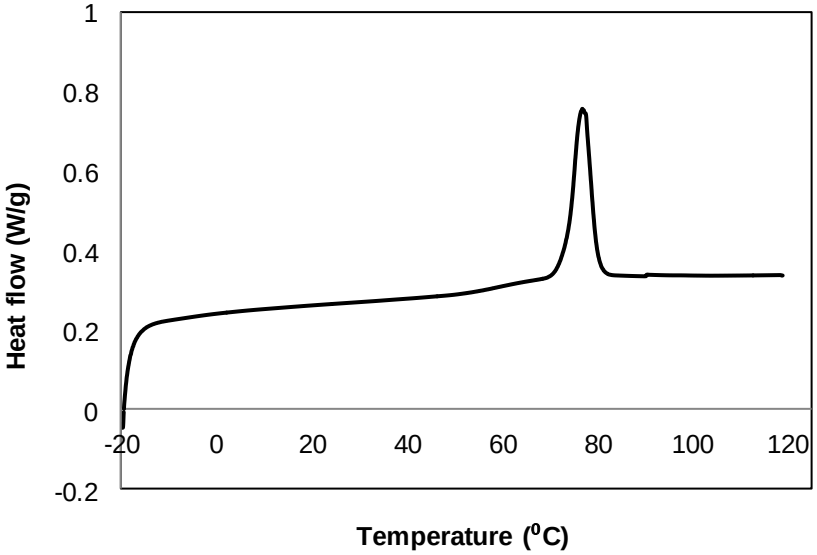

Figure 5.4. DSC thermogram for Latex E. (Exo Down)

Figure 5.5 shows a clear relationship between the temperature of drying and the film topography. When the drying temperature of the films was increased, the topography evolved from a highly rough film to a flat continuous and transparent coating. This phenomenon has an effect on the contact angle value. Figure 5.6 shows how the contact angle decreased as the

drying temperature increased, from values of θ >150º below the melting temperature, to values of θ ≈111º that correspond to the flat surface where the hydrophobicity was determined by the nature of the fluorinated material. The effect of the drying temperature on the roughness of the films is quantified in Figure 5.7 that presents the roughness profiles measured by AFM in Latex E films dried at ambient temperature and 90ºC. It can be observed that whereas RMS is 765 nm at 23ºC, it is only 4 nm at 90ºC.

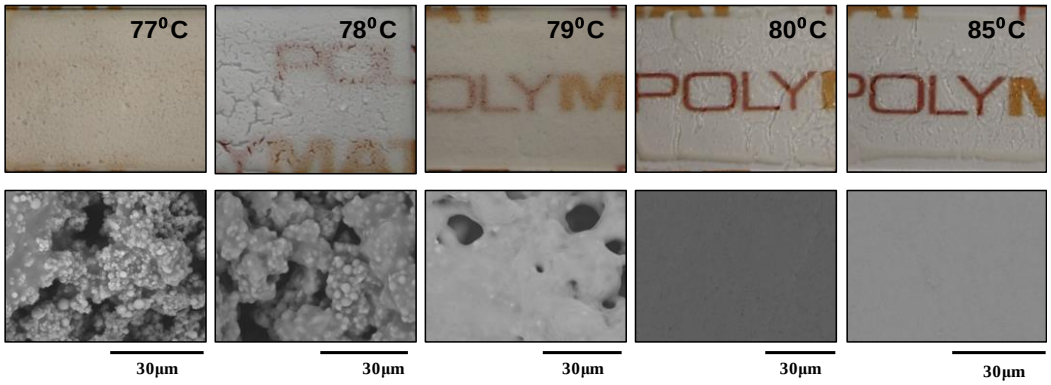

Figure 5.5. Film formation at different drying temperatures.

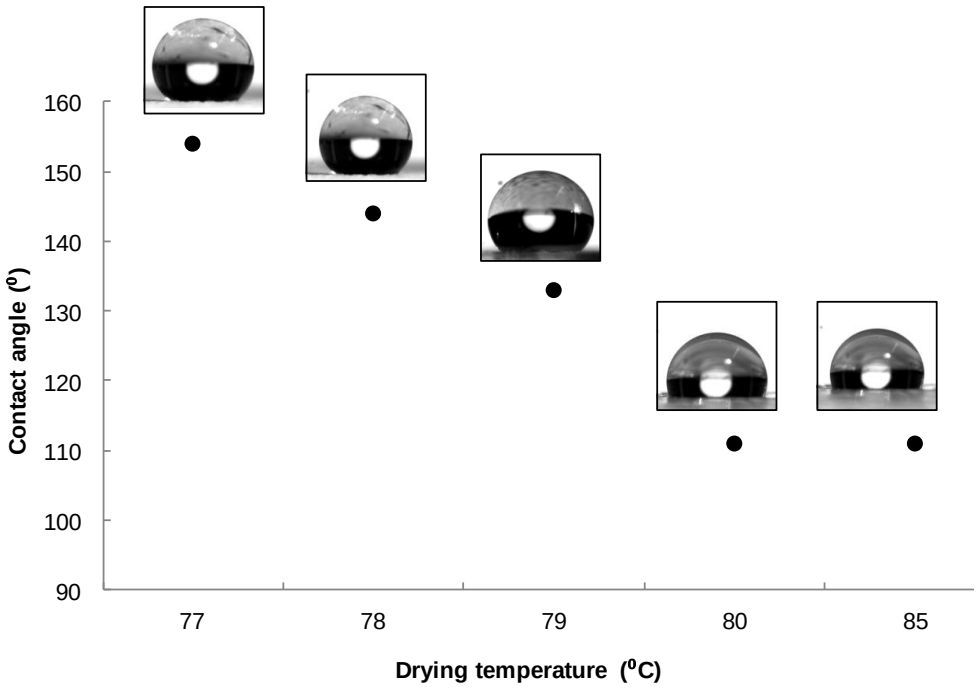

Figure 5.6. Contact angle as a function of the drying temperature.

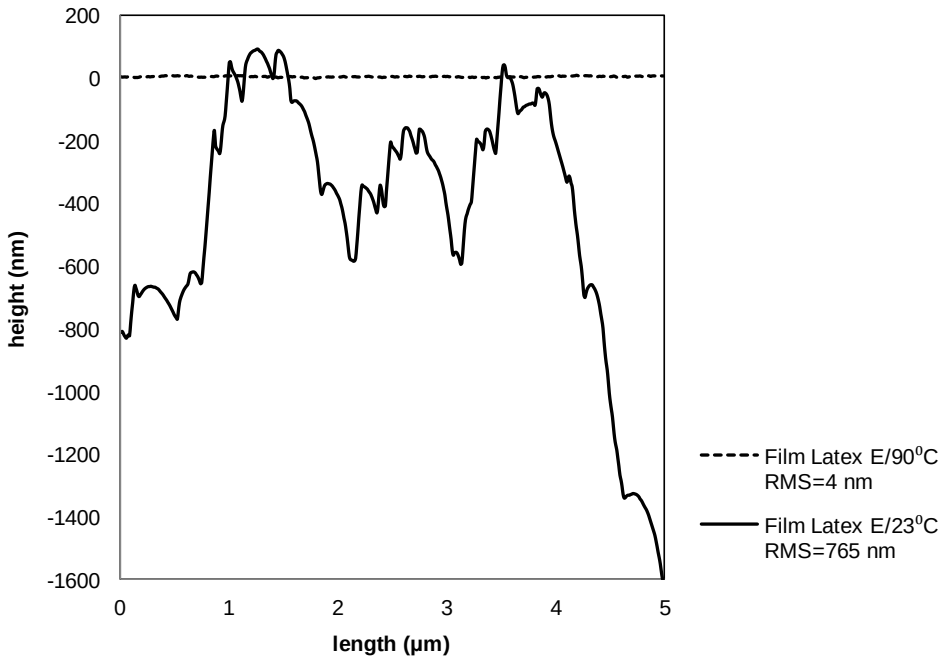

Figure 5.7. Roughness profile of the films formed from Latex E dried at ambient temperature and 90ºC. RMS values for each sample are included in the legend.

The open-time strategy was implemented by using Latex 1 (MMA/BA/MAA copolymer) as film forming latex and Latex E as hydrophobic latex. In order to implement the strategy, the film forming process of Latex 1 was first monitored by determining the rate of water loss by gravimetry and the mobility of the particles in the film by means of the Horus apparatus. The results are given in Figure 5.8. It can be seen that water evaporated continuously, but in terms of the mobility of the particles, the film formation can be divided into three stages. Stage I corresponds to the case in which the particles move relatively free in the film. This period finalized in about 3 minutes. At the end of this stage, the water content in the film was still around 30 wt%. A clear change in the mobility of the particles due to the reduction of water

present in the system determined the onset of the second stage (Stage II) in which interparticle interaction affected the motion of the particles and they rearrange and organize. During Stage II, the water content in the film decreased to a value of around 5 wt%. At the beginning of the particle deformation stage (Stage III), the speckle rate decreased sharply indicating a drastic reduction of the mobility of the particles inside the film. The little amount of water that is still present in the system corresponds to the one trapped in the voids between particles that exponentially disappeared as particles deformed completely. The open-time can be associated to Stage II. Therefore, Figure 5.8 provides the information needed to implement the open-time strategy.

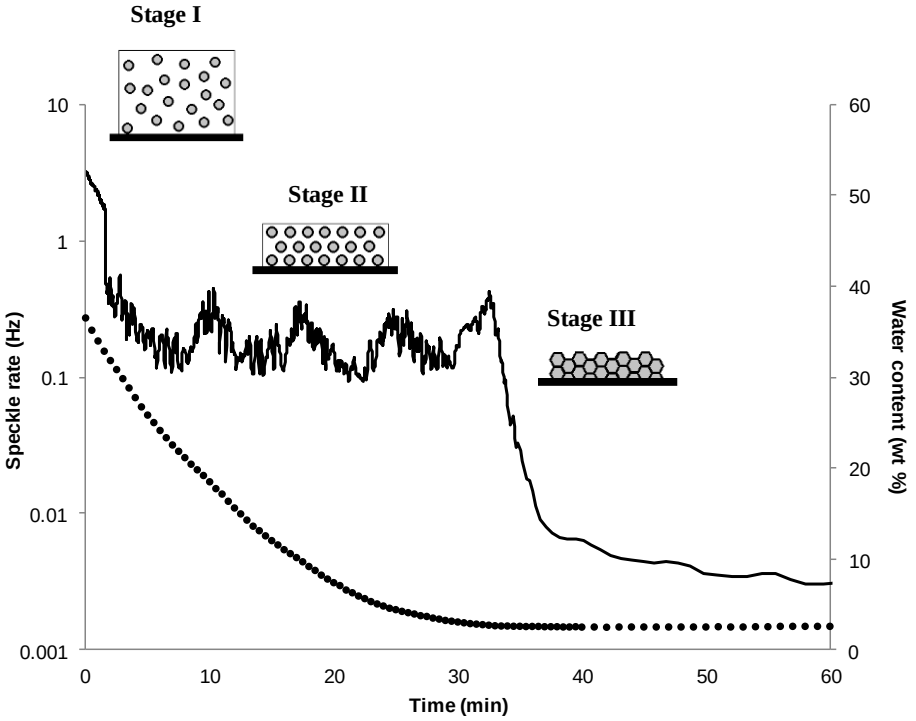

Figure 5.8. Water content (wt%) as a function of time (dotted line) and speckle rate variation with time (obtained from the Horus apparatus) for Latex 1.

A film of Latex 1 was cast and allowed to dry during 5 minutes. Then, Latex E was sprayed on the film during 60 seconds. The amount of polymer added was 4.35 mg/cm^2. In another experiment, this amount of polymer was added in two steps, the first one at 5 minutes (30 seconds of spraying) and the second one at 15 minutes (30 seconds of spraying). Once the films were dried, in order to improve the mechanical strength of the film, the samples were annealed at 78ºC during two hours in order to improve the penetration of the hard particles in the soft matrix and to slightly fuse the primary particles of Latex E. 78ºC was used because the hard particles started to melt above this temperature (see Figure 5.5) and it was well above the Tg of the soft polymer, which formed film at ambient temperature.

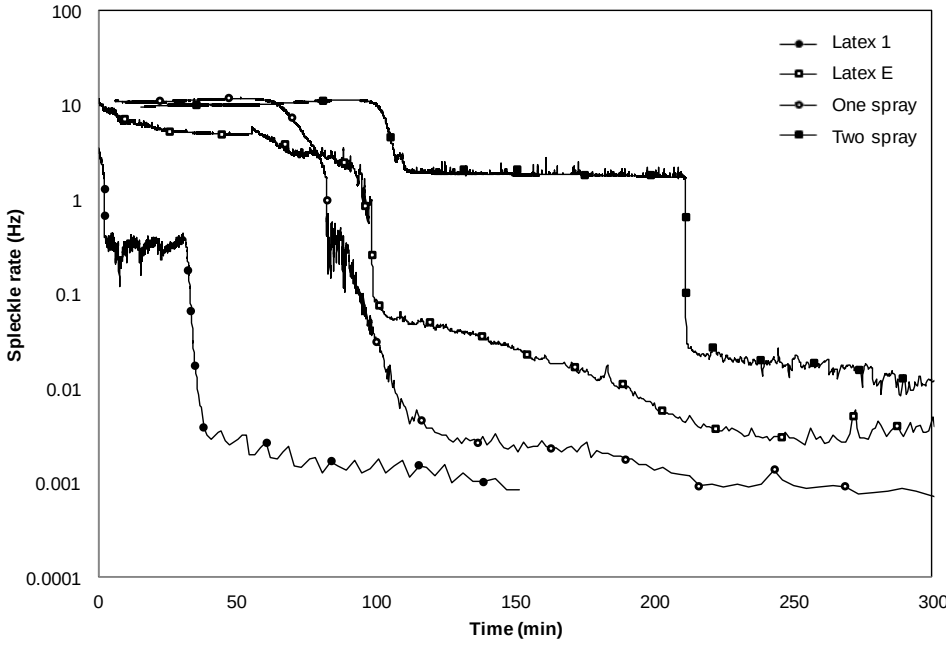

Figure 5.9. Speckle rate variation with time (obtained from the Horus apparatus).

Figure 5.9 shows the drying kinetics for four different films, including the high solids content latex (Latex 1) presented also in Figure 5.8, the PFDA latex (Latex E) and the films produced in “One step spray coating” and “Two step spray coating” procedures. For the sprayed films, the Horus measurement started just after the spraying stage and that is the reason why the curves do not start at time zero and they start at minutes 5 or 15 depending on the case. Latex E contained 80% of water in its formulation; therefore the drying process was much longer than for Latex 1 that only contained around 38% of water. Thus, when Latex E is sprayed onto Latex 1, the drying time was extended until all the water coming from the sprayed latex evaporated.

The films prepared using these procedures presented a translucent appearance (see Figure 5.10) due to the incorporation of large fractal aggregates on the top surface of the coating and they were mechanically consistent and of good quality.

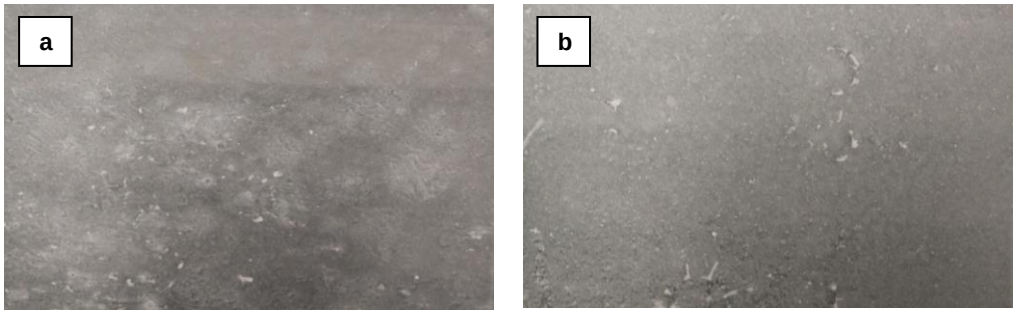

Figure 5.10. Films produced by “One step spray coating” (a) and “Two step spray coating” (b) procedures following the open-time strategy.

SEM micrographs of the top and bottom interfaces were taken from both films. Figure 5.11 shows that both surfaces are fully covered by a large number of hard particles (b.1 and b.2 micrographs). When lower magnification images are analyzed, aggregations of particles are observed (a.1 and a.2). These aggregations are more frequent in the film sprayed twice (image a.2). The presence of these aggregates on the top surface of the film may have an important effect on the wettability of the substrate due to the fact that they considerably increased the roughness profile. SEM images of the film-substrate interface (c.1 and c.2 micrographs) showed no evidence of sedimentation. However, the contour of some particles inserted in the film matrix can be identified indicating that during the drying process a fraction of the particles was able to penetrate into the softer layer of the film.

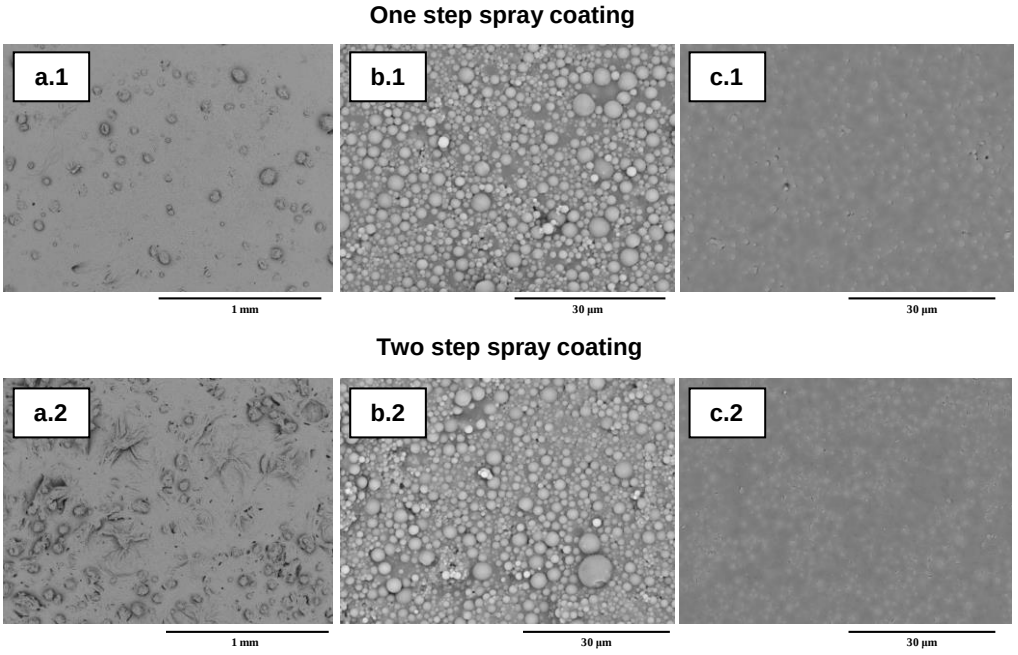

Figure 5.11. SEM micrographs of the films produced by one and two step spray coating techniques. a, b) Air-film interface, c) Film- substrate interface.

The contact angle of these surfaces was analyzed finding important differences between the spraying procedures. It is important to remark that the contact angle value of the MMA/BA/MAA film used as primer was 70º±1. Taking this into consideration, the improvements achieved in contact angle are remarkable. The contact angle value was higher for the film sprayed in two steps, reaching the superhydrophobic regime (θ >150º). In this case, it was difficult to deposit a 10 µl water droplet on top of the film. The probability of the water droplet deposition is the fraction of successful attempts as can be seen in Table 5.4. For the films sprayed in two steps only 28 % of the dispensed droplets stayed on top of the surface. In the rest of the cases, droplets stayed in the syringe because the force of adhesion between the water droplet and the syringe was higher that the force of adhesion between the water droplet and the film as it is shown in Figure 5.12. A sliding angle of 0º was attributed to this situation since the water cannot stay in a static position on top of the surface. In the 28% of the cases, when the water could be deposited on top of the surface, the sliding angle was measured reaching an average value of 27º. A representative value of the sliding angle of the complete surface would be an average between the points in which the droplet cannot be deposited (sliding angle equal to 0º) and the points in which the droplet can stay on top of the surface (average sliding angle of 27º). The average value of the whole surface was 7º (Table 5.4). Additionally, the one step spray coating technique gave surfaces which were highly hydrophobic and presented really low values of contact angle hysteresis, but they did not reach the superhydrophobic threshold.

Table 5.4. Wetting properties of the spray coated films.

Coating technique	Probability of water droplet deposition (%)	θ_{water}(º)	Sliding angle (º)	Contact angle hysteresis (º)
One step spray	100	138±2	>90	≈7
Two step spray	28	152±4	≈7	≈5

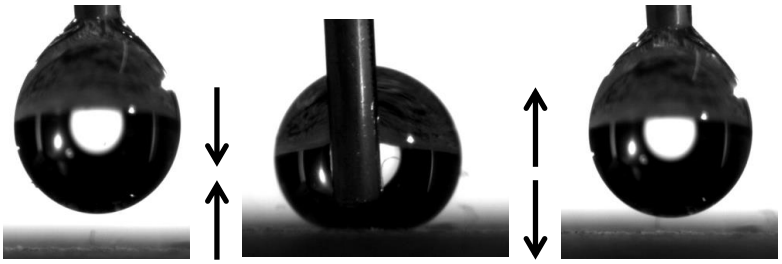

Figure 5.12. Representation of the superhydrophobic nature of the two step sprayed coating.

The superhydrophobic behavior of the two step sprayed surfaces can be attributed to the highly roughness profiles that are created by this technique. Figure 5.13 shows the roughness profiles of the two sprayed coatings and also that of the film formed from Latex 1. The surface sprayed twice is much rougher than the surface sprayed one time explaining the differences in contact angles. As expected, a flat film was obtained from Latex 1 at ambient temperature. These profiles are in agreement with the RMS values shown in the legend of Figure 5.13 extracted from the whole area of the image.

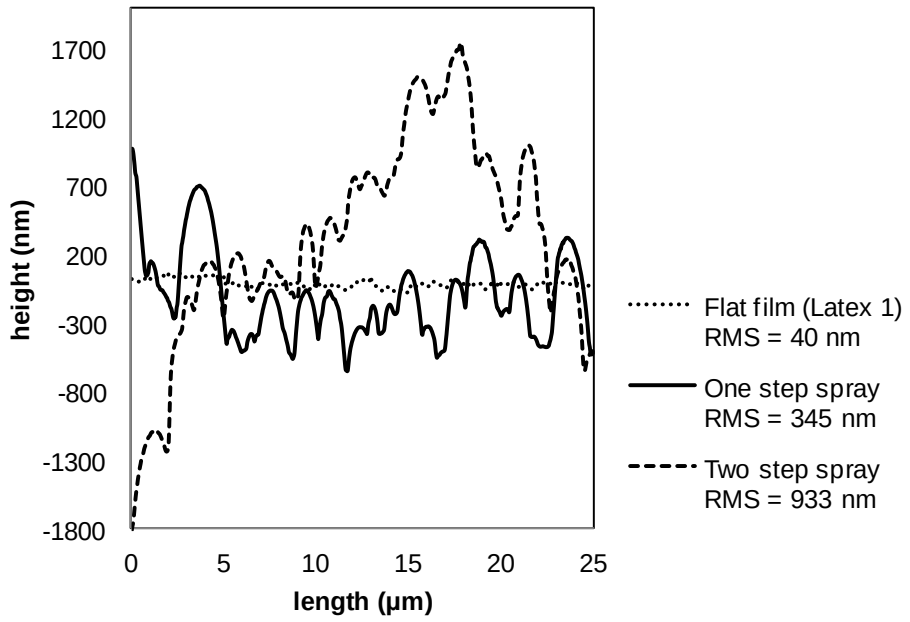

Figure 5.13. Roughness profile of the films formed from Latex 1 (flat surface) and from the one and two spraying procedures. RMS values for each sample are included in the legend.

5.3.1. Mechanical strength

One of the weak points of the superhydrophobic coatings is their usually low mechanical strength. If the particles are not incorporated into the film strong enough, they can be removed from the surface and the film loses its hydrophobic character. In order to evaluate how strong were the particles attached to the surface, different experiments were carried out. In a first experiment, a sharp blade (Figure 5.14,a) was passed five consecutive times on top of the film. In a second experiment, a scrub resistance test was performed (Figure 5.14,b). This test was

performed in complete dry conditions, without any liquid media. A dry wild boar hair brush (Figure 5.14,c, in accordance with DIN 53 778) was passed on top of each surface for 50 cycles (100 passes).

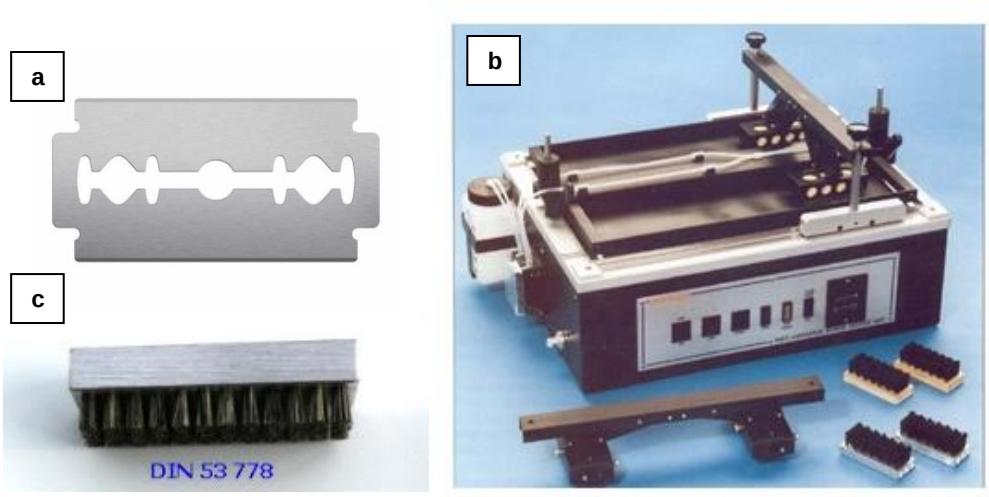

Figure 5.14. Sharp blade (a), scrub test equipment (b) for mechanical strength measurements and wild boar hair brush (c) used in the scrub resistance test.

After both experiments, the surfaces were evaluated visually, and by SEM and AFM microscopy and the water contact angles were measured. Figure 5.15 shows the aspect of each film after both experiments. Visually, the films did not show any significant damage as compared with the initial aspect shown in Figure 5.10.

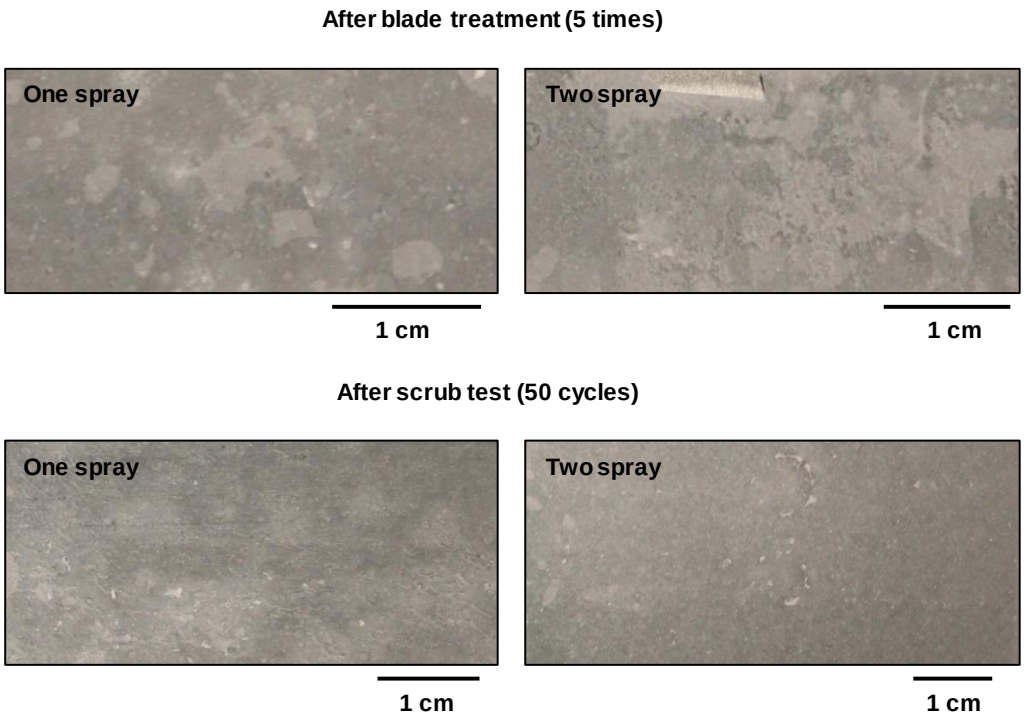

Figure 5.15. Images from the films after the different treatments.

SEM micrographs of both films show that passing a sharp blade on top of the surface five times did not produce an important damage on the surface. As can be observed in Figure 5.16, where the images of the samples before and after the treatment are presented, the base of the coatings remained covered with the hard particles and only the peaks of the big aggregates were partially damaged (Figure 5.16,d).

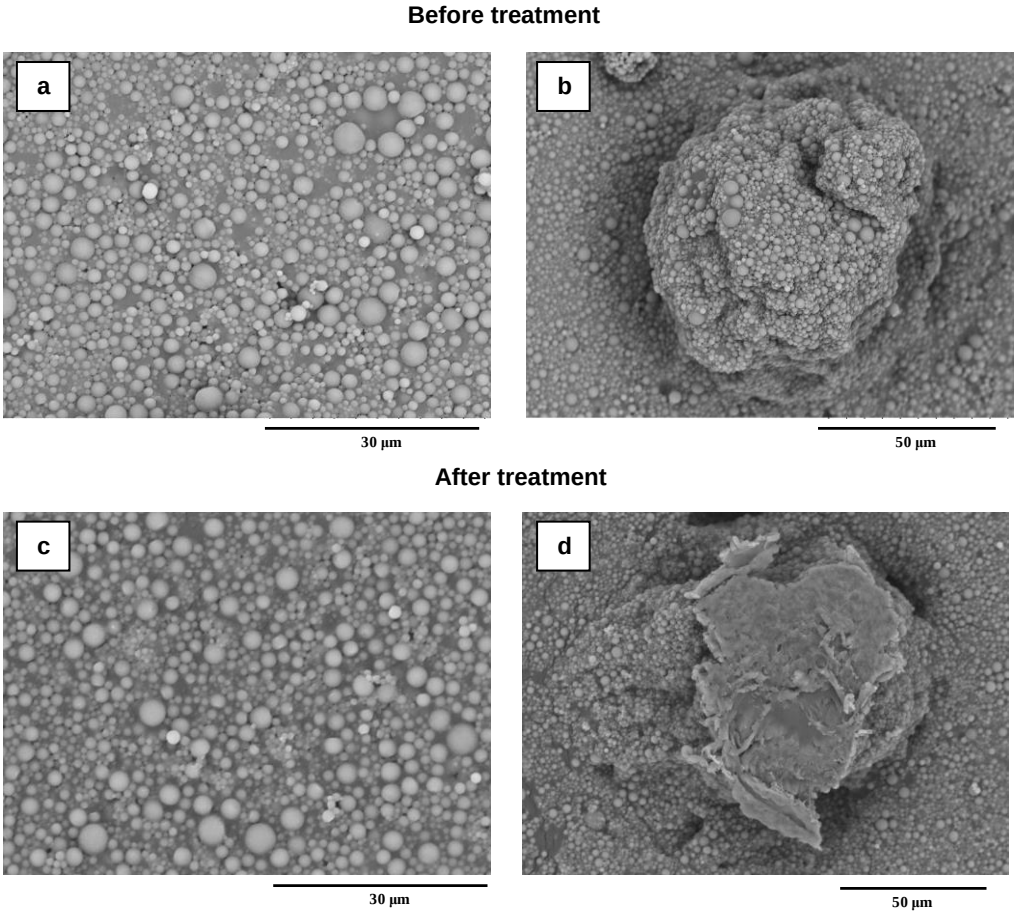

Figure 5.16. SEM micrographs of the films before and after passing a sharp blade five times a,c) One spray coating. b,d) Two spray coating.

The scrub test is much more aggressive and as can be observed in the SEM micrographs, the surface was more damaged (Figure 5.17). One spray coatings showed surfaces that were highly affected by the treatment (Figures 5.17, a and c). However, the surfaces sprayed twice showed better resistance to the scrub test (Figures 5.17, b and d). It

seems that the big aggregates were the ones seriously damaged. On the other hand, the small particles were less affected.

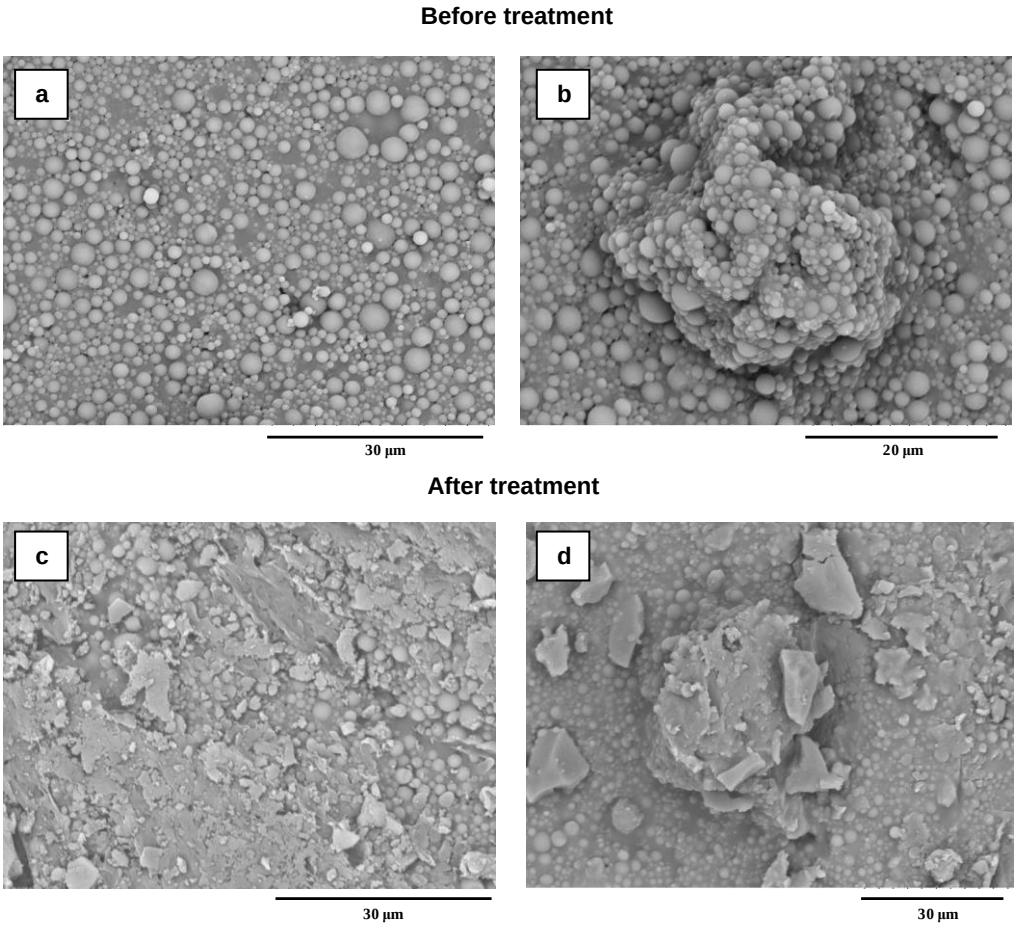

Figure 5.17. SEM micrographs of the films before and after scrub test. a,b) One spray coating. b,d) Two spray coating.

The roughness profiles were measured by AFM. Figure 5.18 shows that the roughness of the one spray coating was not substantially affected by the treatments, and the scrub test slightly increased the roughness. On the other hand, the roughness of the coating sprayed twice was substantially reduced by the treatments. This had an effect on the contact angles that were almost unaffected for the one step spray coating, but that were reduced for the two step coating (see Table 5.5). This reduction suggests that the large aggregates played a key role in achieving superhydrophobicity. In any case, it is remarkable that even when subjected to harsh treatments, the films retained a large fraction of their properties.

Table 5.5. Contact angles before and after the mechanical strength tests.

Coating technique	No post treatment	Blade (5 times)	Scrub test (50 cycles)
One step spray coating	138±2	138±1	136±1
Two step spray coating	152±4	145±4	140±3

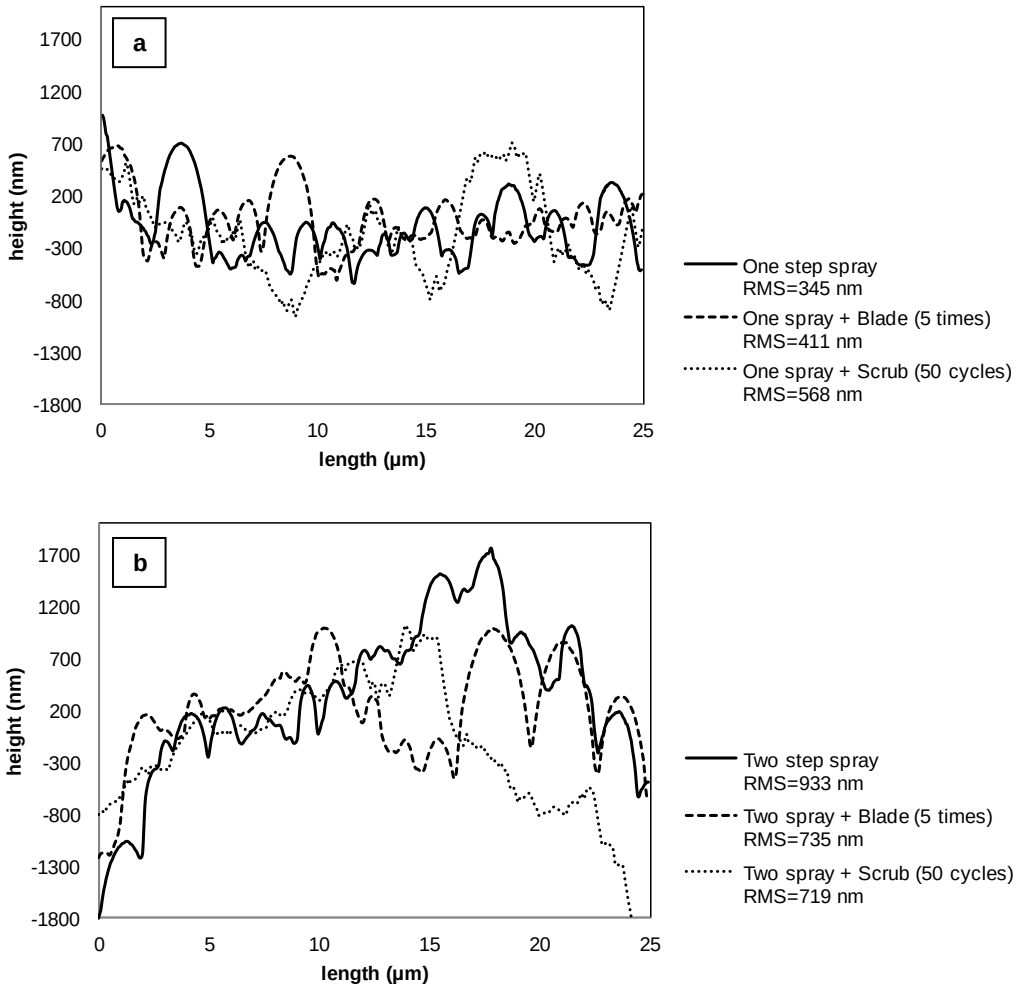

Figure 5.18. Roughness profiles from the sprayed films before and after the blade and scrub treatments. a) One spray coating, b) Two spray coating. RMS values for each sample are included in the legend.

5.3.2. Oleophobicity

An added value to superhydrophobicity is oil repellency or oleophobicity. Superhydrophobic surfaces are commonly wetted by oils or low surface tension liquids reducing their range of applications[25]. Consequently water and oil repellent surfaces are becoming very demanded in antifouling, anti-icing or anticontamination applications[26,27], the development of biomedical devices or fuel transportation[28]. Oils and organic liquids have considerably lower values of surface tension than that of water, therefore, to create oleophobic surfaces, the surface energy of the solid surface should be lower than that of the oil[29]. In this situation, it is more difficult to achieve high contact angles, and to reach the superoleophobic threshold ($\Theta > 150^{o}$) is extremely complicated. Indeed, calculations suggest that the creation of such materials would require lower surface energy than that of any known material and even, Lotus leaves which are well known for their extreme superhydrophobicity, are easily wetted by low surface tension liquids such as hexadecane leading to contact angles around 0^{o} [30]. This challenge has motivated many researchers to develop superoleophobic surfaces combining low surface energy materials and patterned surfaces and paying special attention to the formation of hierarchical structures and re-entrant textures[28,30,31].

The formation of superoleophobic surfaces is out of the scope of this work, but oleophobicity of the coatings produced was characterized in order to know the potential application of the produced materials. For this purpose, the contact angle with olive oil (γ = 32.28 mN/m) and hexadecane (γ = 27.47 mN/m) was measured. The oleophobicity of the superhydrophobic film formed from Latex E was measured as a function of the temperature of drying as it was done for the water in Figure 5.6. In Figure 5.19 it can be observed that the

contact angle for both liquids decreased as the drying temperature of the film increased because the films become flatter when the casting temperature approached the melting temperature (see Figure 5.5). It is worth mentioning that Latex E dried at ambient temperature gave contact angle values of 138 and 132º for olive oil and hexadecane respectively, which are reasonably high oleophobic values.

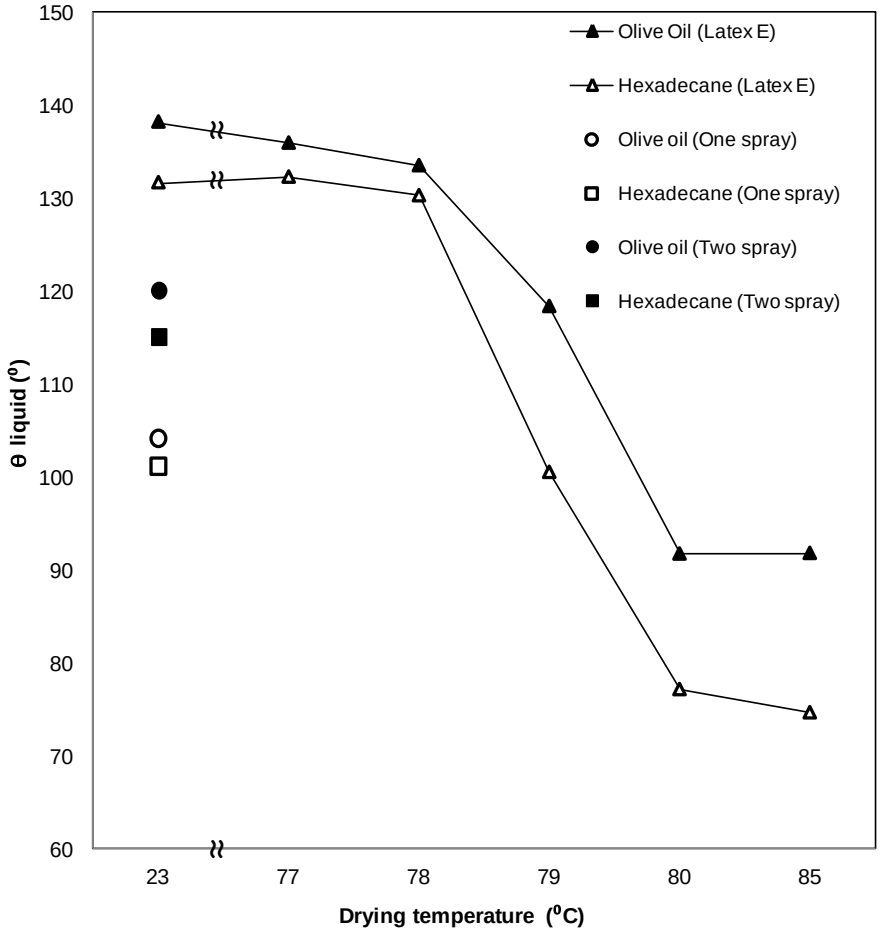

Figure 5.19. Olive oil and hexadecane contact angles for the different surfaces.

The oleophobicity of the films produced by the “One and Two step spray coating procedures” was measured. The films sprayed one time (open square and circle, Figure 5.19) showed modest oleophobicity (contact angles: 104º±1 and 101º±1 respectively for olive oil and hexadecane). However, the films sprayed twice (black square and circle, Figure 5.19) showed improved oleophobicity giving contact angles of 120º±1 and 114º±1 of contact angle for olive oil and hexadecane.

The sliding angle of the olive oil and hexadecane was measured for the one and two spray coatings finding that even in vertical surfaces, these liquids did not slide (Figure 5.20).

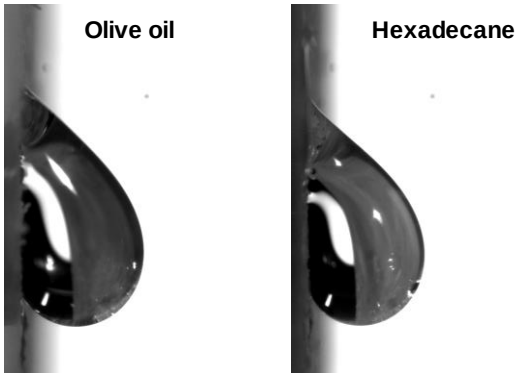

Figure 5.20. Olive oil and hexadecane droplets at 90º of tilting angle for the two spray coating.

This phenomenon is similar to the so-called “petal effect” in which surfaces exhibit high contact angles that can reach the superhydrophobic regime but they present large contact angle hysteresis and strong adhesion of the droplets to the surface[32,33]. The fundamental reason is that the liquid wets the whole surface, namely Wenzel’s model applies.

5.3.3. Icephobicity

The development of surfaces able to prevent ice formation and accumulation is of great interest because ice complicates the operation of many systems such as wind turbines[34–36], aircrafts[36–39], power lines[36,38,40,41], telecommunication devices[36,38,41] and air conditioning equipments[42,43]. To solve this problem, many surface techniques based on chemical, thermal and mechanical methods have been tested but most of them rely on the use of expensive equipment and complicated procedures[42]. The application of glycol based fluids[37,44] or the use of sacrificial coatings (silicon grease[45], sol-gel systems[46,47]) have proven to be efficient solutions, however, they are expensive methods that need periodic re-application and have detrimental consequences for the environment. This situation has prompted researchers to develop new anti-icing systems and also to investigate the relationship between water wettability and ice adhesion. Indeed, this relationship is not clear and there are some works that observe a direct relationship between surface hydrophobicity and reduced ice adhesion[48,49] while others do not find a clear trend[50,51].

The reduction of ice adhesion requires the reduction of surface wettability[38] and therefore the design of superhydrophobic surfaces constitute a potential option to develop low ice adhesion surfaces, specially from fluorinated polymers, which present the lowest surface energy values. However, superhydrophobic surfaces which are water repellent under regular conditions lose their water repellency when water vapour condenses on the surface[52–54]. It was demonstrated that water condensation on superhydrophobic surfaces produces an increase in contact angle hysteresis and reduces the water droplet mobility. The water droplet coalesces with the water condensed on top and between the pillars of the rough surface and produces a

transition from Cassie's state (water stands on the pillars) to Wenzel's state (water penetrates in the structure)[55]. This effect can produce an increase in the ice adhesion strength because the convex and concave structures of the surface may have an anchoring effect[56].

The hydrophobic and superhydrophobic coatings produced in this work were tested in order to evaluate the potential application of these surfaces as antiicing coatings. For the sake of comparison, the film produced from the MMA/BA/MAA latex was also tested. The antiicing properties were analyzed in terms of ice adhesion strength, response under water vapour condensation conditions, and ice formation and accumulation using supercooled water.

Ice adhesion strength was characterized using a TA.HD plus texture analyzer equipment (Stable Micro Systems). The films were casted onto glass substrates (10 x 5 cm). Spectrophotometer cuvettes (1.2 x 1.2 x 4.5 cm) were used as molds to build ice blocks on top of the coatings. The open side of the cuvette was placed on top of each coating and the borders were sealed with molding paste. A hole was done in the bottom part of the cuvette and 4 ml of water were introduced with a syringe. The samples were then introduced into a freezer to form the ice blocks and stayed there for two days. In this test, the texture analyzer was used in a peel mode experiment to remove the ice block from the substrate by pulling from an adhesive tape that surrounds the frozen cuvette as it is shown in Figure 5.21.

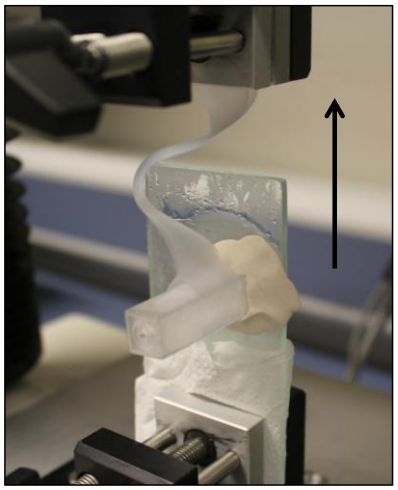

Figure 5.21. Representation of the ice adhesion strength test

When the ice block is removed from the substrate, different types of fracture[57] can occur as it is represented in Figure 5.22. The adhesive failure where the ice is completely removed from the surface at the bond line between the two materials leaving a clean film surface would be the ideal situation in this case. On the other hand, an ice residue can be left on the film surface (ice failure) and also depending on the strength of the film-ice adhesion, the film can be separated from the glass substrate completely or the ice can detach part of the surface of the film (film failure). In this test, the ice adhesion strength was evaluated visually by observing the different failures of each sample.

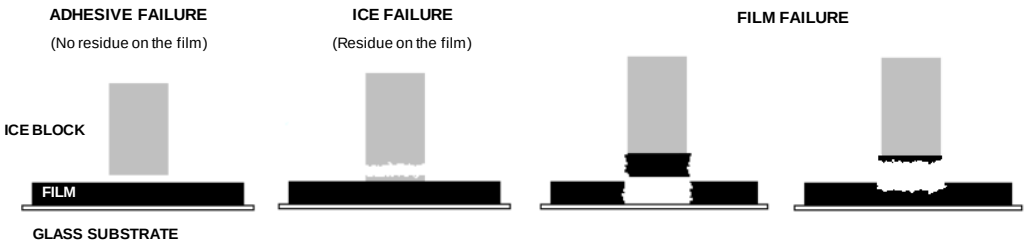

Figure 5.22. Types of failure in the ice adhesion test

Additionally, in another set of experiments the effect of the water vapour condensation was studied. The experiments were carried out in an OCA 20 Instrument (Dataphysics) equipped with a cooling chamber (Figure 5.23). Films were placed on the base of the chamber. Such a base can be cooled down. The experiments started at 23ºC and 55% relative humidity and the film was cooled down until -8.5 ºC. Therefore, condensation of water vapour occurred. With this set up, two different experiments were done. First, a 10 μl water droplet was placed on the film before starting the cooling and the evolution of the contact angle of this droplet was measured as a function of the temperature of the base. Second, the contact angle of newly dispensed droplets was measured at certain temperatures in order to see the effect of the condensation on the film surface.

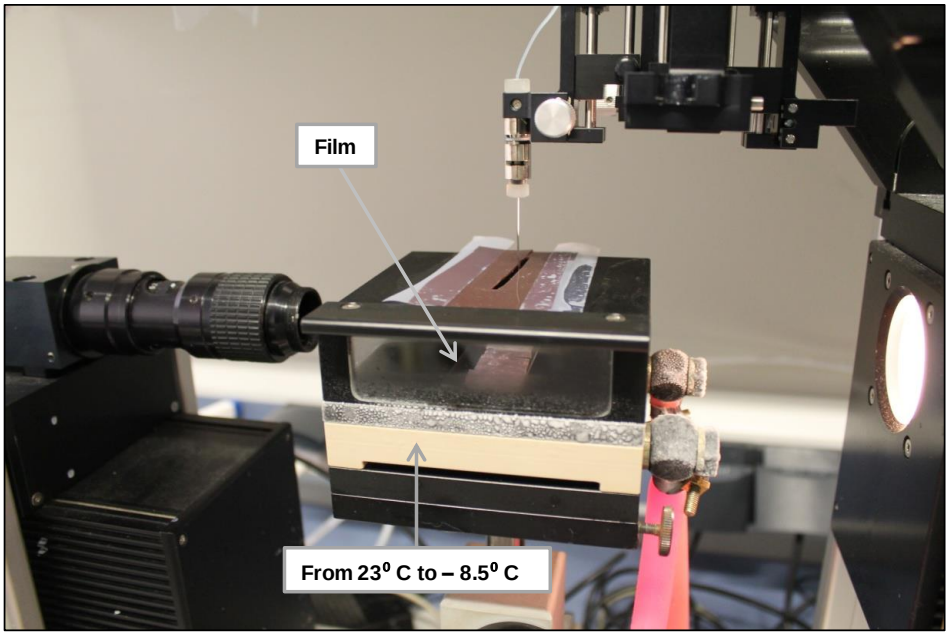

Figure 5.23. Set up for contact angle measurement equipped with a cooling chamber.

Finally, ice formation and accumulation on the surface of the films was studied. The samples were stored in the freezer and after a certain time, supercooled water was poured on top of the surfaces. The ice formation on top of the surface was evaluated visually for the different samples.

5.3.3.1. Ice adhesion strength

Ice adhesion has been tested by many researchers[36,38,45,48–51] but still there is not a clear trend about the relationship between hydrophobicity, roughness and ice adhesion. In order to examine ice adhesion in the systems developed in this work, the ice adhesion strength of the films formed in Section 5.3, specifically, the “Two Spray”, “One Spray” and the “MMA/BA/MAA” films was tested and compared with a smooth hydrophobic surface from the PFDA latex (Latex E). Latex E was not film forming at ambient temperature, therefore, the latex was melted and a film was formed with the help of a hot press (T≈150ºC). The four samples were evaluated as previously described and the images of the samples after the ice block removal are presented in Figure 5.24.

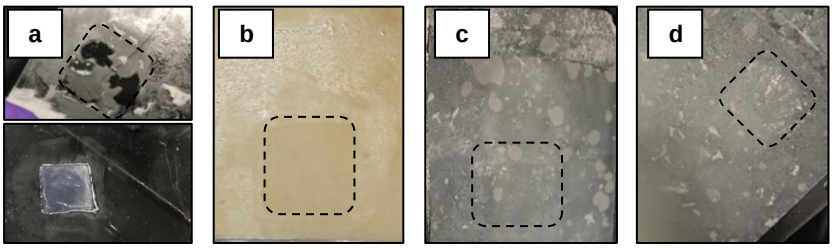

Figure 5.24. Photographs of the samples after the test. a) MMA/BA/MAA smooth film, b) Smooth PFDA film (Latex E 150ºC), c) One step spray film, d) Two step spray film.

As can be observed from the results in Figure 5.24, the worst response to ice adhesion was given by the MMA/BA/MAA smooth film (Figure 5.24**,** a) because the adhesion ice-film was that strong that the polymer film detached from the substrate (film failure) or a big ice residue is left on the surface (ice failure). From the rest of the experiments, it can be seen that apparently

clean surfaces were left after the test. An adhesive failure leads to a completely clean surface. However, it is not possible to evaluate visually whether some small ice residue was left on the film or if the film was slightly damaged. Only under the same type of failure the results can be compared. The ice-film interfaces for the different samples were not sufficiently analyzed to establish that the same type of failure took place in all the cases. Therefore, the results obtained in the ice adhesion strength test were inconclusive. What it seems clear after analyzing visually the different responses it that those films containing fluorinated polymer on the surface reduce the ice adhesion strength leading to cleaner surfaces as compared with the MMA/BA/MAA film where the film was completely destroyed or a big ice residue was left on the surface.

5.3.3.2. Response under water vapour condensation conditions

In another set of experiments, the effect of water vapour condensation on contact angle was studied above and below freezing temperature. Loss of superhydrophobicity has been observed even in Lotus leaves when water vapour condenses on the surface[58,59] since the water vapour is able to penetrate into the asperities of the surface and condensates on top of it.

Two different experiments were carried out and the results are shown in Figure 5.25. The contact angle value was measured at different temperatures of the base of the chamber. The system was cooled down according to the temperature profile represented in Figure 5.26. Considering that the studied films were deposited on a thin glass slide, similar temperature can

be expected for the film surface. In the experiments presented in Figure 5.25 a, a 10 μl water droplet was deposited on the surface at the beginning of the experiments (23ºC) and the contact angle of the droplet was measured at different temperatures.

Figure 5.25 a shows that the contact angle decreased as temperature decreased. It is worth pointing out that this effect was not due to a decrease of the surface tension of water, γ_W, because actually, γ_W increases as temperature decreases[60]. The decrease of the contact angle was more pronounced below the freezing point and the effect was stronger for the sprayed films than for both flat films and the film directly cast from Latex E.

It is worth pointing out that when the water droplet reaches the freezing point there is a change in the appearance of the droplet that produces a reduction in the contact angle (Figure 5.27).

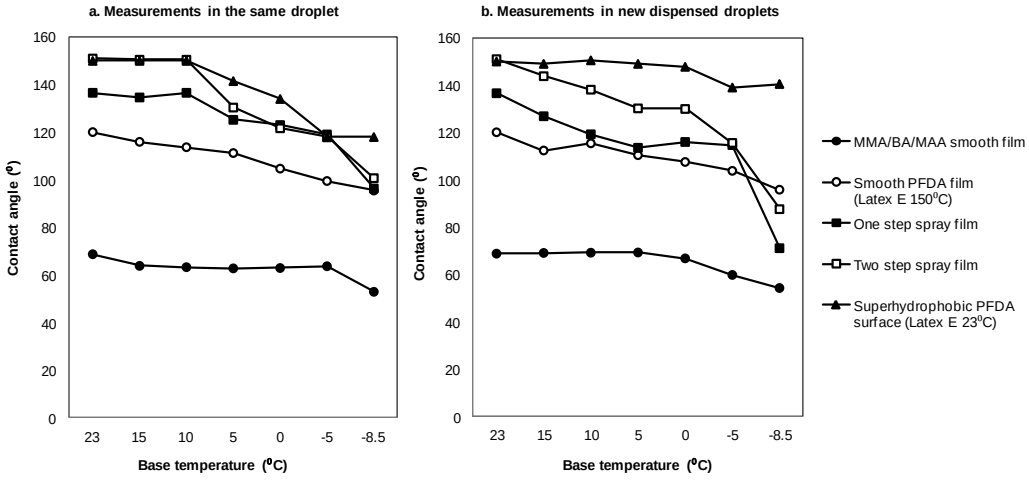

Figure 5.25. Contact angle measured as a function of the chamber base temperature.

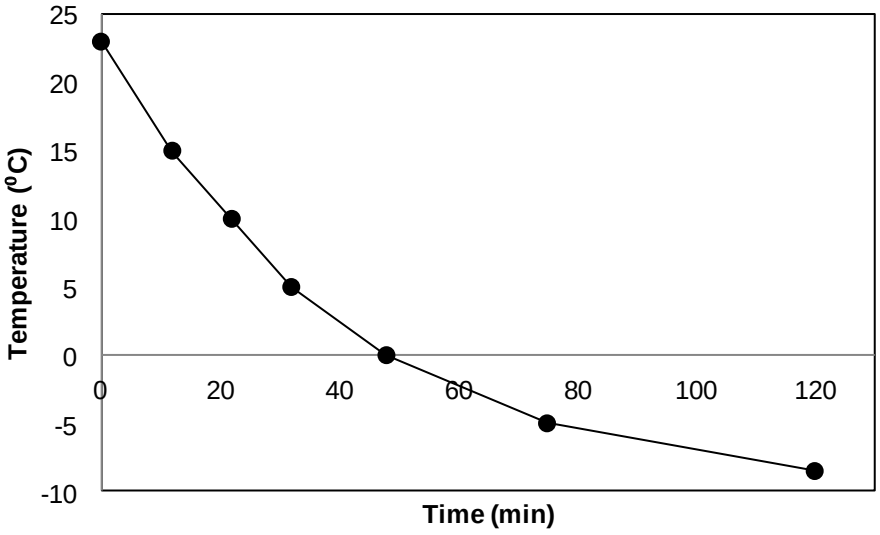

Figure 5.26. Temperature profile for experiments in Figure 5.25.

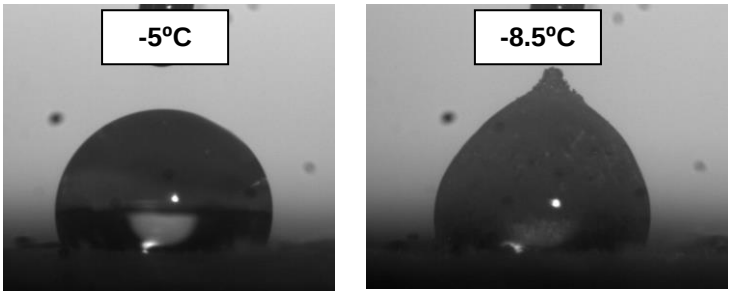

Figure 5.27. Change in the appearance of the droplet at the freezing point.

In experiments of Figure 5.25 b, the contact angle of water droplets is measured in different points of the film at each temperature, dispensing new droplets in every point. In these

results, also, the effect of decreasing temperature was stronger for T < 0ºC and more accused for the sprayed films.

The effect of temperature might be attributed to an accelerated condensation at lower temperatures, which modified the nature of the film surface making it more hydrophilic. The stronger effect observed for the sprayed films might be due to the effect of the hydrophilic MMA/BA/MAA substrate that may favour the formation of water/ice films within the pores.

On the other hand, the superhydrophobic PFDA surface from Latex E was the less affected by the water vapour condensation. This suggests that the porosity of the system was so high that when water vapour condensated, formed small droplets into the structure of the film and the time of the experiment was not enough to substantially modify the surface of the film, which retained part of its hydrophobicity at subzero temperatures.

5.3.3.3. Ice formation and accumulation using supercooled water

Following a similar procedure to the one described by Cao and coworkers[61], icing experiments were carried out using laboratory-made supercooled water. Bottles containing 500 ml of ultrapure water and the different films placed on top of aluminum plates and tilted at an angle of 10º were stored in the freezer at a temperature of -24ºC for 3 hours. After this time, the water was poured on top of the film in about 10 seconds. This step was done inside the freezer trying to reduce as much a possible the condensation of the water vapour on the film surface. The occurrence of icing was evaluated visually. Figure 5.28 shows the aspect of the different surfaces after the test. As can be seen, ice was formed both on the films and on the

aluminum plates. The only surface that did not show ice formation was the film cast from Latex E at room temperature (Figure 5.28, c). The reason for this better performance could be the higher roughness of the sample and consequently the higher hydrophobicity that led to sliding angles close to zero degrees. Additionally, it is necessary to consider the fact that the sample was a powder, and although the tilting angle was very low, the upper layers of the powdery surface could be removed by the water.

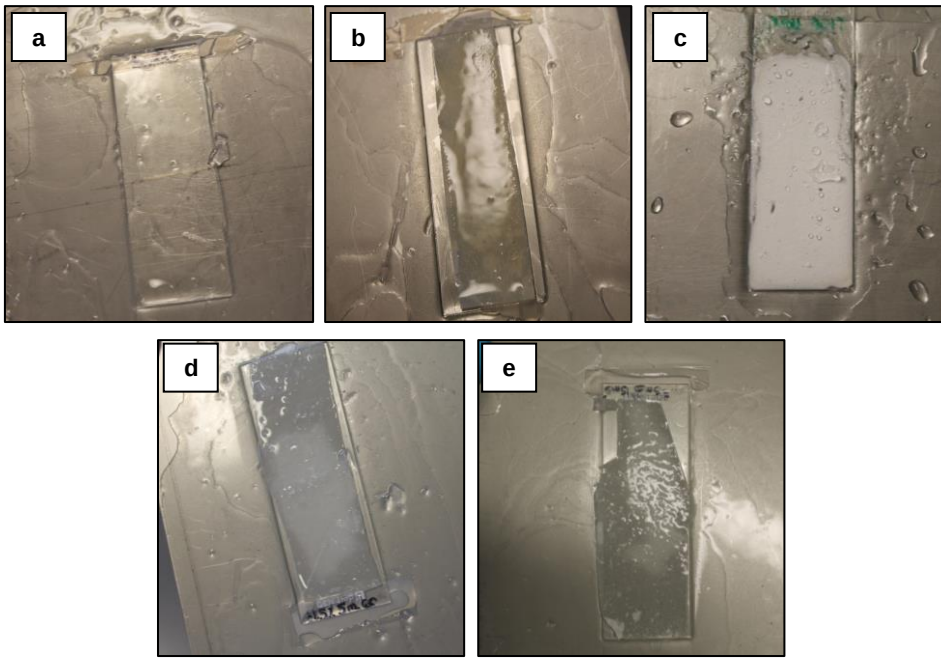

Figure 5.28. Aspect of the films after pouring supercooled water on top of their surface. a) MMA/BA/MAA smooth film, b) Smooth PFDA film (Latex E 150ºC), c) Superhydrophobic PFDA surface (Latex E 23ºC), d) One step spray film, e) Two step spray film. The films were tilted 10º.

In order to avoid ice formation, water should slide down the surface while it is being poured. Therefore, the films should be tilted at angles above their sliding angle. It was observed that the film cast from Latex E had tilting angles close to zero degrees and therefore no ice was formed on top of its surface. However, as was explained in the characterization of the contact angle of the sprayed surfaces and shown in Table 5.4, the sprayed surfaces present a heterogeneous microstructure which also affects the sliding angle. For instance, the films sprayed twice had an average sliding angle of 7º but in the regions where the water droplet could be deposited, the average sliding angle was around 27º. On the other hand, the films sprayed in one step showed sliding angles higher than 90º. In order to check if the tilting angle made a difference on ice formation, the experiments for the once and twice sprayed coatings were repeated at 40º of tilting. The images after the experiment are presented in Figure 5.29. Although ice covers the surface of both samples, it can be observed how for the case of the film sprayed once the layer is thicker and more visible than for the case of the film sprayed twice.

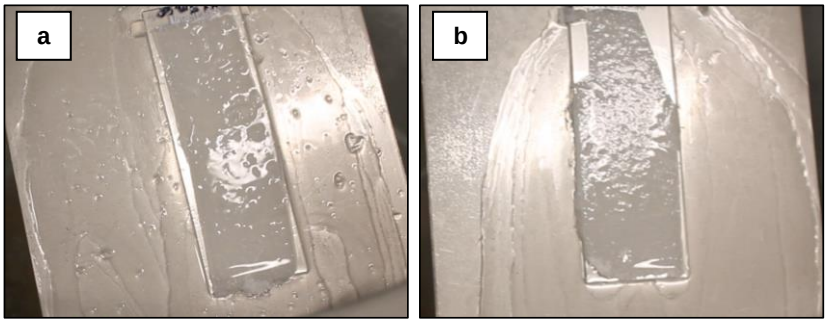

Figure 5.29. Aspect of the films after pouring supercooled water on top of their surface. a) One step spray film, b) Two step spray film. The films were tilted 40º.

Complete icephobicity was not achieved probably due to the fact that although it was attempted to reduce water vapour condensation by doing the experiments inside the freezer, condensation still occurred and it had a tremendous effect as it was proved in previous experiments.

Although the sprayed coatings did not show total efficiency as antiicing materials, they showed potential to reduce the ice adhesion strength and ice formation and accumulation as compared with the conventional MMA/BA/MAA coating, maintaining as well part of its hydrophobic character under severe water vapour condensation conditions.

5.4. Conclusions

In this work, a new method that allows the formation of superhydrophobic coatings with good film forming properties and mechanical strength is presented. The method involves the use of film forming coatings that are cast on the substrate and during the open time of these films a second dispersion is sprayed on the first film. This method can be cost efficiently applied to large and complex surfaces overcoming some of the previous approaches that involve highly expensive techniques which are not applicable to cover large and irregular surfaces. A key aspect of this development is the use of a fractal dispersion of a hydrophobic hard polymer. A method to synthesize relatively high solids fractal dispersions during the polymerization process is presented. Miniemulsion polymerization of PFDA was used and the surfactant and the initiator systems were used to control the fractal structure. This one step method is advantageous with respect to the previous methods that require two steps and

usually achieve low solids contents. A MMA/BA/MAA high solids film forming latex was used as a first coating. Contact angles > 150º, sliding angles of 7º and contact angle hysteresis ≈ 5º that belong to the superhydrophobic regime were obtained. The films showed oleophobic behaviour giving a contact angle of 120º for olive oil and good mechanical strength retaining an acceptable hydrophobicity (θ = 140º) after 50 cycles of an aggressive scrub test.

Icephobicity of the sprayed materials was tested and compared with a conventional MMA/BA/MAA coating. Although ice formation and accumulation on top of the surface still occurred for the sprayed systems, they demonstrated potential to reduce ice adhesion strength to the surface as compared to the MMA/BA/MAA film, maintaining their hydrophobic character under water vapour condensation conditions.

5.5. References

(1) Mandelbrot, B. B. *The Fractal Geometry of Nature*; **1982**; Vol. 1.

(2) Fractals and the Fractal Dimension. Retrieved from: http://www.vanderbilt.edu/AnS/psychology/cogsci/chaos/workshop/Fractals.html

(3) Lattuada, M.; Wu, H.; Hasmy, A.; Morbidelli, M. Estimation of Fractal Dimension in Colloidal Gels. *Langmuir* **2003**, *19*, 6312–6316.

(4) Deng, X.; Mammen, L.; Butt, H. J.; Vollmer, D. Candle Soot as a Template for a Transparent Robust Superamphiphobic Coating. *Science* **2012**, *335*, 67–70.

(5) Lazzari, S.; Nicoud, L.; Jaquet, B.; Lattuada, M.; Morbidelli, M. Fractal-like Structures in Colloid Science. *Adv. Colloid Interface Sci.* **2016**, 1–13.

(6) Kim, A. Y.; Berg, J. C. Fractal Aggregation: Scaling of Fractal Dimension with Stability Ratio. *Langmuir* **2000**, *16*, 2101–2104.

(7) González, A. E.; Martínez-López, F.; Moncho-Jordá, A.; Hidalgo-Álvarez, R. Concentration Effects on Two- and Three-Dimensional Colloidal Aggregation. *Physica A* **2002**, *314*, 235–245.

(8) Wu, H.; Lattuada, M.; Morbidelli, M. Dependence of Fractal Dimension of DLCA Clusters on Size of Primary Particles. *Adv. Colloid Interface Sci.* **2013**, *195-196*, 41–49.

(9) Eggersdorfer, M. L.; Pratsinis, S. E. The Structure of Agglomerates Consisting of Polydisperse Particles. *Aerosol Sci. Technol.* **2012**, *46*, 347–353.

(10) Jullien, R. The Application of Fractals to Colloidal Aggregation. *Croat. Chem. Acta* **1995**, *65*, 215–235.

(11) Schaefer, D. W.; Martin, J. E.; Wiltzius, P.; Cannell, D. S. Fractal Geometry of Colloidal Aggregates. *Phys. Rev. Lett.* **1984**, *52*, 2371–2374.

(12) Weitz, D. A.; Oliveria, M. Fractal Structures Formed by Kinetic Aggregation of Aqueous Gold Colloids. *Phys. Rev. Lett.* **1984**, *52*, 1433–1436.

(13) Li, D.-H.; Ganczarczyk, J. Fractal Geometry of Particle Aggregates Generated in Water and Wastewater Treatment Processes. *Environ. Sci. Technol.* **1989**, *23*, 1385–1389.

(14) Jia, Z.; Wu, H.; Morbidelli, M. Thermal Restructuring of Fractal Clusters: The Case of a Strawberry-like Core-Shell Polymer Colloid. *Langmuir* **2007**, *23*, 5713–5721.

(15) Schaefer, D. W.; Keefer, K. D. Structure of Random Porous Materials: Silica Aerogel. *Phys. Rev. Lett.* **1986**, *56*, 2199–2202.

(16) Jouault, N.; Vallat, P.; Dalmas, F.; Said, S.; Jestin, J.; Boué, F. Well-Dispersed Fractal Aggregates As Filler in Polymer- Silica Nanocomposites: Long-Range Effects in Rheology. *Macromolecules* **2009**, *42*, 2031–2040.

(17) Marcilla, R.; Blazquez, J. A.; Rodriguez, J.; Pomposo, J. a.; Mecerreyes, D. Tuning the Solubility of Polymerized Ionic Liquids by Simple Anion-Exchange Reactions. *J. Polym. Sci. Part A Polym. Chem.* **2004**, *42*, 208–212.

(18) Aguirreurreta, Z.; de la Cal, J. C.; Leiza, J. R. PhD Thesis: Water-Borne Coatings and Pressure-Sensitive Adhesives Produced with Polymerizable Surfactants, **2016**.

(19) Autran, C.; de la Cal, J. C.; Asua, J. M. (Mini)emulsion Polymerization Kinetics Using Oil-Soluble Initiators. *Macromolecules* **2007**, *40*, 6233–6238.

(20) Brun, A.; Dihang, H.; Brunel, L. Film Formation of Coatings Studied by Diffusing-Wave Spectroscopy. *Prog. Org. Coatings* **2008**, *61*, 181–191.

(21) Brun, a.; Brunel, L.; Snabre, P. Adaptive Speckle Imaging Interferometry (ASII): New Technology for Advanced Drying Analysis of Coatings. *Surf. Coatings Int. Part B* **2006**, *89*, 251–254.

(22) Aguirreurreta, Z.; Dimmer, J. A.; Willerich, I.; De La Cal, J. C.; Leiza, J. R. Water Whitening Reduction in Waterborne Pressure-Sensitive Adhesives Produced with Polymerizable Surfactants. *Macromol. Mater. Eng.* **2015**, *300*, 925–936.

(23) Retrieved from: http://www.formulaction.com/microrheology-horus.html.

(24) Horus Technology. *Adaptive Speckle Imaging Interferometry: Measurement Principle*.

(25) Pan, Z.; Zhang, W.; Kowalski, A.; Zhao, B. Oleophobicity of Biomimetic Micropatterned Surface and Its Effect on the Adhesion of Frozen Oil. *Langmuir* **2015**, *31*, 9901–9910.

(26) Raynolds, S.; Read, R. E. Oil and Water Repellent, **1970**.

(27) Kota, A. K.; Tuteja, A. Superoleophobic Surfaces. In *Advances in Fluorine-Containing Polymers*; **2012**; pp 171–185.

(28) Wong, T.-S.; Kang, S. H.; Tang, S. K. Y.; Smythe, E. J.; Hatton, B. D.; Grinthal, A.; Aizenberg, J. Bioinspired Self-Repairing Slippery Surfaces with Pressure-Stable Omniphobicity. *Nature* **2011**, *477*, 443–447.

(29) Jung, Y. C.; Bhushan, B. Wetting Behavior of Water and Oil Droplets in Three-Phase Interfaces for Hydrophobicity/philicity and Oleophobicity/philicity. *Langmuir* **2009**, *25*, 14165–14173.

(30) Tuteja, A.; Choi, W.; Ma, M.; Mabry, J. M.; Mazzella, S. A.; Rutledge, G. C.; McKinley, G. H.; Cohen, R. E. Designing Superoleophobic Surfaces. *Science* **2007**, *318*, 1618–1622.

(31) Kota, A. K.; Kwon, G.; Tuteja, A. The Design and Applications of Superomniphobic Surfaces. *NPG Asia Mater.* **2014**.

(32) Feng, L.; Zhang, Y.; Xi, J.; Zhu, Y.; Wang, N.; Xia, F.; Jiang, L. Petal Effect: A Superhydrophobic State with High Adhesive Force. *Langmuir* **2008**, *24*, 4114–4119.

(33) Nosonovsky, M.; Bhushan, B. Lotus Versus Rose: Biomimetic Surface Effects. In *Green Tribology: Biomimetics, Energy Conservation and Sustainability*; **2012**; pp 25–40.

(34) Parent, O.; Ilinca, A. Anti-Icing and de-Icing Techniques for Wind Turbines: Critical Review. *Cold Reg. Sci. Technol.* **2011**, *65*, 88–96.

(35) Dalili, N.; Edrisy, A.; Carriveau, R. A Review of Surface Engineering Issues Critical to Wind Turbine Performance. *Renew. Sustain. Energy Rev.* **2009**, *13*, 428–438.

(36) Meuler, A. J.; Smith, J. D.; Varanasi, K. K.; Mabry, J. M.; Mckinley, G. H.; Cohen, R. E. Relationships between Water Wettability and Ice Adhesion. *ACS Appl. Mater. Interfaces* **2010**, *2*, 3100–3110.

(37) Authority, C. A. *Aircraft Icing Handbook*; **2000**.

(38) Sayward, J. M. *Seeking Low Ice Adhesion*; **1979**.

(39) Eyre, F. W. & A. *The Detection of Frozen Contamination on Aircraft Surfaces*; **2002**.

(40) Laforte, J. L.; Allaire, M. A.; Laflamme, J. State-of-the-Art on Power Line de-Icing. *Atmos. Res.* **1998**, *46*, 143–158.

(41) Volat, C.; Farzaneh, M.; Leblond, A. *De-Icing / Anti-Icing Techniques for Power Lines: Current Methods and Future Direction*; **2005**.

(42) Gwak, Y.; Park, J.-I.; Kim, M.; Kim, H. S.; Kwon, M. J.; Oh, S. J.; Kim, Y.-P.; Jin, E. Creating Anti-Icing Surfaces via the Direct Immobilization of Antifreeze Proteins on Aluminum. *Sci. Rep.* **2015**, *5*.

(43) Sforza, P. M. *Commercial Airplane Design Principles*; **2014**.

(44) United States Environmental Protection Agency; *Storm Water Technology Fact Sheet. Airplane Deicing Fluid Recovery Systems*; **1999**.

(45) Baker, H. R.; Bascom, W. D.; Singleterry, C. R. The Adhesion of Ice to Lubricated Surfaces. *J. Colloid Sci.* **1962**, *17*, 477–491.

(46) Ayres, J.; Simendinger, W. H.; Balik, C. M. Characterization of Titanium Alkoxide Sol-Gel Systems Designed for Anti-Icing Coatings: I. Chemistry. *J. Coatings Technol. Res.* **2007**, *4*, 463–471.

(47) Ayres, J.; Simendinger, W. H.; Balik, C. M. Characterization of Titanium Alkoxide Sol-Gel Systems Designed for Anti-Icing Coatings: II. Mass Loss Kinetics. *J. Coatings Technol. Res.* **2007**, *4*, 473–481.

(48) Dotan, A.; Dodiuk, H.; Laforte, C.; Kenig, S. The Relationship between Water Wetting and Ice Adhesion. *J. Adhes. Sci. Technol.* **2009**, *23*, 1907–1915.

(49) Petrenko, V. F.; Peng, S. Reduction of Ice Adhesion to Metal by Using Self-Assembling Monolayers (SAMs). *Can. J. Phys.* **2003**, *81*, 387–393.

(50) Kulinich, S. A.; Farzaneh, M. How Wetting Hysteresis Influences Ice Adhesion Strength on Superhydrophobic Surfaces. *Langmuir* **2009**, *25*, 8854–8856.

(51) Landy, M.; Freiberger, A. Studies of Ice Adhesion. I. Adhesion of Ice to Plastics. *J. Colloid Interface Sci.* **1967**, *25*, 231–244.

(52) Lafuma, A.; Quéré, D. Superhydrophobic States. *Nat. Mater.* **2003**, *2*, 457–460.

(53) Quéré, D.; Lafuma, A.; Bico, J. Slippy and Sticky Microtextured Solids. *Nanotechnology* **2003**, *14*, 1109–1112.

(54) Jo, H.; Hwang, K. W.; Kim, D.; Kiyofumi, M.; Park, H. S.; Kim, M. H.; Ahn, H. S. Loss of Superhydrophobicity of Hydrophobic Micro/nano Structures during Condensation. *Sci. Rep.* **2015**, *5*.

(55) Wier, K. A.; McCarthy, T. J. Condensation on Ultrahydrophobic Surfaces and Its Effect on Droplet Mobility: Ultrahydrophobic Surfaces Are Not Always Water Repellant. *Langmuir* **2006**, *22*, 2433–2436.

(56) Yang, S.; Xia, Q.; Zhu, L.; Xue, J.; Wang, Q.; Chen, Q.-M. Research on the Icephobic Properties of Fluoropolymer-Based Materials. *Appl. Surf. Sci.* **2011**, *257*, 4956–4962.

(57) Bennett, S. J.; Devries, K. L.; Williams, M. L. Adhesive Fracture Mechanics. *Int. J. Fract.* **1974**, *10*, 33–43.

(58) Cheng, Y. T.; Rodak, D. E.; Wong, C. A.; Hayden, C. A. Effects of Micro- and Nano-Structures on the Self-Cleaning Behaviour of Lotus Leaves. *Nanotechnology* **2006**, *17*, 1359–1362.

(59) Cheng, Y.-T.; Rodak, D. E. Is the Lotus Leaf Superhydrophobic? *Appl. Phys. Lett.* **2005**, *86*, 1–3.

(60) Vargaftik, N. B.; Volkov, B. N.; Voljak, L. D. International Tables of Surface Tension of Water. *J. Phys. Chem. Ref. Data* **1983**, *12*, 817–820.

(61) Cao, L.; Jones, A. K.; Sikka, V. K.; Wu, J.; Gao, D. Anti-Icing Superhydrophobic Coatings. *Langmuir* **2009**, *25*, 12444–12448.

Chapter 6. Incorporation of waterborne fluoropolymers in paint formulation

6.1. Introduction

Waterborne coatings are becoming increasingly demanded due to environmental concerns that regulate the use of VOCs. Nowadays around 80% of the paints sold in the residential market are water-based[1]. There are several reasons for this change. Water-based paints are less hazardous for both human health and for the environment and also, they offer excellent durability, quick drying times, less odor emission and excellent adhesion. Additionally, compared to solvent-borne products, lower amounts of water based paint are required to cover the same surface area and the materials used to paint (spray guns or brushes) are cleaned easily[2].

Water, UV resistance or the ability of the paint to resist to changes in temperature are some of the factors that determine the durability of paints and coatings in general. Waterborne coatings are especially sensitive to water due to the fact that most of the components of the formulation are water compatible. This may lead to poor water resistance and blistering on the paint surface, especially when water is accumulated on top of the coating as it may occur in many outdoor applications. It has been found that the incorporation of hydrophobic components into the formulation as well as the use of hydrophobic polymer binders such as long chain methacrylates and styrene is an efficient way to improve water resistance of paints[3].

Among the different hydrophobic binders, fluorinated polymers are well known to have excellent water repellency. Moreover, fluorinated polymers can greatly enhance the properties of coatings used in modern industrial, household and construction products. These materials

combine a wide variety of interesting properties that are beneficial for coating formulations such as low surface energy, insulating properties, impermeability to gases, high resistance to water, oil, chemicals, corrosion and UV radiation as well as low dirt pick up[4–7]. Indeed, many fluorinated polymers (e. g. polytetrafluoroethylene (PTFE, Teflon), polyvinylfluoride (PVF), polyvinylidene fluoride (PVDF) or fluoroethylene vinyl ether (FEVE)) are already being used in the market as a part of industrial settings, insulation systems and food and automotive industry[8]. According to a recent report by the market research firm, The Freedonia Group, the demand for fluoropolymers is expected to increase at 5.3% annually to $2.3 billion in 2019[9] driven by the interest of fluoropolymers in construction, electrical and electronic markets. Even if it is undeniable that the high performance of fluoropolymers comes with a significantly higher cost compared to conventional acrylics or silicon-based coatings, the future perspective of the increasing market of fluoropolymers together with the interesting range of possibilities that these materials offer justifies the interest on the research and industrialization of these fluorinated polymers. Demand for cost effective, high performing, multifunctional coatings that enable materials to perform efficiently under extreme conditions with minimal environmental impact (energy consumption, VOC emissions, toxicity, carbon footprint, etc.) continues to increase. These specialty fluoropolymers possess many characteristics that make them ideally suited for use in such novel coating formulations.

The aim of the present work is to study the effect of the incorporation of fluorinated polymers in paint formulations and evaluate the performance of these polymers. Fluorinated homopolymer and copolymer latexes using 1H,1H,2H,2H-perfluorodecyl acrylate (PFDA) as fluorinated monomer, 2-ethylhexyl acrylate (2EHA) as comonomer to improve film formation properties and methacrylic acid (MAA) were synthesized and incorporated into a commercial

paint formulation. Preliminary studies showed that apart from increasing the hydrophobicity of the paint, the fluorinated polymer resins provide an interesting matting appearance to the final surface. This gives an added value to the potential application of fluoropolymers in paints.

In paint technology, the terms gloss and matte refer to visual appearance of a finish with respect to its gloss level. Glossy paints reflect most light in the specular (mirror-like) direction and they provide a bright sheen when they are dried. On matte paints most of the light scatters in a range of angles and they show little to no sheen when they are dried. The differences between gloss and matte affect the physical appearance of coatings and also practical aspects such as surface cleanability or texture. Matte surfaces are generally more complicated to clean, but they cover better imperfections in the surface. For example, in some coating applications scratches, craters and impurities on the substrate are not easily recognized if the surface has a matte finish, whereas glossy surfaces show every single imperfection[10–12].

Figure 6.1 shows a schematic representation of both glossy and matte surfaces. As can be observed, only part of the incident light is directly reflected, the rest passes into the paint film and is internally scattered and absorbed by pigments and the substrate.

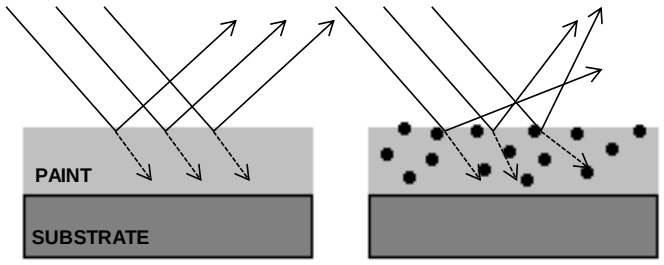

Figure 6.1. Gloss and matte surfaces

In order to achieve a perfect matte surface, the incoming light should be scattered. For this purpose, a micro-rough surface is necessary in order to reflect the incident light in a diffuse manner. Different additives are used in order to introduce micro-roughness to the surface such as silica particles, waxes, fillers or some organic materials. This microscopic components stay at the upper interface without being noticed visually or in the texture of the surface. Many parameters influence the matting effect including particle size, particle size distribution and the amount of matting agent used. In general, the higher the concentration of the matting agent in the formulation, the stronger the matting effect. The matting power of matting additives depends on their chemical, morphological, and physical properties. Matting agents with smaller average particle size provide a modest matting effect, but they produce smooth paint films. In contrast, products with larger particle sizes are stronger in matting efficiency, but the paint film surface is not so smooth[12,13].

However, the use of matting agents has some inconveniences. It represents an additional step to the process, and a good dispersion of the matting agent needs to be ensured. Otherwise, it will aggregate and create defects in the final surface. Furthermore, some matting agents are expensive and their incorporation to the paint does not give any additional advantage to the final coating. The substitution of the matting agent with a polymer that can provide the paint with the matte appearance and also, improve some additional properties would be particularly valuable.

In this chapter, the synthesis of waterborne fluoropolymer resins and the effect of their incorporation as additives into paint formulation on different properties including matting

efficiency were investigated. Most of this work was carried out in Nuplex Resins (Bergen Op Zoom, The Netherlands) although some specific characterization was performed at POLYMAT.

6.2. Experimental

6.2.1. Preliminary studies

The formulation for a commercial white pigmented paint (shown in Table 6.1) was chosen as a reference for this study. As can be observed, the formulation is divided in two main parts: the mill-base and the let-down. The mill-base is the fraction of the paint where the pigments are dispersed. The let-down constitutes the other fraction of the paint that contains the resins, solvents and additives. To obtain the final paint, the mill-base is added to the let-down under stirring. The main resin of this formulation is a commercial resin named as Stq Nu which has a minimum film formation temperature of around 60ºC and a solids content of 44 wt%.

Table 6.1. Paint formulation for resin Stq Nu

Component	***Grams***
MILL-BASE	
Nu Bc resin	5.12
Demiwater	7.36
Solvent 1	0.34
Defoamer 1	0.04
Pigment	13.05
LET-DOWN	
Stq Nu resin	59.72
Demiwater	2.92
Solvent 1	3.88
Solvent 2	2.58
Solvent 3	1.29
Defoamer 2	0.37
Surfactant	0.37
Matting agent	2.86
Thickener	0.09
Total	*100.00*

The different additives of the formulation cannot be revealed due to confidential issues; however some fundamental aspects of them are summarized in Table 6.2.

Table 6.2. General description of the resins and additives used in this work.

Additive	***Description***
Nu Bc resin	*Nuplex Owned Block Copolymer Pigment Stabilizer*
Stq Nu resin	*Nuplex Owned Gradient Morphology Binder*
Defoamer 1	*VOC-free silicon-containing defoamer*
Defoamer 2	*Polyether siloxane copolymer emulsion*
Surfactant	*Silicon-containing surface additive*
Matting agent	*Micronized, modified polyethylene wax*
Thickener	*Associative thickener. Water soluble non ionic polyurethane*

In this preliminary study, two fluorinated copolymers, p(PFDA/2EHA/MAA) (80.8/17.7/1.5) and p(PFDA/2EHA) (90/10) synthesized by miniemulsion polymerization following the procedure described in Chapter 3 were used. The fluorinated waterborne dispersions, with 40% of solids content, were incorporated into the paint formulation where 50 wt% of the polymer of the Stq Nu resin was substituted by the fluorinated polymer. The general formulation is shown in Table 6.3.

Table 6.3. Paint formulation for resin Stq Nu and fluorinated resin in a 50:50 wt ratio.

Component	***Grams***
MILL-BASE	
Nu Bc resin	*4.74*
Demiwater	*6.82*
Solvent 1	*0.32*
Defoamer 1	*0.04*
Pigment	*12.08*
LET-DOWN	
Stq Nu resin	*29.86*
Fluorinated resin[a]	*32.84*
Demiwater	*2.71*
Solvent 1	*3.59*
Solvent 2	*2.39*
Solvent 3	*1.20*
Defoamer 2	*0.34*
Surfactant	*0.34*
Matting agent	*2.64*
Thickener	*0.08*
Total	*100.00*

[a] p(PFDA/2EHA/MAA) (80.8/17.7/1.5) or p(PFDA/2EHA) (90/10) in each case.

The paints were casted onto glass substrates with a wet film thickness of 120 μm and dried under controlled conditions at 23ºC and 55% of relative humidity. These paints presented good appearance and wetting properties (see Figure 6.2).

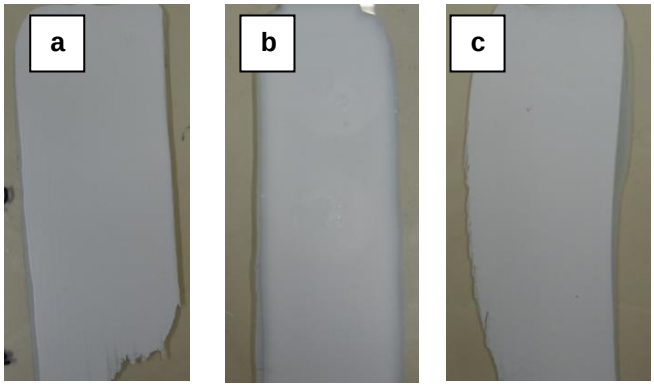

Figure 6.2. Paints from the formulations based on a. Stq Nu b. Stq Nu & p(PFDA/2EHA/MAA) (80.8/17.7/1.5) c. Stq Nu & p(PFDA/2EHA) (90/10).

After 14 days of drying, gloss, hardness and contact angle were measured for the different paints. The detailed description of the techniques used to measure these properties is included in the Section 3 of this chapter. Figure 6.3 shows the results for gloss at 20º and 60º and the contact angle values and hardness of the three different paints are presented in Figure 6.4. For the sake of simplicity, the resins in this work will be named using letter C indicating copolymer and a number, indicating the weight content of the fluorinated monomer in the formulation. In this way, in the graphs, the copolymer p(PFDA/2EHA/MAA) (80.8/17.7/1.5) is named as C80 and the copolymer p(PFDA/2EHA) (90/10) is named as C90.

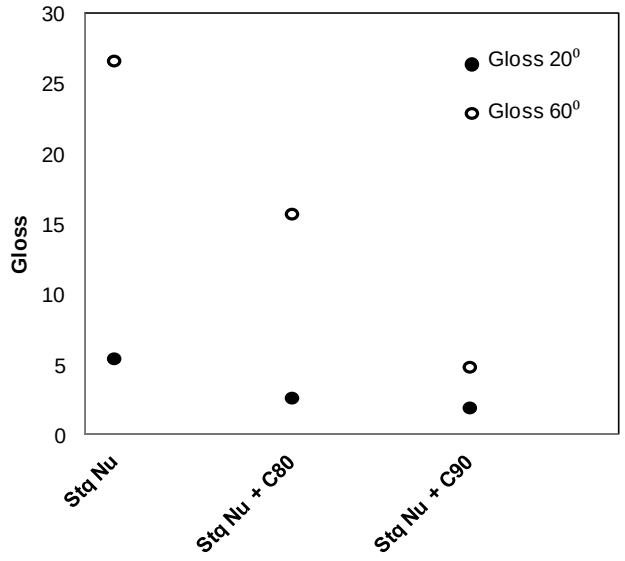

Figure 6.3. Gloss at 20º and 60º for paints in Figure 6.2.

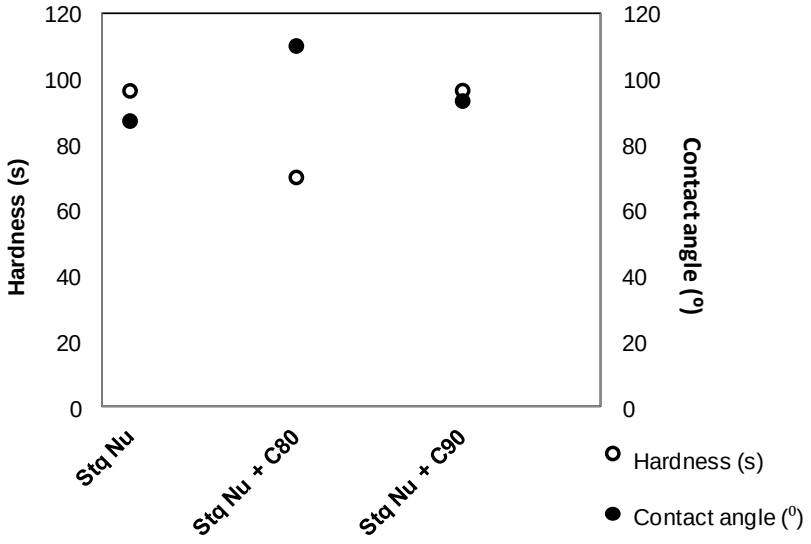

Figure 6.4. Hardness and contact angle for paints in Figure 6.2.

The previous graphs show that those paints containing fluoropolymer have lower gloss values, i.e. they are more matte, than the reference containing the Stq Nu resin. Regarding the contact angle, the paints that contain fluoropolymer show higher contact angle values and therefore, they are more hydrophobic. The paint that contained the C80 fluorinated copolymer is softer according to the hardness values; however with the C90 copolymer it is possible to achieve hardness values similar to the reference.

After these promising previous results, the work focused on the investigation of the properties that fluorinated polymers give to the final paints when they are incorporated in the formulation. Several properties such as matting efficiency, hydrophobicity and hardness, among others were studied.

6.2.2. Incorporation of fluorinated resins in paint formulation

6.2.2.1. Synthesis of the fluorinated resins

To prepare waterborne dispersions of these fluorinated materials is necessary to consider the hydrophobic nature of the fluorinated monomers. These monomers are water-insoluble and as they do not diffuse through the aqueous phase, they cannot be polymerized in conventional emulsion polymerization. The incorporation of hydrophobic monomers in the polymer backbone is easier in miniemulsion polymerization. In this process, the monomer is dispersed in an aqueous solution of surfactant using a homogenization device. The particles are formed by polymerizing the monomer droplets. This avoids the need of monomer mass transport through the water[14]. The miniemulsion preparation in laboratory scale was explained in Chapter 3, where a Branson Sonifier was used. However, since this part of the work was

carried out in an industrial environment, considerations about the possibilities of miniemulsion in industry should be taken into account. Indeed the miniemulsification process is the bottleneck for the industrial implementation of miniemulsion polymerization. Several devices can be used to produce the miniemulsification of the coarse emulsion, but among them, high pressure homogenizers (HPHs) seem to be a promising choice for industrial scale as large capacity HPHs are available[15]. In these equipments, the coarse emulsion is passed through the narrow gap of a valve. At the entrance of the gap, the droplets suffer elongational flow and the elongated droplets are broken up by the turbulence created at the exit of the gap. This process results in a tremendous increase of the surface area of the droplets, and if they are not rapidly covered by surfactant, droplet coagulation occurs. A consequence of the droplet break-up and coagulation processes is that both the size and the broadness of the droplet size distribution decrease with the number of passes or homogenization cycles, therefore, several passes are often needed to achieve small droplet sizes[16,17].

Figure 6.5 shows the high pressure homogenizer APV-1000 used in this work. It has two valves, and the conditions of operation were $P_{max} \approx 800$ bar and $P_{min} \approx 120$ bar ($\approx 15\%$ P_{max}). It was very important to stir the coarse emulsion in the metallic cup during the process to avoid phase separation during the miniemulsification stage.

Figure 6.5. High Pressure Homogenizer for miniemulsification

Three different fluorinated dispersions were produced with this technique, and the formulations are shown in Table 6.4. As can be observed, the same nomenclature as in previous section is followed to describe the synthesized polymers. The monomer mixture was varied to produce a fluorinated homopolymer (C100) and two different copolymers (C88 and C80) where the monomer ratio between PFDA and 2EHA was varied to modulate the properties of the final polymer. Methacrylic acid (MAA) was incorporated into the formulation to improve stability and compatibility with the rest of the components added during the paint formulation. AMBN (2,2'-azodi(2-methylbutyronitrile)) was used as oil soluble initiator and Dowfax 2A1 (alkyl diphenyloxide disulfonate) was used as surfactant (anionic).

Table 6.4. Formulation of the fluorinated homopolymer and copolymers.

ORGANIC PHASE		***AQUEOUS PHASE***		$d_{droplet}$ (nm)	$d_{particle}$ (nm)
MONOMER RATIO[a] (wt/wt/wt)	***INITIATOR[b]***	***EMULSIFIER[b]***	***WATER***		
PFDA/2EHA/MAA (100/0/0) ***C100***	*AMBN 1 wt%*	*DOWFAX 2A-1 1 wt%*		*154*	*228*
PFDA/2EHA/MAA (88.6/9.9/1.5) ***C88***	*AMBN 1 wt%*	*DOWFAX 2A-1 1 wt%*	*≈60 wt%*	*150*	*236*
PFDA/2EHA/MAA (80.8/17.7/1.5) ***C80***	*AMBN 1 wt%*	*DOWFAX 2A-1 1 wt%*		*156*	*240*

[a] Monomer represents 40% of the total weight of the formulation

[b] based on the total weight of monomer

For the preparation of the miniemulsions, the organic phase (monomer and initiator) and the aqueous phase (emulsifier and water) were mixed separately for 15 minutes and then, they were mixed together for another 15 minutes obtaining a coarse emulsion. This emulsion was charged to the homogenizer for the miniemulsification process. Several cycles were necessary to achieve a target droplet size of around 150 nm and a good miniemulsion stability.

Figure 6.6 represents the evolution of the droplet size with the number of cycles of homogenization for the three different compositions.

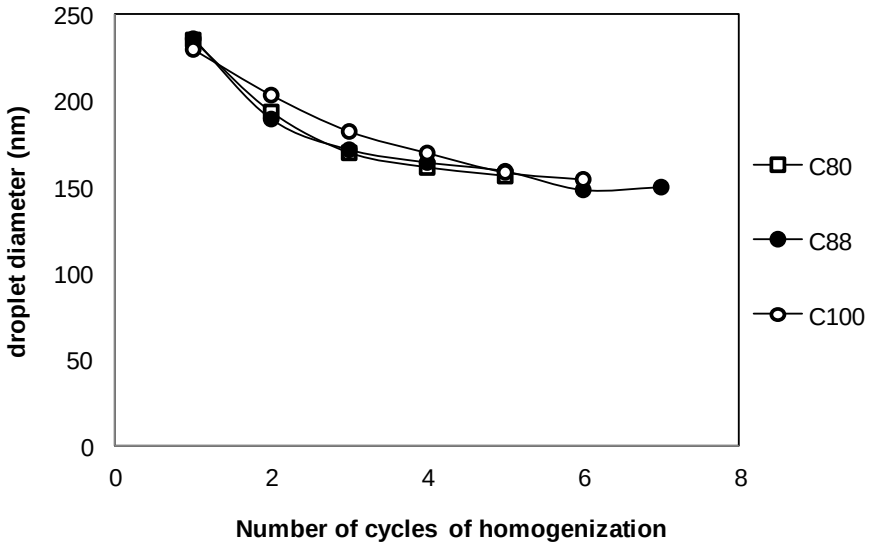

Figure 6.6. Evolution of droplet size with the number of cycles of homogenization.

After the homogenization stage, the miniemulsions were charged into the reactor and polymerized in a batch process at 70ºC during 4 hours. Full conversion was achieved as determined gravimetrically.

The pH of the final latexes was acidic (pH = 3,5 - 4) during the reaction to avoid the polymerization of MAA in the water phase. To incorporate the resins into paint formulation, the resin should be in basic conditions in order to improve their stability and compatibility with the rest of the additives of the paint formulation. A 25 % wt ammonium hydroxide solution in water was used to increase the pH to basic conditions (pH = 7,5 – 8).

6.2.2.2. Paints

The fluorinated resins were incorporated in the paint formulation based on the Stq Nu resin and their properties studied. In order to investigate the matting efficiency of the fluorinated polymer resins, paints with and without a commercial matting agent were formulated. The matting agent that the formulation initially contains is a micronized, modified polyethylene wax for solvent borne and aqueous coating systems for improving surface protection and for matting. It is presented as a white powder with a melting point of 115ºC.

Two different approaches were tested to study the matting efficiency of the fluorinated resins:

- Total substitution of the matting agent by the fluorinated resins
- Partial substitution of the matting agent by the fluorinated resins

In the first approach, the three different fluorinated polymer resins were incorporated to the formulation in 5, 10 and 16 wt% with respect to the final paint where the polymer ratios between the Stq Nu resin and the fluorinated resin were respectively, 82/18, 65/35 and 51/49.

In the second approach, 1/3 of the appropriate amount of matting agent given by the initial formulation was incorporated to those paints containing 16 wt% of each of the fluorinated resins.

The fluorinated resin added to the paints in each case substituted a certain amount of the Stq Nu resin in order to have similar solids content in all the formulations. The formulations for the different paints containing fluorinated resin are shown in Table 6.5.

Component	C80 5%	C88 5%	C100 5%	C80 10%	C88 10%	C100 10%	C80 16%	C88 16%	C100 16%	C80 16% + 1/3 M.A.	C88 16% + 1/3 M.A.	C100 16% + 1/3 M.A.
							Grams					
MILL-BASE												
Nu Bc resin	4.59	4.59	4.41	3.85	3.85	3.90	3.32	3.32	3.32	3.28	3.28	3.28
Demiwater	6.61	6.61	6.34	5.54	5.54	5.61	4.77	4.77	4.77	4.72	4.72	4.72
Solvent 1	0.31	0.31	0.29	0.26	0.26	0.26	0.22	0.22	0.22	0.22	0.22	0.22
Defoamer 1	0.04	0.04	0.04	0.03	0.03	0.03	0.03	0.03	0.03	0.03	0.03	0.03
Pigment	11.71	11.71	11.23	9.82	9.82	9.95	8.46	8.46	8.46	8.37	8.37	8.37
LET-DOWN												
Stq Nu resin	53.59	53.59	51.38	44.93	44.93	45.52	38.69	38.69	38.69	38.30	38.30	38.30
Demiwater	2.62	2.62	2.52	2.20	2.20	2.23	1.89	1.89	1.89	1.87	1.87	1.87
Solvent 1	3.48	3.48	3.34	2.92	2.92	2.96	2.51	2.51	2.51	2.49	2.49	2.49
Solvent 2	2.32	2.32	2.22	1.94	1.94	1.97	1.67	1.67	1.67	1.66	1.66	1.66
Solvent 3	1.16	1.16	1.12	0.97	0.97	0.99	0.84	0.84	0.84	0.83	0.83	0.83
Defoamer 2	0.33	0.33	0.32	0.28	0.28	0.28	0.24	0.24	0.24	0.24	0.24	0.24
Surfactant	0.33	0.33	0.32	0.28	0.28	0.28	0.24	0.24	0.24	0.24	0.24	0.24
Fluorinated resin (FR)	12.84	12.84	16.41	26.91	26.91	25.96	37.07	37.07	37.07	36.70	36.70	36.70
Thickener	0.08	0.08	0.08	0.07	0.07	0.07	0.06	0.06	0.06	0.06	0.06	0.06
Matting agent	x	x	x	x	x	x	x	x	x	0.99	0.99	0.99
total	*100.00*	*100.00*	*100.00*	*100.00*	*100.00*	*100.00*	*100.00*	*100.00*	*100.00*	*100.00*	*100.00*	*100.00*
Solids Content of the Fluorinated Resin	*0.40*	*0.40*	*0.30*	*0.40*	*0.40*	*0.42*	*0.45*	*0.45*	*0.45*	*0.45*	*0.45*	*0.45*
Solids Content of Setaqua 6717	*0.44*	*0.44*	*0.44*	*0.44*	*0.44*	*0.44*	*0.44*	*0.44*	*0.44*	*0.44*	*0.44*	*0.44*
wt % Fluorinated Resin in the final paint	*5.14*	*5.14*	*4.92*	*10.76*	*10.76*	*10.90*	*16.68*	*16.68*	*16.68*	*16.52*	*16.52*	*16.52*
wt % Setaqua 6717 in final paint	*23.58*	*23.58*	*22.61*	*19.77*	*19.77*	*20.03*	*17.02*	*17.02*	*17.02*	*16.85*	*16.85*	*16.85*
wt % polymer in paint	*28.71*	*28.71*	*27.53*	*30.53*	*30.53*	*30.93*	*33.70*	*33.70*	*33.70*	*33.37*	*33.37*	*33.37*
ratio Setaqua 6717/Fluorinated Resin	*0.82*	*0.82*	*0.82*	*0.65*	*0.65*	*0.65*	*0.51*	*0.51*	*0.51*	*0.51*	*0.51*	*0.51*

Table 6.5. Formulation for the paints containing fluorinated polymer.

In addition to the paints that contain fluorinated polymer, two reference paints were made in order to compare the different evaluated properties: i) a matte reference that corresponded to the formulation presented in Table 6.1, containing the Stq Nu resin, but no fluoropolymer and the appropriate amount of matting agent given by the formulation, and ii) a glossy reference that contained the same components as the matte one except that no matting agent was added in this case.

All the paints were formulated in two steps. The mill-base was prepared separately and stored. For the paint formulation, the components of the let-down were added and premixed for 15 minutes in a Dispermat Mixer and afterwards, the mill-base was added to the let-down and mixed for another 15 minutes. Once the paint was prepared, it was stored for some time to settle in the pot. The different paints containing fluoropolymer and the references, casted onto glass substrates, are shown in Figure 6.7. All the paints presented good appearance, excellent wetting and good film properties at room temperature.

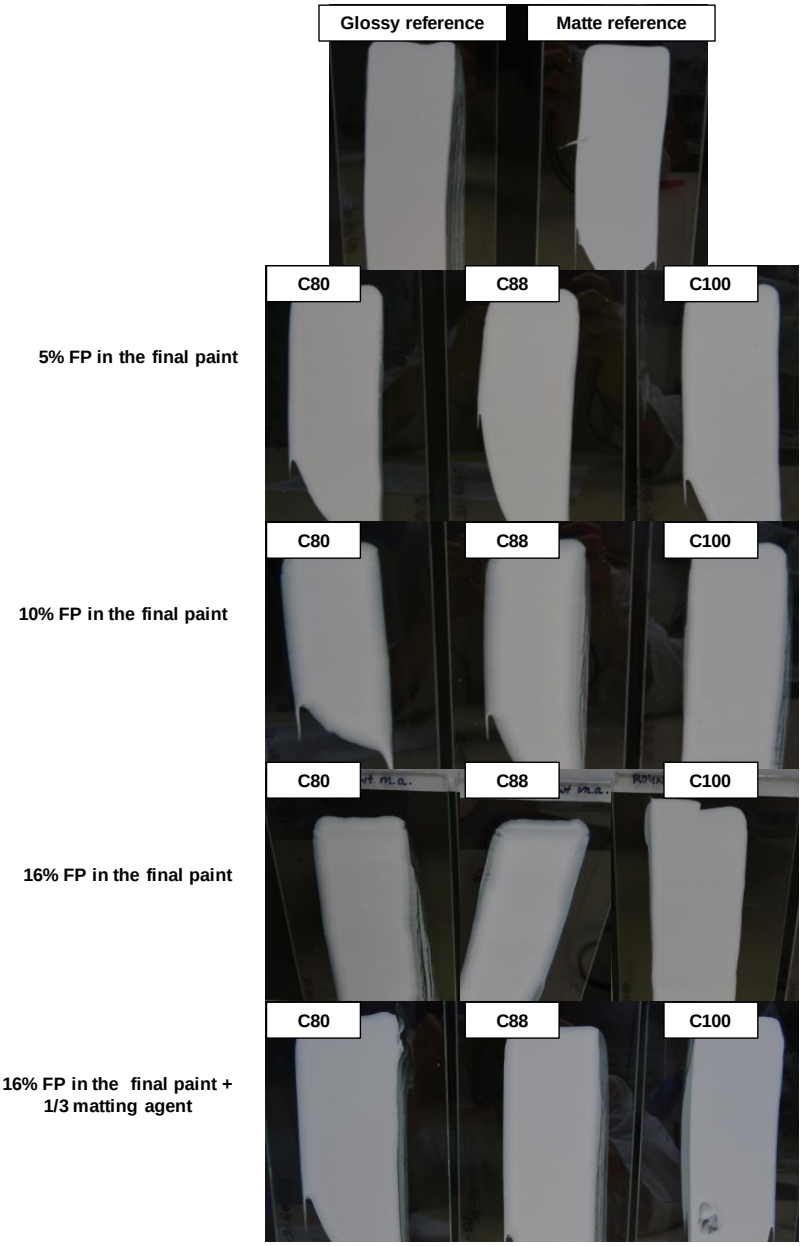

Figure 6.7. Paints with different amounts of fluorinated polymer and reference paints.

6.3. Results and discussion

The performance of fluorinated polymers in paints was evaluated by comparison with the glossy and matte references.

6.3.1. Gloss and Contact Angle

The paints were cast onto LENETA cards and dried for 14 days at 23ºC and 55% of relative humidity. The gloss was measured with a glossmeter from BYK Instruments at 20º and 60º.

In Figure 6.8 the gloss at 20º and 60º is represented with respect to the composition of fluorinated polymer into the final paint, for the paints without matting agent. As can be observed, gloss decreased with the increase of the fluoropolymer content in the paint, but still a 16% was not enough to reach the matting values of the matte reference. The matting efficiency of the homopolymer is lower than the one of the copolymers. This behavior was unexpected because the fluorinated homopolymer particles were hard and maintained their spherical shape after film formation, which could disperse light and produce the matting effect (see Figure 6.1). On the contrary, it was observed that the copolymers, which due to their softer nature were likely deformed during the film formation, gave lower gloss values and therefore a stronger matte effect.

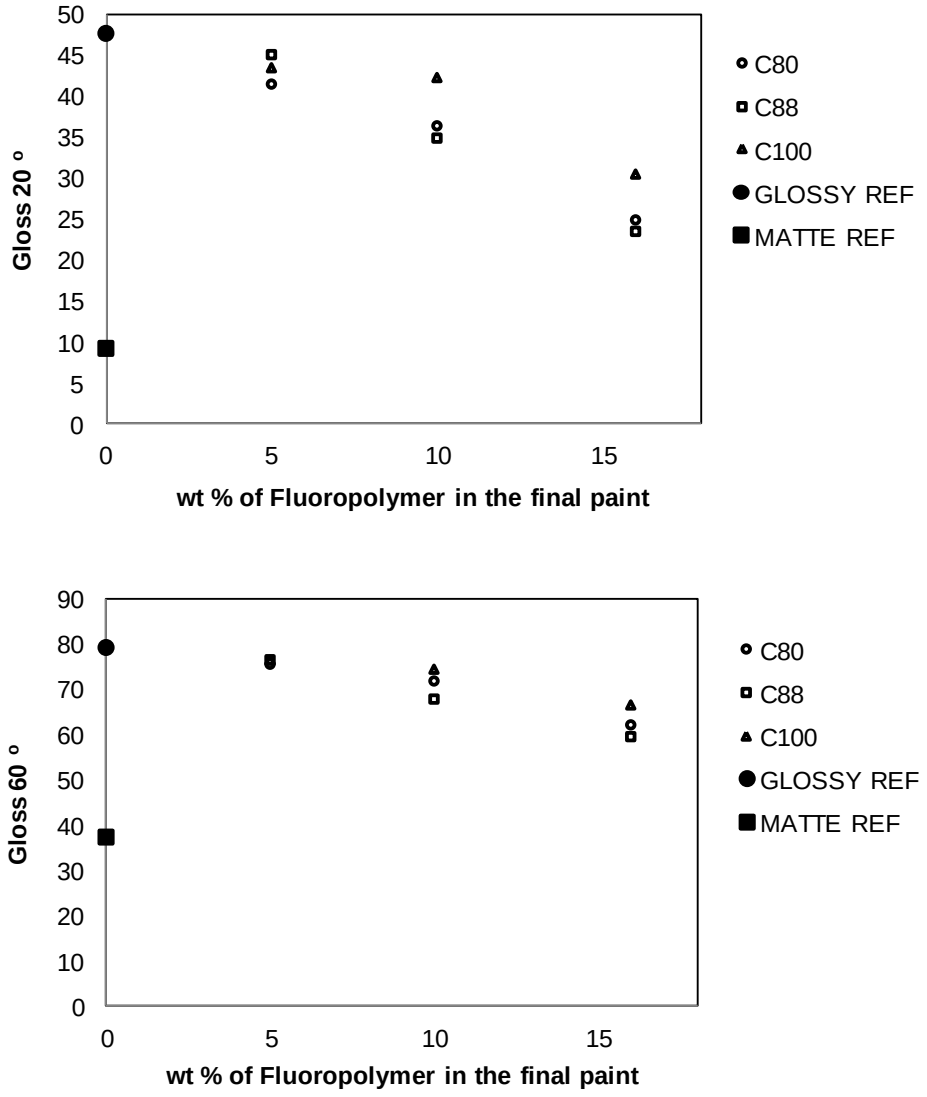

Figure 6.8. Gloss at 20º and 60º with respect to the concentration of fluoropolymer in the final paint.

Figure 6.9 compares the gloss of the films containing 16% of the fluorinated polymers and 1/3 of the appropriate amount of matting agent given by the original formulation with those with 16% of the fluorinated polymers and no matting agent as well as with the glossy and matte references.

It can be observed that gloss decreased sharply when 1/3 of the appropriate amount of matting agent was included in the formulation. Again, the gloss values of paints with the copolymers are lower than the gloss of the PFDA homopolymer paint, and the softer resin (C80) seemed to be the most effective one for the matting effect. It is important to notice that the C88 + 1/3 of matting agent combination reached the matting efficiency of the matte reference and with the C80 + 1/3 of matting agent lower gloss values than the reference can be achieved, what means that a higher amount of matting agent could be replaced in the system.

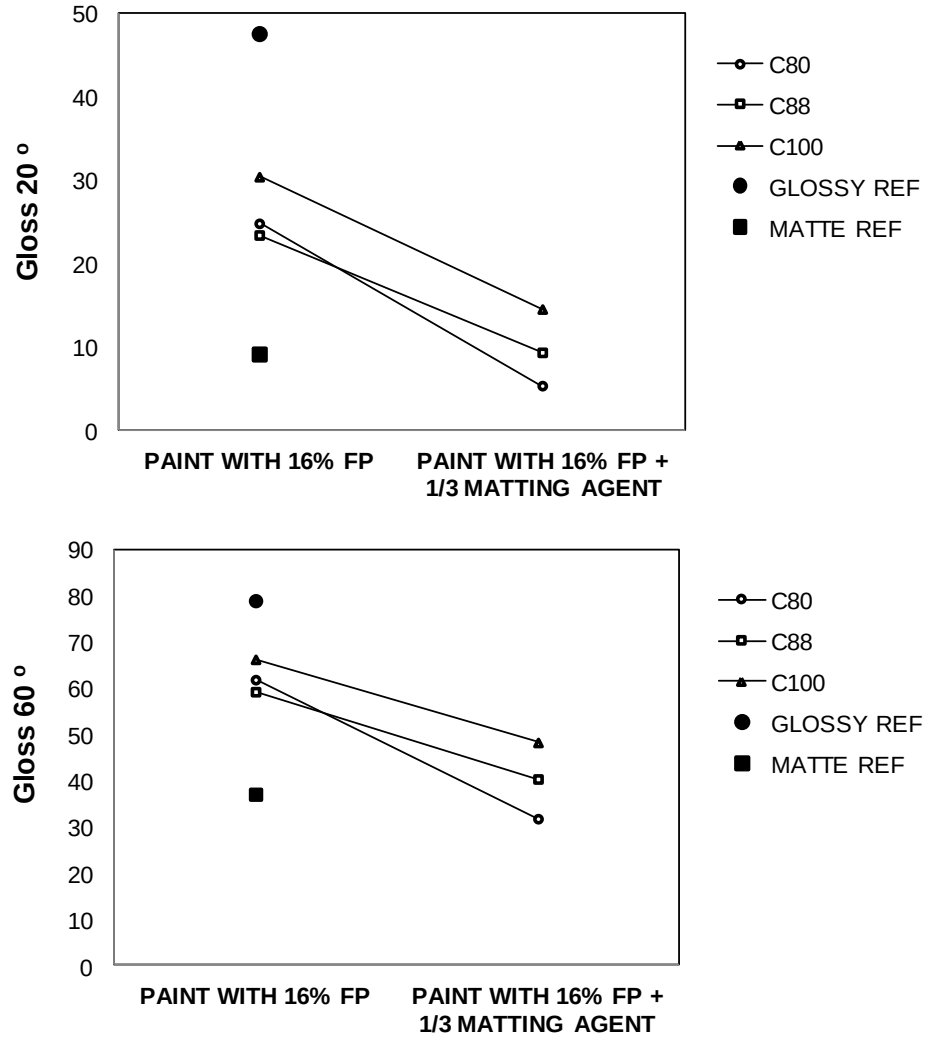

Figure 6.9. Gloss at 20^0 and 60^0 with and without the introduction of 1/3 of the appropriate amount of matting agent.

The contact angle of the different paints was measured and the values are presented in Figure 6.10.

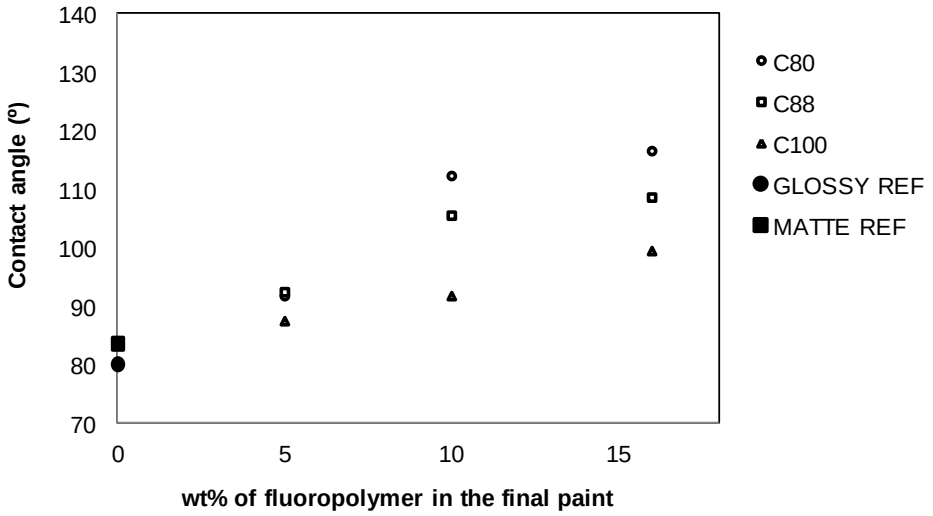

Figure 6.10. Water contact angle with respect to the concentration of fluoropolymer in the final paint.

For the case of the paints with fluoropolymer, the contact angle is always higher than the references and also increased with the increase in the percentage of fluorinated polymer in the formulation. The contact angles of both the glossy and matte references were similar, namely, the introduction of the matting agent in the system did not affect significantly the hydrophobicity of the surface. The paint containing the C80 copolymer was the more hydrophobic one, giving higher contact angles than the C88 copolymer. Moreover, the paint containing the homopolymer was the less hydrophobic one, which was against the expectations for this material that was supposed to give the higher contact angle values.

Figure 6.11 shows how with the introduction of 1/3 of matting agent in the system, the contact angle value of the paints barely changed. This effect confirms that the introduction of matting agent in the system does not improve the hydrophobicity of the final surface.

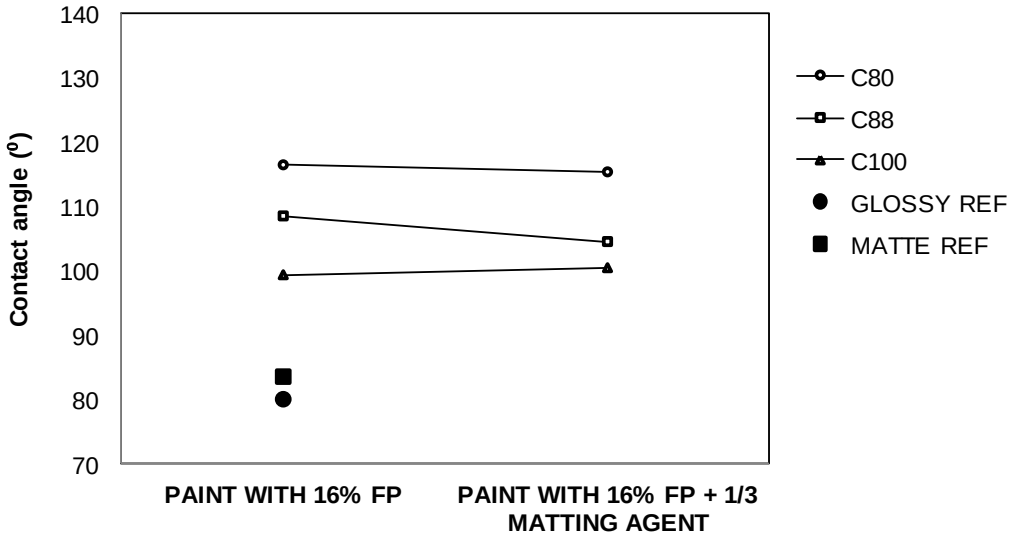

Figure 6.11. Water contact angle with and without the introduction of 1/3 of the appropriate amount of matting agent.

The surface of the paints was studied in order to understand the unexpected behavior in gloss and contact angle observed in Figure 6.8 and Figure 6.10. According to the definition of the matting effect, it can be understood that due to the presence of certain heterogeneities or roughness in the system, the light is dispersed into different directions creating the matting appearance. Following this idea, by the incorporation of fluorinated homopolymer particles on the top surface of the film, higher matting efficiency can be expected. The results in Figure 6.8 showed that the higher matting effect was achieved by the paints containing C80 copolymer, instead of the ones containing the fluorinated homopolymer. Additionally, the paints containing

C80 copolymer were also the most hydrophobic ones, although the fluorinated homopolymer is the most hydrophobic according to its nature. In order to understand these results, SEM microscopy was used to study the morphology of the top and bottom surfaces of the different paints. SEM micrographs were taken from the top and bottom interfaces of both glossy and matte references (Figure 6.12) and also for the different paints containing fluorinated polymer (Figure 6.13 and Figure 6.14).

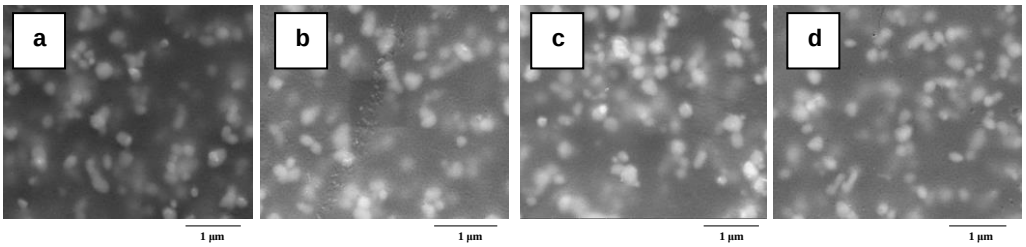

Figure 6.12. Top and bottom views of glossy and matte references. a) glossy reference top, b) glossy reference bottom, c) matte reference top, d) matte reference bottom.

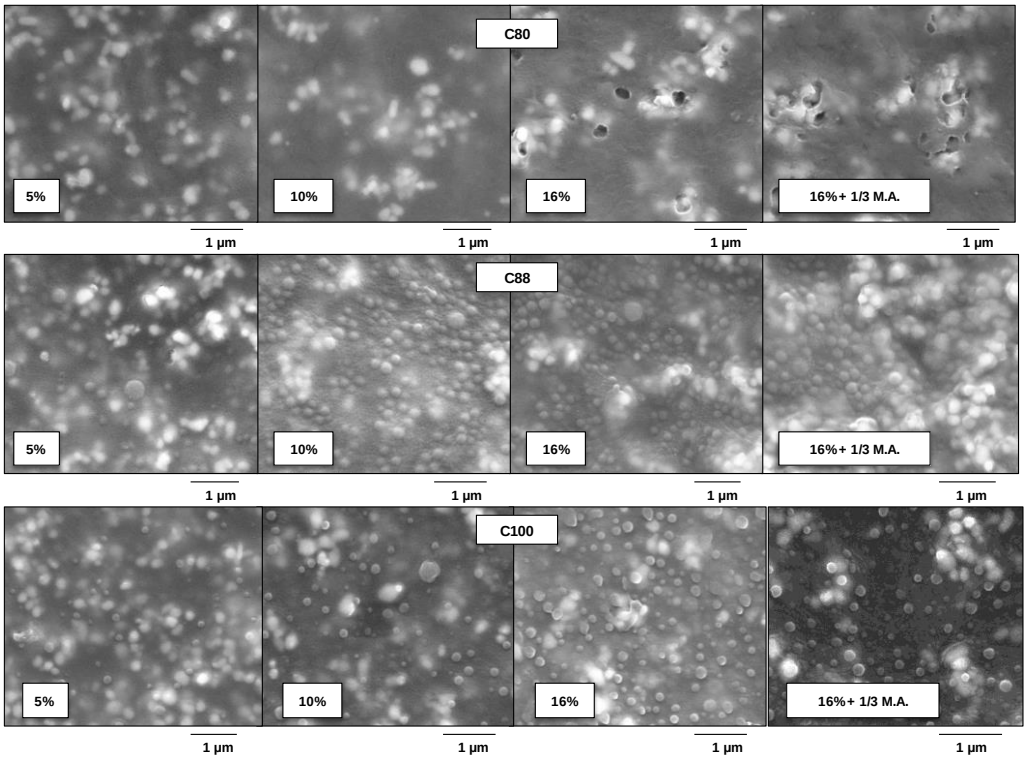

Figure 6.13. Top views of paints containing fluoropolymer.

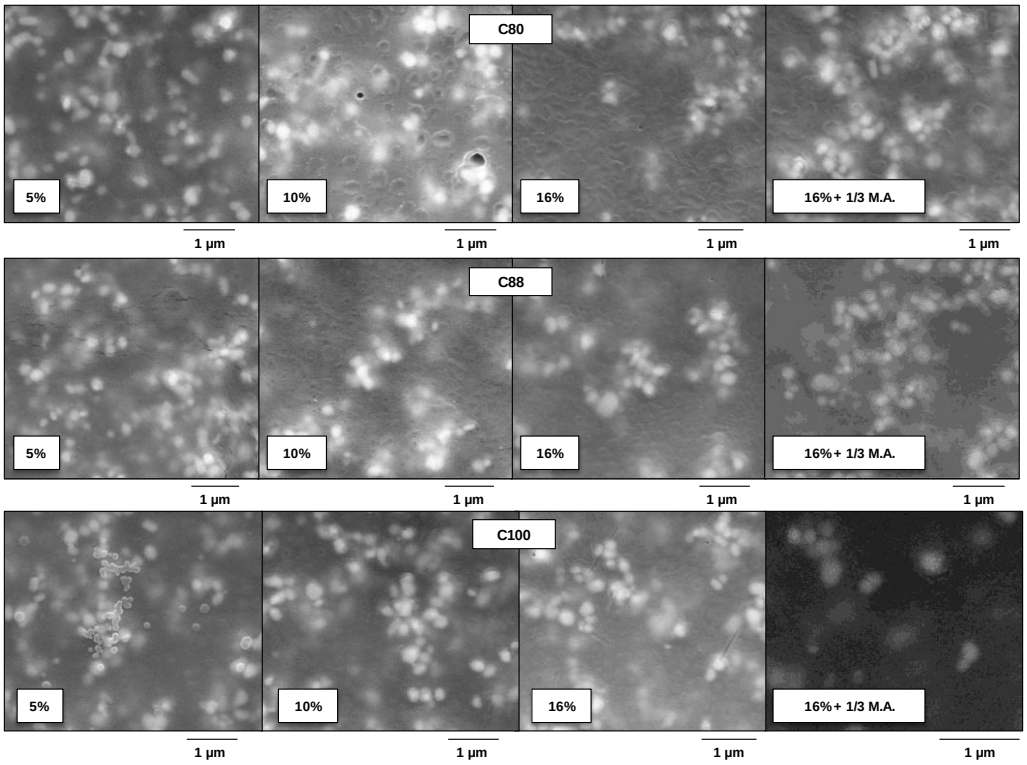

Figure 6.14. Bottom views of paints containing fluoropolymer.

According to Figure 6.12, both references do not show almost any difference between each other. For the case of the top views of the paints with fluorinated polymers, there is a clear difference between the different interfaces. The paints with the C80 copolymer showed a layer of fluorinated polymer on top of the surface, while the paints with the C88 copolymer and the fluorinated homopolymer C100 present a large number of hydrophobic particles undeformed on the top surface due to the harder nature of these materials. The bottom views of the different paints show that there is no sedimentation of the fluorinated particles to the bottom of the film.

According to the images, it can be concluded that the presence of the C80 copolymer layer on top of the film covering efficiently all the surface could be the reason why these paints present lower gloss values, and consequently higher matting appearance. The gloss of the fluorinated copolymer C80, which was the only one that had good film forming properties at ambient temperature, was characterized obtaining a value of 38 at 20º and 63 at 60º. These values are similar to the ones obtained for the paints containing 16% of C80 fluoropolymer. This could be an indication that confirms the presence of the C80 copolymer on the top surface and moreover, the low gloss obtained by the C80 paints may come from the nature of the C80 polymer. On the other hand, the presence of the fluorinated particles on top of the surface, isolated and maintaining the spherical shape does not seem to be efficient enough to achieve the matting effect.

Lower magnification images were taken from the references and from the paints containing 16% of the fluorinated polymer and the ones containing 16% of the fluorinated polymer and 1/3 of matting agent. As can be observed in Figure 6.15, the samples that contained matting agent in the formulation presented big aggregates on the surface. Since these aggregates are bigger in size than the incorporated fluoropolymer particles, they provide higher matting efficiency, but also, they create more imperfections in the surface.

Additionally, the paints containing the C80 copolymer showed the highest contact angles, although the fluorinated copolymer C88 and the fluorinated homopolymer C100 are more hydrophobic in nature. The presence of the C80 fluorinated copolymer layer covering the top of the surface can be the reason why these materials are more hydrophobic than the ones that present the hydrophobic particles that remain underformed and isolated on the top surface.

As was demonstrated by Gao and coworkers, the contact angle value is determined by the interactions between the liquid and the solid at the three phase contact line where the liquid, solid and air coexist and the interfacial area of contact between the solid and the liquid is irrelevant[18]. Taking this into consideration, in those paints containing C80 copolymer, it is more likely that the water droplet touches the fluorinated copolymer because particles are deformed and the soft polymer covers almost all the surface, whereas for the case of the C88 and C100, since particles remain spherical and they do not deform, the possibility of finding a particle at the three phase contact line is lower reducing the overall value of contact angle.

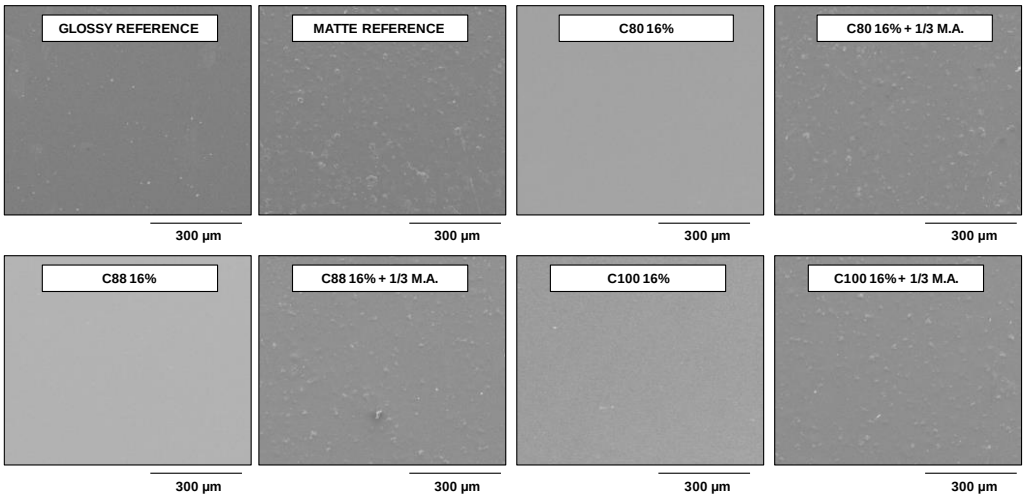

Figure 6.15. Lower magnification images (300µm) of the references and the paints containing 16% of fluoropolymer and 1/3 of matting agent.

Due to the fact that particle sedimentation of hard homopolymer particles was observed in Chapter 3 of this work, SEM micrographs from the cross section of the samples containing C100 homopolymer particles were done to the paints C100 16% and C100 16% + 1/3 M.A. In

Figure 6.16, the brighter regions correspond to the pigment and the while the spherical particles correspond to the homopolymer. The C100 particles are distributed all over the section of the films indicating that no sedimentation was occurring probably due to a higher viscosity of the overall system.

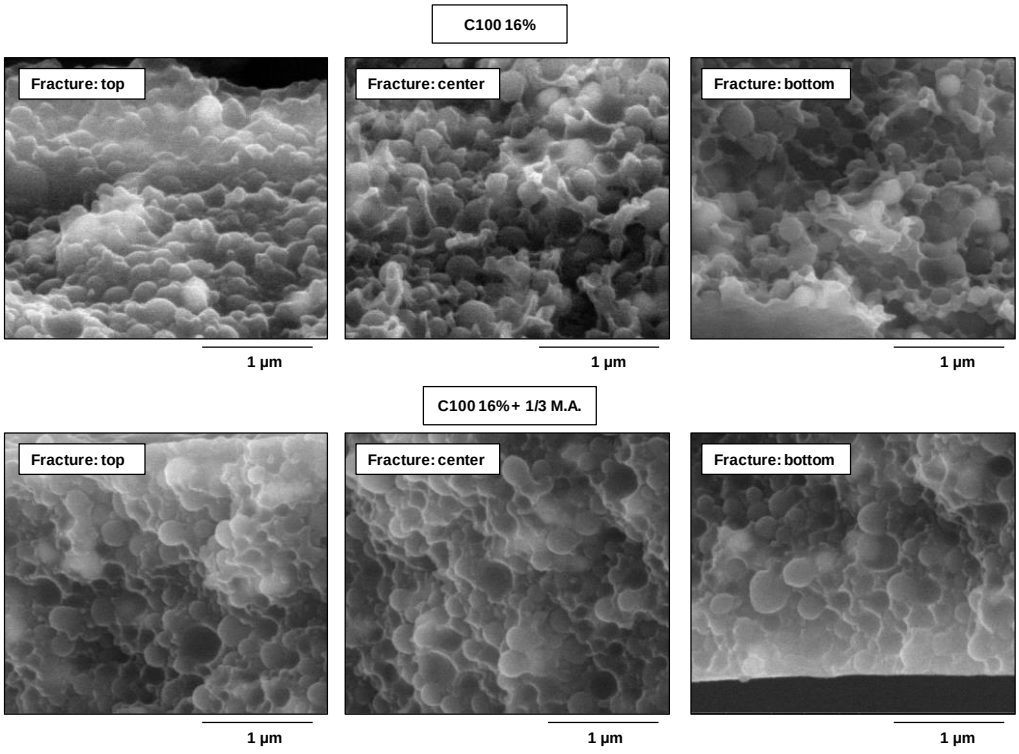

Figure 6.16. Cross section views of paints containing fluorinated homopolymer particles.

In order to look for differences in roughness for the different paints, AFM micrographs were taken from the paints containing 16% of fluorinated polymer, from the ones containing 16% of fluorinated polymer and 1/3 of matting agent and from both references. The images are

shown in Figure 6.17 together with the RMS values for the different paints. (RMS is the root mean square average of height deviations taken from the mean image data plane).

As can be observed, in the paints containing C88 and C100 polymer dispersions, the hard particles can be perfectly distinguished in the top surface. However, the C80 copolymer deforms and no spherical particles can be identified.

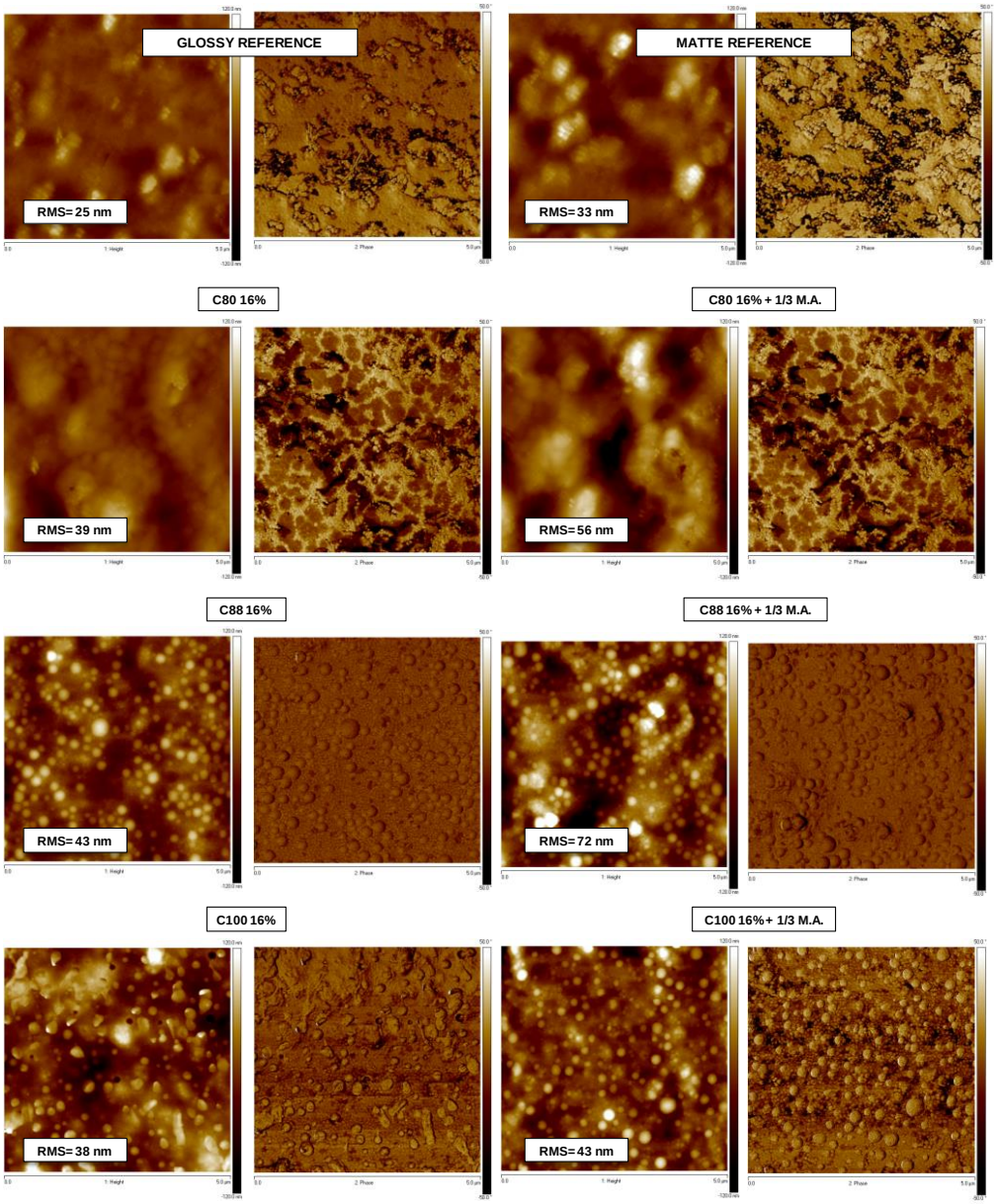

Figure 6.17. Height (120 to -120 nm) and phase (50 to -50º) AFM micrographs of the paints containing 16% of the fluorinated polymers and 1/3 of matting agent. (Image 5µm x 5µm)

Although C88 and C100 retain their spherical shape, the roughness of the surface does not seem to increase significantly according to the RMS values. Therefore, the effect on gloss and contact angle cannot be attributed to variations of roughness.

The phase images of the paints show the different materials present in the surface. Phase deviations in AFM are related to the differences in the viscoelastic properties of the materials present in a surface[19] and generally, more rigid materials appear as brighter while less rigid materials are represented with darker colors. In the phase images of Figure 6.17, it can be observed that the images for the paints containing fluoropolymer are very different from the references. These paints contain many components in the formulation so the identification of the different components can be quite complicated. In order to compare the images between each other, all of them have the same phase scale (from 50 to -50º). The C80 fluoropolymer can be identified in the dark deformed regions of the C80 samples, due to the fact that this polymer is softer than the Stq Nu resin. The spherical particles of the C88 resin showed similar rigidity to the paint matrix due to the similar color and in the case of the C100 samples, brighter homopolymer particles can be identified due to the harder nature of this polymer compared to the matrix. These images are in agreement with the SEM observations and it seems that those underformed particles stay more localized in the surface of the paint while in the paint containing the C80 copolymer the soft hydrophobic polymer covers more area thanks to the deformation of the particles.

6.3.2. Hardness

The hardness is defined as the resistance of a coating to a mechanical force, such as pressure, rubbing or scratching[20]. In practice, different testing methods can be used and in this case, pendulum hardness was employed. This method evaluates hardness by measuring the damping time of an oscillating pendulum. The pendulum rests with 2 stainless steel balls on the coating surface. A physical relationship exists between oscillation time, amplitude and the geometric dimensions of the pendulum. The viscoelastic behavior of the coating determines its hardness. When the pendulum is set into motion, the balls roll on the surface and put pressure on the coating. Depending on the elasticity, the damping will be stronger or weaker. If there are no elastic forces, the pendulum will damp stronger. High elasticity will cause weak damping. There are two types of pendulums standardized for this test method, König and Persoz. The König pendulum was used in this work.

Additionally, the thermal transitions of the different components of the formulation were analyzed by means of Differential Scanning Calorimetry in a DSC, Q1000 (TA Instruments). The heating rate used was 10ºC/min over a temperature range from -80 to 150ºC under nitrogen atmosphere. Figure 6.18 shows the results for the different paints with and without matting agent. As can be observed, the C80 resin is the softer one with a Tm around 18ºC followed by the C88 resin which is harder with a Tm around 45ºC. The C100 resin is highly crystalline with a melting peak at a temperature around 76ºC. The transition that appears at a temperature around 62ºC corresponds to the Tg of the Stq Nu resin and also, the melting peak of the matting agent can be identified at a temperature around 115ºC (Figure 6.18,b).

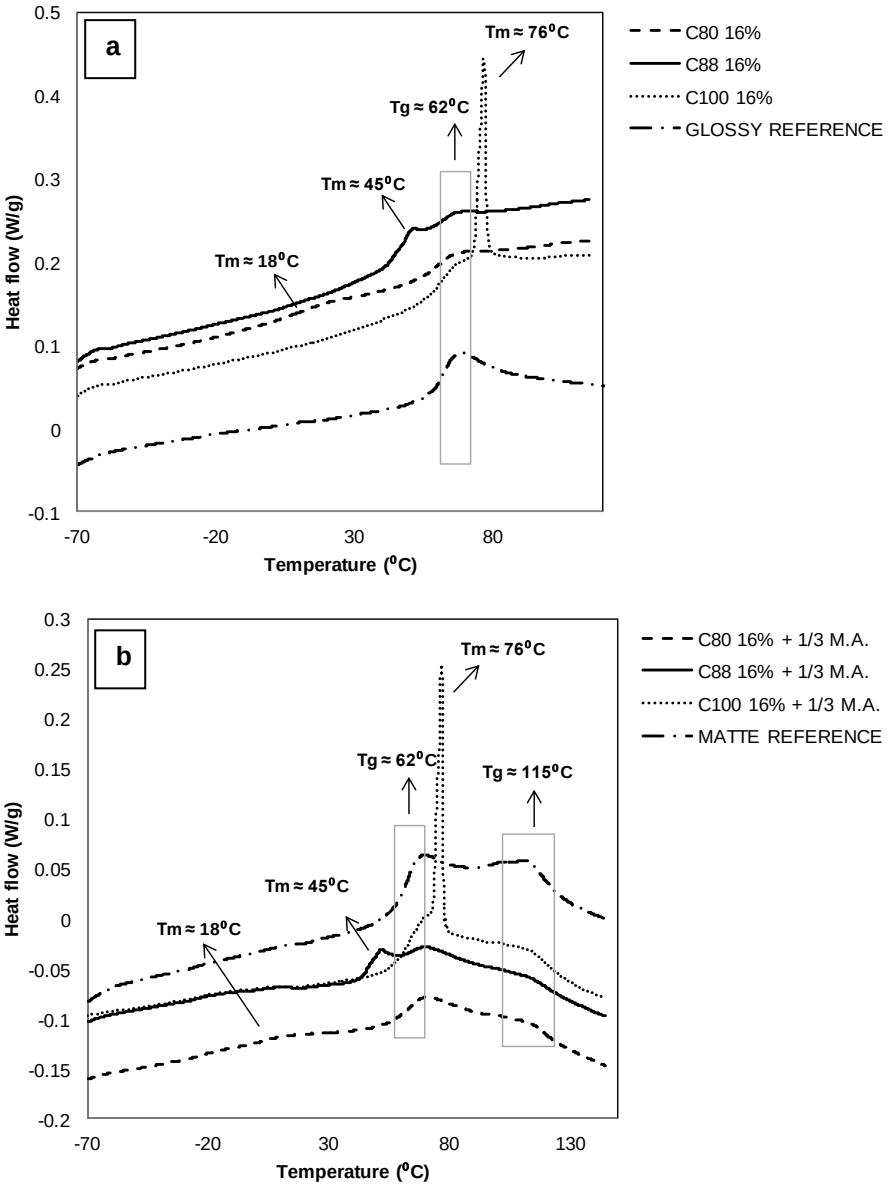

Figure 6.18. DSC thermograms for the paints without (a) and with (b) matting agent. (Exo Down)

The hardness of the paints, casted onto glass substrates was measured after 14 days of drying. The values for the paints without matting agent and for the references are presented in Figure 6.19.

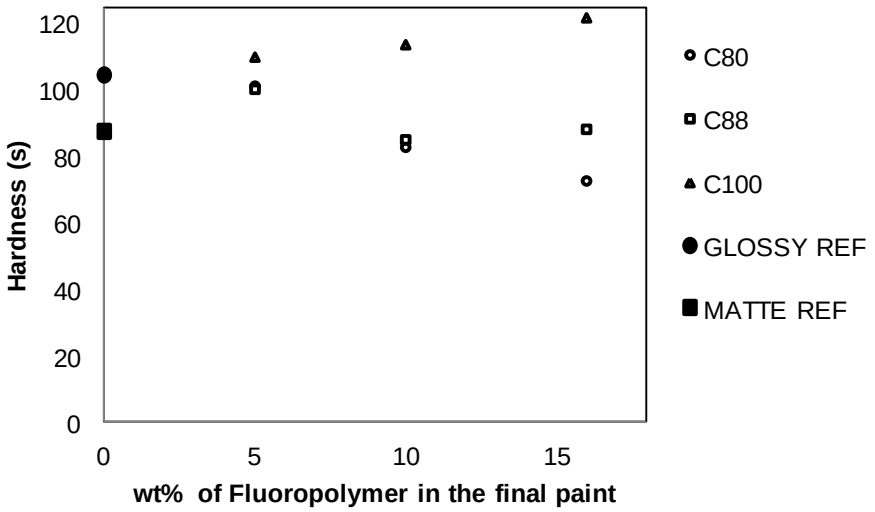

Figure 6.19. Hardness with respect to the concentration of fluoropolymer in the final paint.

The hardness of the paints decreased with the increase in the fluoropolymer content, with both copolymers because C80 and C88 were softer than the Stq Nu resin. C80 copolymer gave softer paints than the C88 copolymer due to its lower Tm (see Figure Figure 6.18,a). The incorporation of the fluorinated homopolymer increased the hardness of the paint because of the hard nature of homopolymer (Tm ≈ 76ºC, Figure 6.18,a).

Figure 6.20 shows the variation of the hardness of the paints when 1/3 of matting agent was introduced in the system.

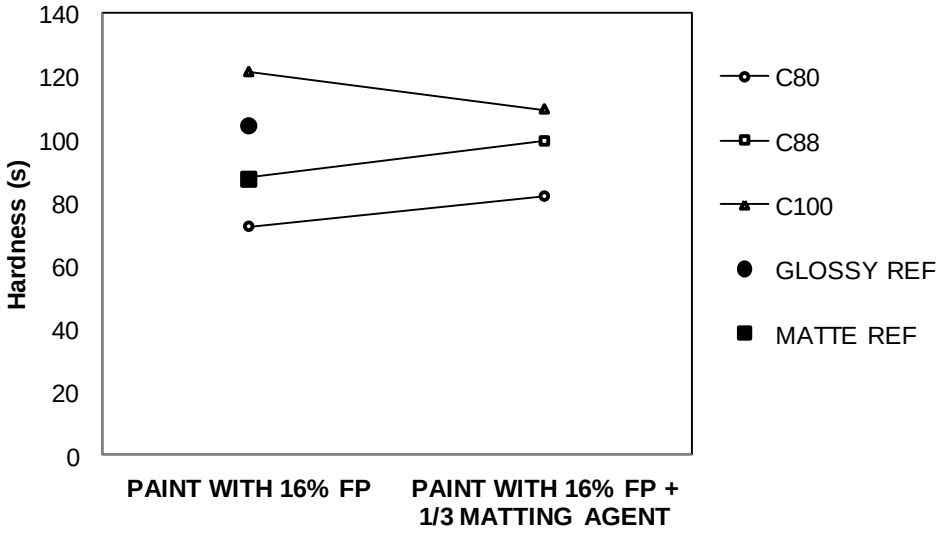

Figure 6.20. Hardness with and without the introduction of 1/3 of the appropriate amount of matting agent.

With the introduction of 1/3 of the appropriate amount of matting agent, the hardness of both paints with fluorinated copolymers increased (C80 and C88), and the hardness of the homopolymer paint decreased (C100). The increase for C80 and C88 was due to the substitution of the soft polymer by the harder matting agent. In the case of the PFDA homopolymer, the hard crystalline homopolymer was substituted by the matting agent which was softer than PFDA. With the homopolymer and the C88 we can reach at least the same hardness as with the harder reference (glossy reference).

6.3.3. Chemical Resistance

The chemical resistance to water, a mixture of ethanol and water (1:1) and coffee was tested. The tests were carried out as follows (Figure 6.21):

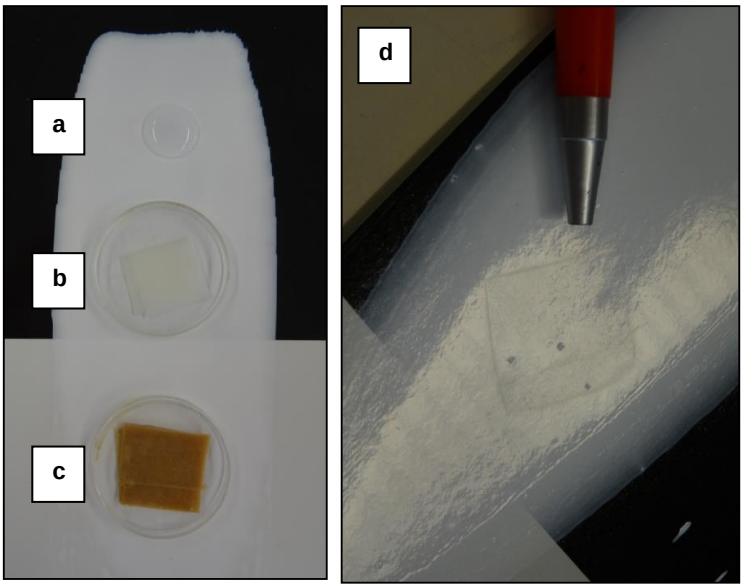

Figure 6.21. Chemical resistance test. a) water resistance 4h, b) ethanol-water resistance 1h, c) coffee resistance 1h, d) damage on the paint surface after ethanol test.

Water resistance:

A drop of water was placed on top of the paint and left in contact with the paint for 4 hours (Figure 6.21,a). After this time, the droplet is gently removed with a clean paper cloth.

Ethanol-water resistance:

An ethanol in water solution was prepared in a 1:1 wt% ratio. A piece of paper cloth was placed on top of the paint and wet with the ethanol solution. The cloth was covered with a glass dish and left in contact with the paint for 1 hour (Figure 6.21,b). After this time, the cloth was removed and the remaining liquid solution was cleaned gently with a clean paper cloth.

Coffee resistance:

A standard coffee solution was prepared dissolving 2 g of Nescafe Coffee in 50 g of water. As in the previous case, a piece of paper cloth was placed on top of the paint and wet with the coffee solution. The cloth was covered with a glass dish and left in contact with the paint for 1 hour (Figure 6.21,c). After this time, the cloth was removed and the remaining liquid coffee was cleaned gently with a clean paper cloth.

The damage that the water, ethanol-water solution and coffee produced to the paint was visually evaluated. The paints were graded from 1 to 5, where 5 is the best, so no damage is produced to the surface and 1 is the worst. The results of the chemical resistance test are shown in Figure 6.22.

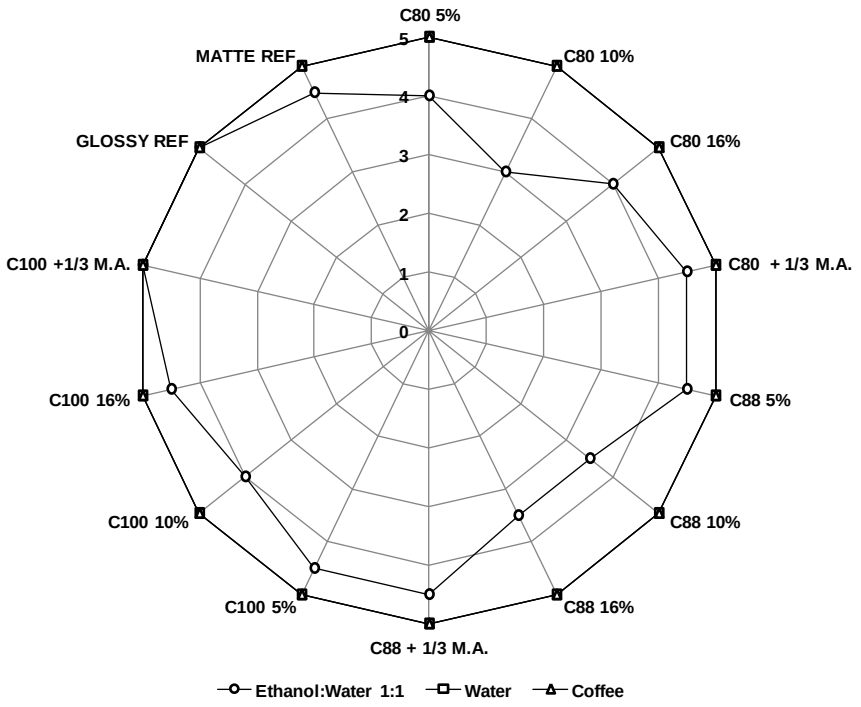

Figure 6.22. Results for the chemical resistance test.

As can be observed, the results for the coffee and water test are 5 for all the cases, what indicates that the resistance of the paints to the coffee and water is excellent.

The ethanol resistance is always more complicated, especially for the case of matte surfaces. The matte paints, in contact with ethanol, are generally damaged showing after the test a shiny surface in the area in contact with the ethanol and with its vapour. The ethanol acts as a cosolvent improving the film formation and leading to a shiny surface. For the case of the glossy paints, since they are already shiny, the effect of ethanol is not almost visible. According to the results in Figure 6.22, the ethanol resistance was especially good for the paint containing

the fluorinated homopolymer and 1/3 of matting agent (C100+1/3 M.A.). The paint with the C88 and 1/3 of matting agent, that gave good results in hardness and low gloss values, showed as well good chemical resistance with a value of 4.5 in the ethanol test.

6.3.4. Water Vapour Resistance

In order to test the water vapour resistance of the paints, walnut wooden panels were coated with the paints. To coat the wooden panels, a first layer of the paint is applied. After 24 hours of drying it is sanded in the direction of the wood grain, and then, a second layer is applied on top of the first one. The paint is left to dry for one week before the test is done.

To perform the test, the following steps are done (see Figure 6.23):

1. The wooden panels are coated as described previously.
2. The wooden panels are placed covering a container with boiling water during 1h.
3. The surface is gently dried with a paper cloth and a cross cut is done in the region of contact.
4. The cut section is placed again covering a container with boiling water during 1 h.
5. Finally, the surface is dried with a paper cloth. Immediately, an adhesive tape is stuck to the surface and sharply removed.

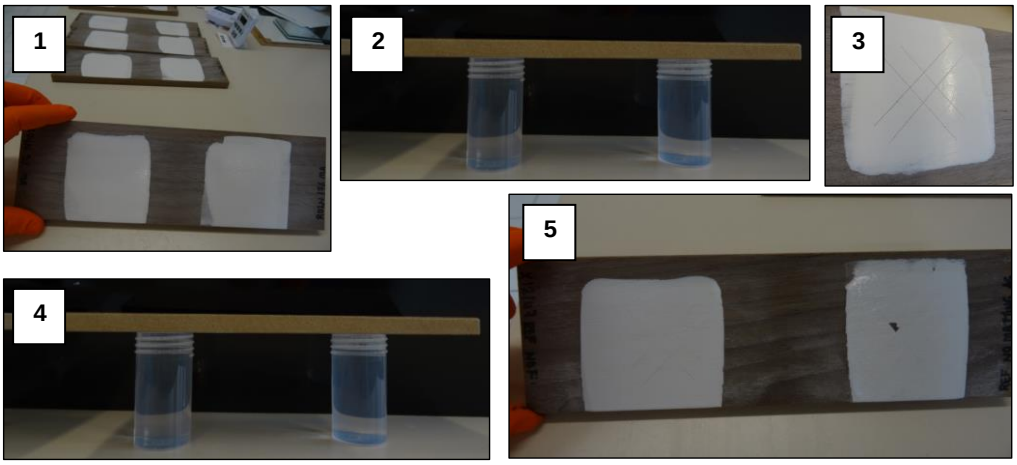

Figure 6.23. Water vapour resistance test

At the end of the test, the only panel that failed and had damage on its surface was the one of the glossy reference, as can be observed in the paint of the right side of picture 5 in Figure 6.23. All the panels coated with the paints containing fluorinated polymer demonstrated to be resistant to water vapour in the conditions of the test.

6.3.5. Water Vapour Resistance in blue pigmented paints

In order to see the effect of the addition of a coloured pigment to the paint, blue pigmented paints were prepared for the different formulations. To prepare these blue pigmented paints, 4 wt% of a blue ink (with respect to the total amount of paint) was added to the white pigmented paints and properly mixed to achieve a good dispersion of the pigment. The paints were casted onto white coated standard Q-panels[21]. Once the panels were dried, they were divided in two parts to perform two different kind of tests. The lower part of the panel was used to evaluate the resistance to water during a long period of time and the upper part of

the panel was used to test the resistance to water vapour. Both procedures are described below.

Water resistance:

The procedure in which this test was carried out is not standardized and can be done in different ways depending on the system. In this particular case, it was set along the way in order to see some differences between the different panels. Since the failure time of contact of the paint with water could not be predicted, the test was done as follows.

A cross cut was done in the lower part of the panel and the panels were immersed in a water bath at ambient temperature for four hours per day during four consecutive days. After this stage, no damage was observed in the paints; therefore, the panels were immersed in a water bath for 48 consecutive hours. The appearance of the panels after the test is shown in Figure 6.24. It can be seen that after this second step, some blisters appeared in both the matte and the glossy references, which is a sign of a lower water resistance.

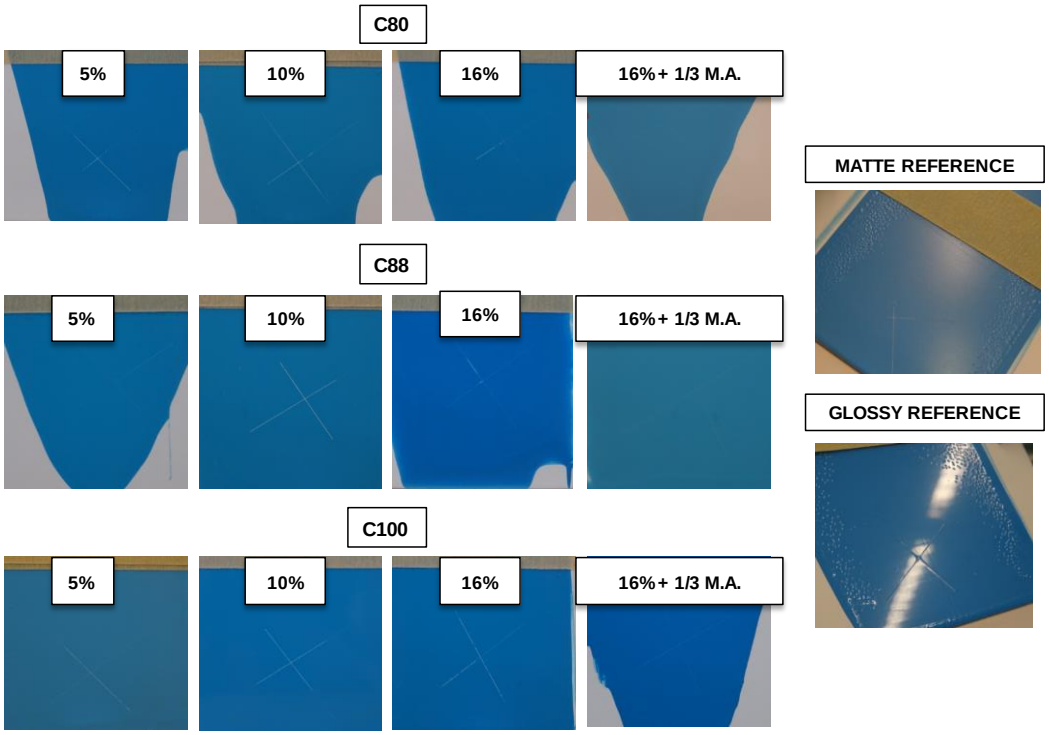

Figure 6.24. Panels after water immersion.

The panels were gently dried with a paper cloth and afterwards, an adhesive tape was stuck to the surface and sharply removed. The results after this treatment are presented in Figure 6.25.

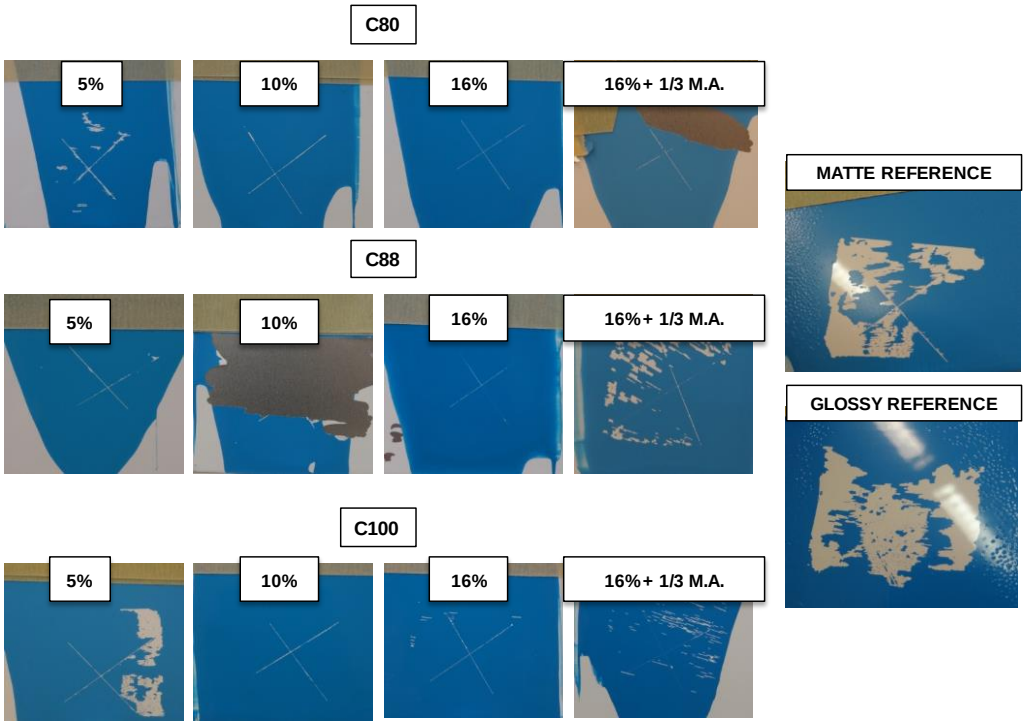

Figure 6.25. Panels after adhesion test.

In the pictures for the different paints, it is clear that both references were highly damaged after the test. The paints containing fluoropolymer seem to resist much better the test, showing little damage and retaining the majority of the paint in most cases. In the case of the paints C80 16% + 1/3 M.A. and C88 10%, it was the white paint that covered the panel the one that failed.

Water vapour resistance:

The upper side of the panels, which was not in contact with water, was used to evaluate the water vapour resistance during a long time exposure. In this case, the blue coated panels

were placed covering a container with boiling water during 4 hours. The boiling water was changed every hour with new boiling water. After four hours of exposure, the damage is evaluated visually. As can be seen in Figure 6.26, the contact with water vapour leaves a circle mark on the paint surface. This circle shape that comes from the shape of the water container is especially visible in the matte reference and the glossy reference also contains some blisters.

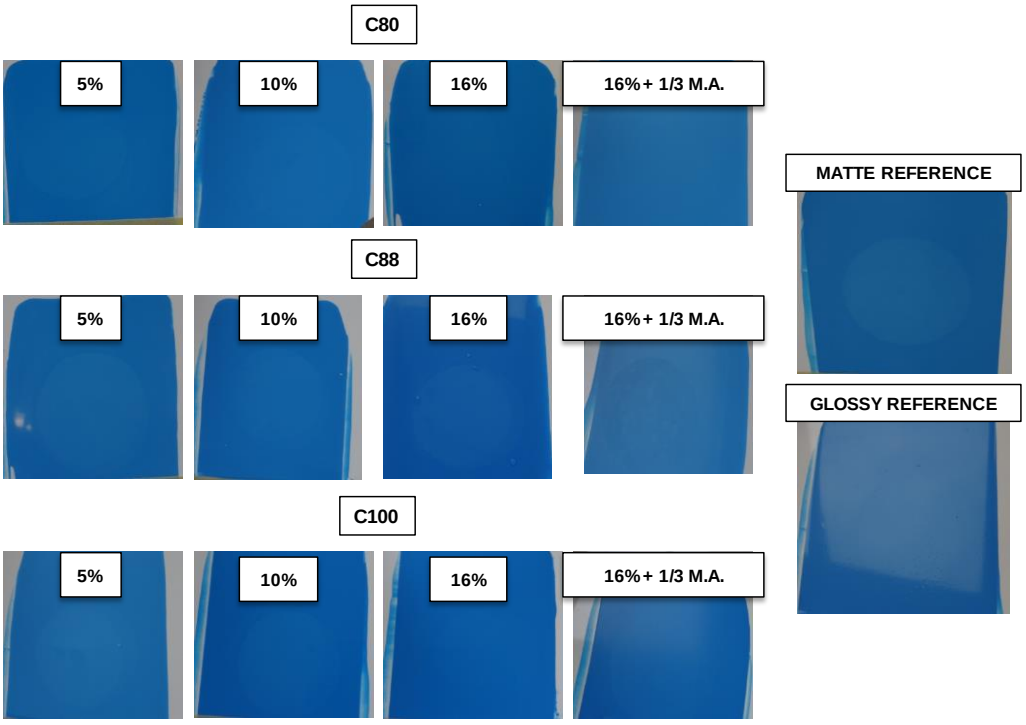

Figure 6.26. Panels after water vapour resistance test.

6.3.6. Surface Cleanability

The surface cleanability is a very important property because it is always desirable for a coating to maintain its surface as clean as possible[22]. Hydrophobic coating technology is one of the most promising approaches to improve surface cleanability and reduce dirt pick up[23]. The surface cleanability was studied through two different approaches:

- Attachment of the dirt to the surface: DIRT PICK UP

- Detachment of the dirt from the surface: SURFACE CLEANING OR EASY TO CLEAN PROPERTIES

The ideal situation to have in a coating would be LOW DIRT PICK UP together with EASY TO CLEAN PROPERTIES, which will result in surfaces that uptake low amount of dirt and are easy to clean since dirt does not adhere so well to the surface.

In this work, the surface cleanability is studied following different procedures. For this purpose, various sets of Q-panels were coated with the different white paints. The procedures are described below.

Outdoor exposition: dirt pick up

The coated panels were placed outdoors during several weeks (Figure 6.27). Since all the panels are exposed to the same atmospheric conditions, the differences in the dirt that they uptake should come from the nature of the material of the coating.

Figure 6.27. Panels exposed outdoors.

In Figure 6.28, the panels are shown after 12 weeks of outdoor exposure. As can be observed, a clean reference has been included, which is a panel with a paint that has not been exposed outdoors. Additionally, for the sake of comparison, a panel with a bad reference was prepared. This paint contained a soft resin from Nuplex that gives bad results on dirt pick up and it is commonly used as a reference.

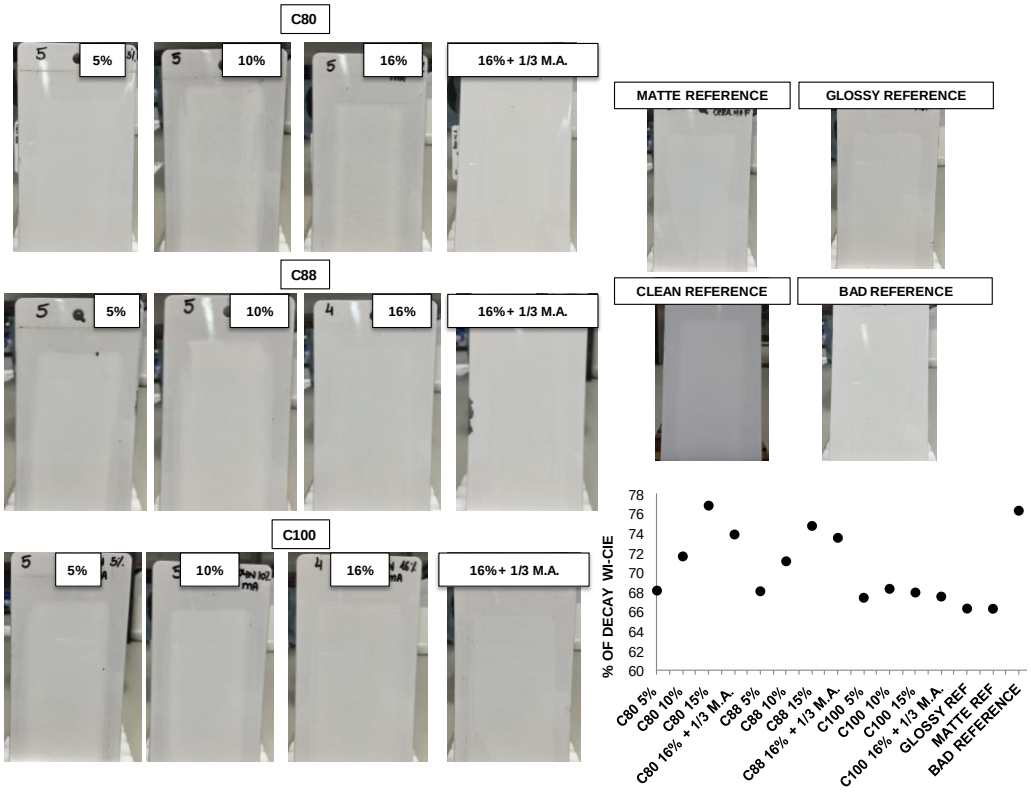

Figure 6.28. Panels after 12 weeks of exposure / % of decay WI-CIE.

Visually, it is complicated to appreciate a difference between the clean panel (CLEAN REFERENCE) and the rest of the panels that were placed outdoors, which in fact is a good sign that shows good resistance to dirt. In order to keep a track of the dirt that each panel is uptaking, the Whiteness Index (WI-CIE) was measured after and before the outdoor exposure. Whiteness is a single number index that indicates the relative degree of whiteness of near-white materials under specific lighting conditions. The CIE Whiteness was developed by the French International Commission on Illumination (also called CIE) and it is the most commonly

used whiteness index. It normally refers to measurements of whiteness done under a standard representation of outdoor daily light (D65 standard illuminant)[24]. The whiteness index of the different panels was measured with a Color i5 Spectrophotometer (X-Rite) before and after the outdoor exposure and the % of decay of WI-CIE is calculated as follows.

$$\%\ \boldsymbol{of\ WI-CIE\ decay} = \frac{(\boldsymbol{WI-CIE_{initial}})-(\boldsymbol{WI-CIE_{after\ 12\ weeks}})}{(\boldsymbol{WI-CIE_{initial}})} \cdot \mathbf{100} \qquad \textbf{(5.1)}$$

According to this expression, those panels that were more damaged by the outdoor exposure will present higher percentages of WI-CIE decay because they will look less white.

As can be observed in the graph in Figure 6.28, the ones with higher values of % of WI-CIE decay correspond to the bad reference and the paint containing 16% of C80 due to the softer nature of this material. The best results (lower values of % of WI-CIE decay) were given by those paints containing the fluorinated homopolymer and the references.

Additionally, the dirt removal or surface cleanability was studied. Carbon black is used as dirt and it was put in contact with the coated panels under different conditions.

WET DIRT CONTACT AT ROOM TEMPERATURE
DRY DIRT CONTACT AT ROOM TEMPERATURE
DRY DIRT CONTACT AT T=80ºC
} SURFACE CLEANING PROPERTIES

Wet dirt contact at room temperature

As it is represented in Figure 6.29, a carbon black dispersion in water (1 wt%) was prepared and 10 droplets of the dispersion were placed on top of each panel. The droplets were left to dry during two days and then, the dirt was removed following always the same procedure. The panels were put in an inverted position and tapping the panel through another surface, the loose dirt was removed. Afterwards, with compressed air, the extra dirt was removed. Finally, with a clean paper cloth and water, the surface was gently cleaned until the point in which no extra dirt could be removed from the panel.

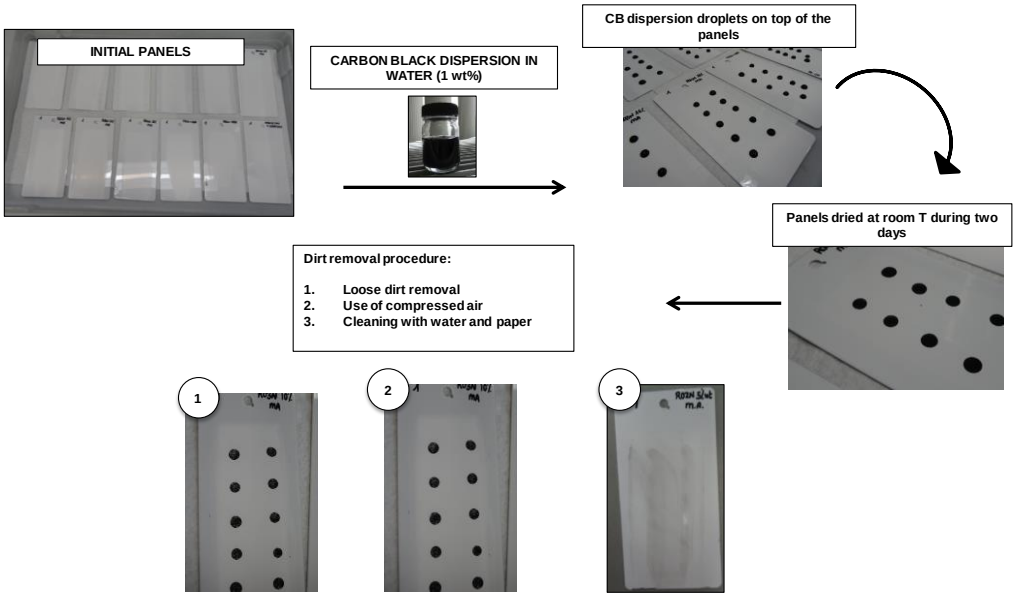

Figure 6.29. Wet dirt contact procedure (T amb)

Dry dirt contact at room temperature

Carbon black in a powder state was firstly dried overnight in the oven and afterwards, left to recover at ambient temperature. As shown in Figure 6.30, six spots of carbon black powder were placed on top of each panel. The powder spots were in contact with the panels for two days and then, the dirt was removed following the same procedure that was described for the wet dirt contact.

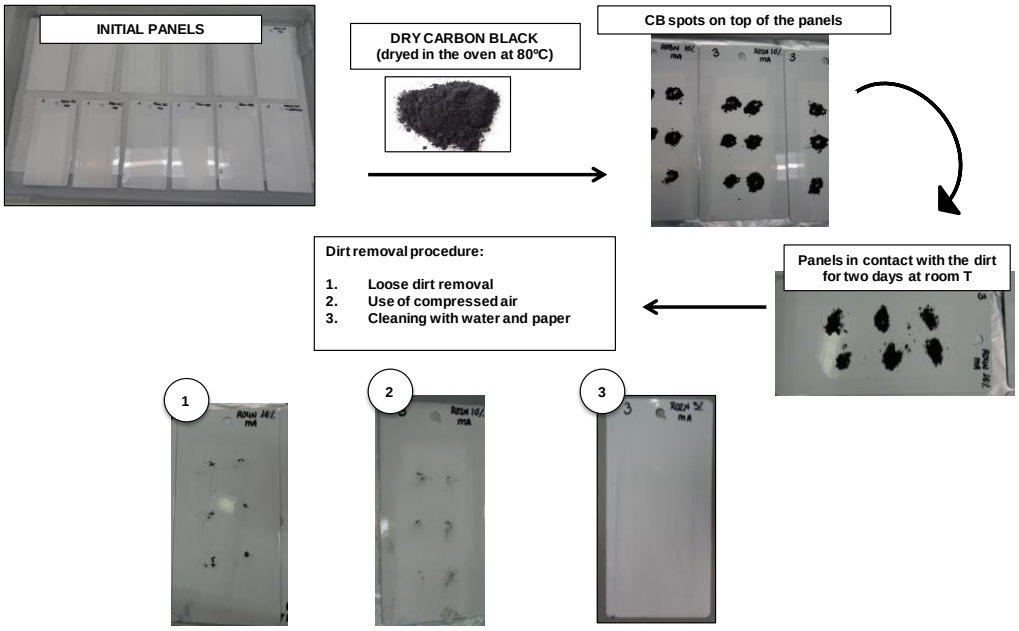

Figure 6.30. Dry dirt contact procedure (T amb)

Dry dirt contact at T=80ºC

As in the previous case, carbon black in a powder state was firstly dried in the oven overnight and afterwards, left to recover ambient temperature. Six spots of carbon black powder were placed on top of each panel. The panels with the powder were kept in the oven at 80ºC during 24 hours and then, they were maintained at ambient conditions for another 24 hours. After that, the dirt was removed following the same procedure previously described. The procedure is represented in Figure 6.31.

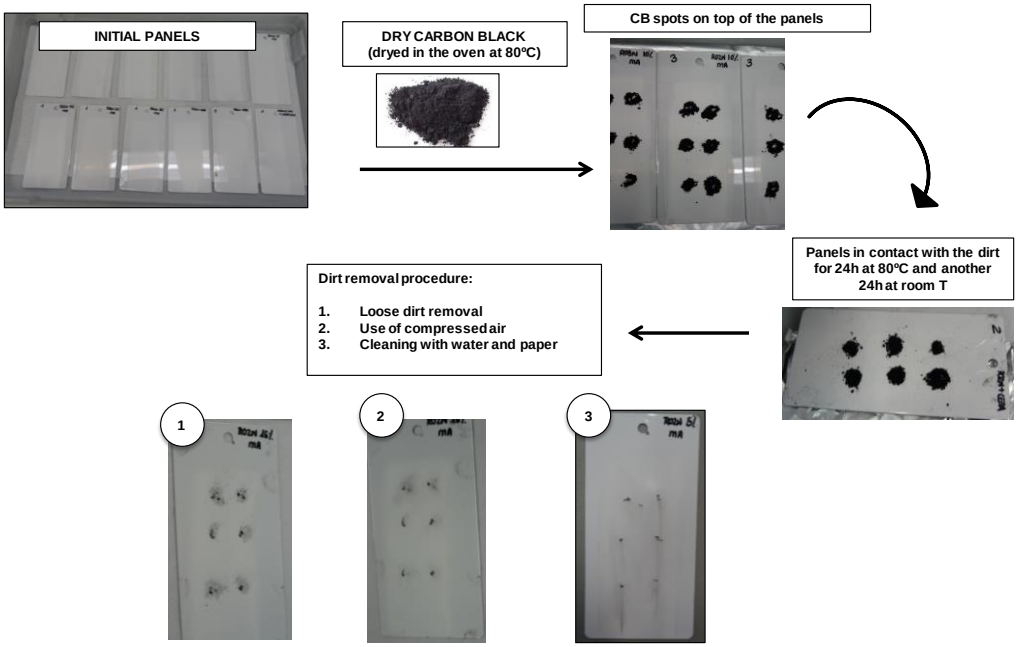

Figure 6.31. Dry dirt contact procedure (T=80ºC)

The panels for the different drying procedures after the cleaning stage are shown in Figure 6.32, Figure 6.33 and Figure 6.34. As a general observation for the three cases, those

panels containing 5% of the fluorinated resin seem to have better easy to clean properties. When the content of C80 and C88 is increased, the cleanability of the surface gets worse probably because the final paint is less hard. On the contrary, when the content of fluorinated homopolymer (C100) is increased, the panels have cleaner appearance and the surface cleanability is improved. It is possible to compare how easy to clean the panels are under the different conditions of the contact with dirt. According to the pictures, those films in contact with the dirt at 80ºC are visually the most affected by the contact of the dirt. This could be expected because a temperature of 80ºC is higher than the Tm of the polymers present in the system and therefore dirt gets more stuck to the paints. In the experiments in which the dirt was tested at ambient temperature, the paints in contact with the dry dirt were more easy to clean than the ones in contact with the wet dirt. This could be due to capillary forces present in the case of the wet dirt contact. As the water is being evaporated, the curvature of the air-water interface, because of the presence of dirt particles, creates a large negative pressure in the fluid which presses the dirt to the paint surface[25].

WET DIRT CONTACT AT ROOM TEMPERATURE

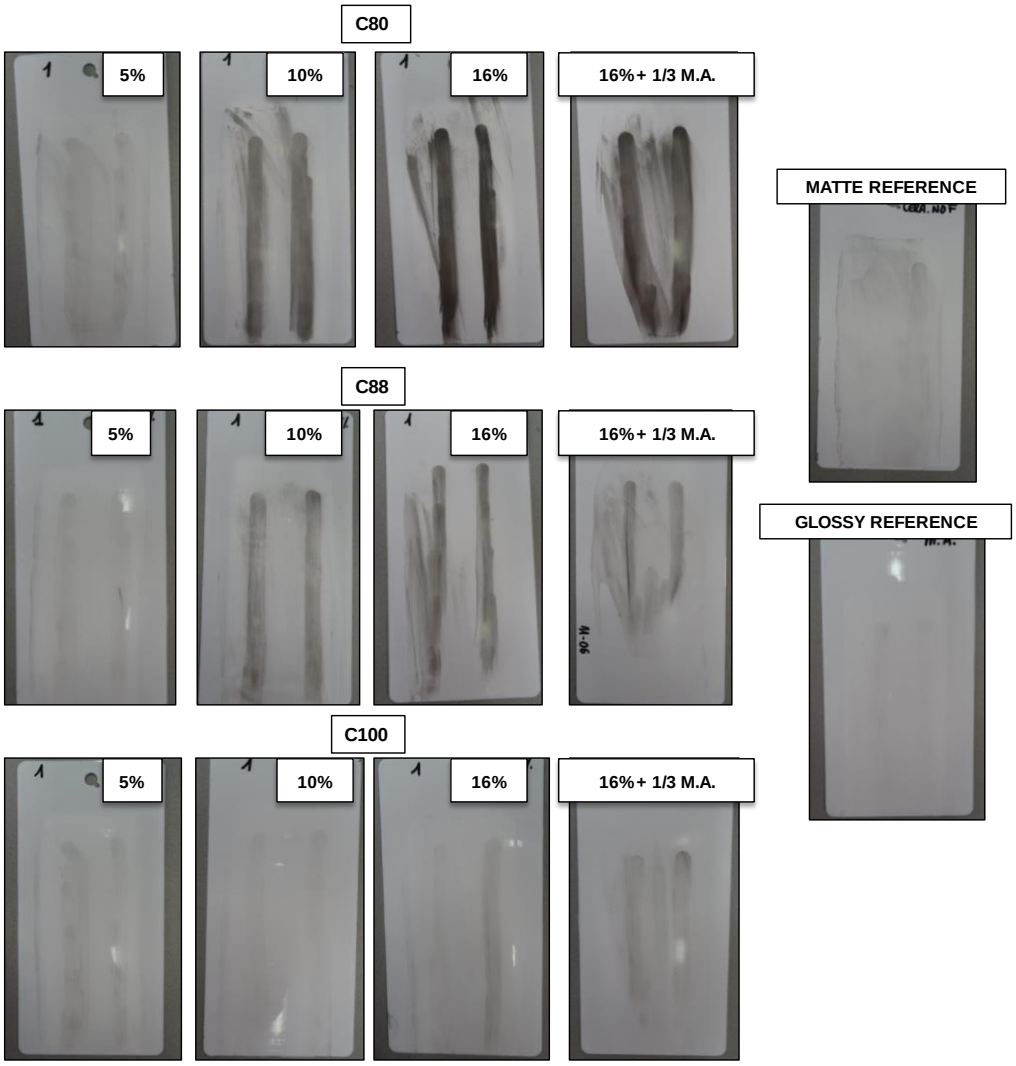

Figure 6.32. Panels for the wet dirt contact after the cleaning procedure.

DRY DIRT CONTACT AT ROOM TEMPERATURE

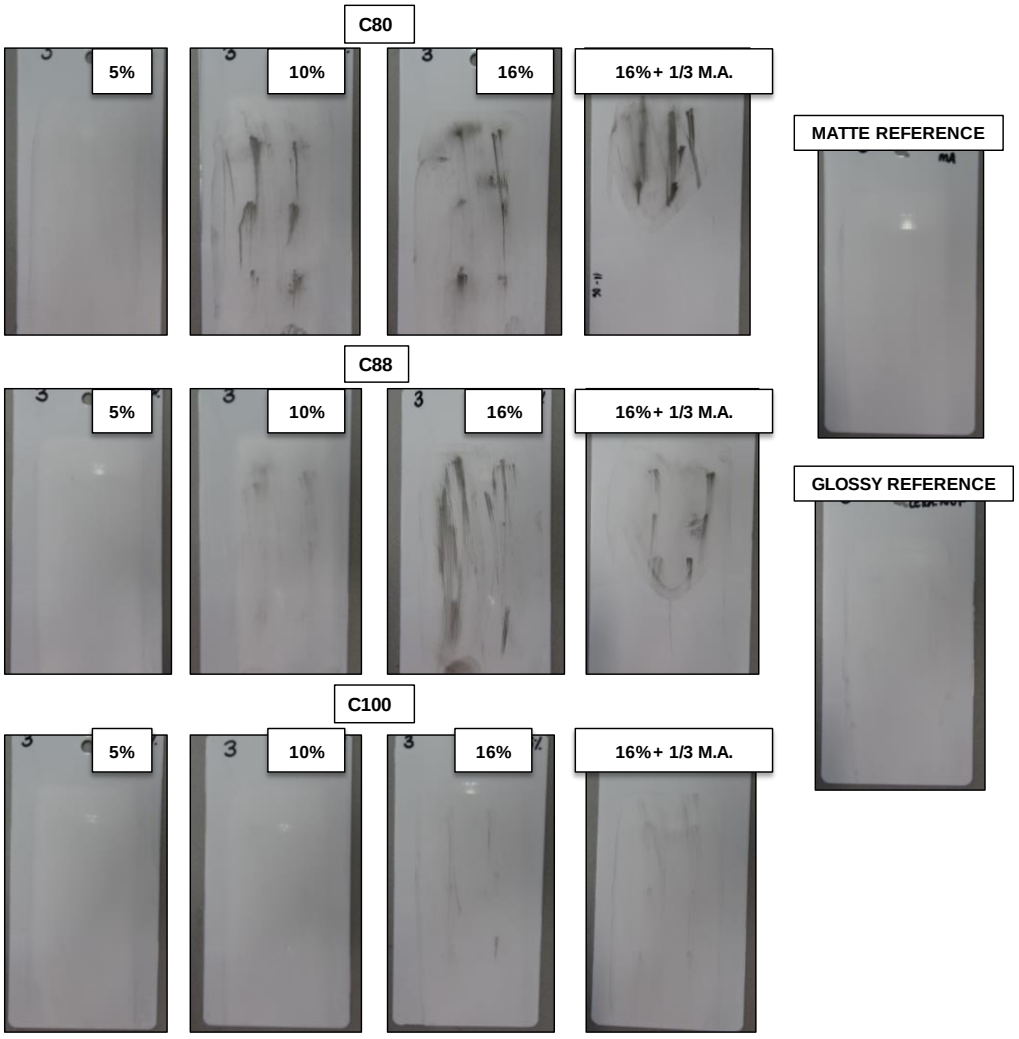

Figure 6.33. Panels for the dry dirt contact (Tamb) after the cleaning procedure.

DRY DIRT CONTACT AT T=80ºC

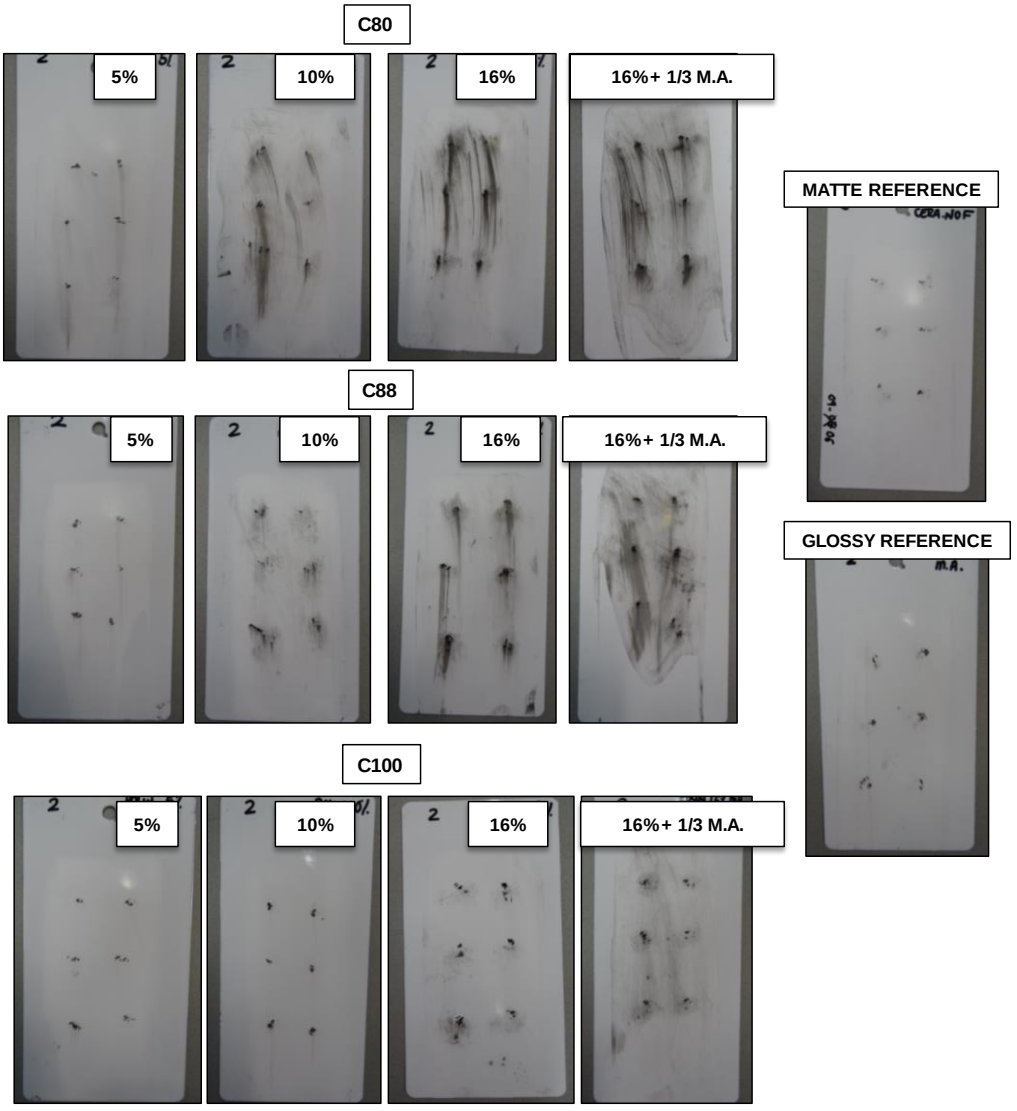

Figure 6.34. Panels for the dry dirt contact (T=80ºC) after the cleaning procedure.

6.3.7. Use of the soft fluorinated resin as plasticizer to reduce VOCs in paints

The development of low VOC paints is a matter of great interest nowadays due to environmental concerns. Indeed the limitations in volatile organic compounds are getting tougher due to their contribution to ozone and smog formation and their connection to respiratory illnesses[26]. The use of water media instead of solvent based processes is already a big improvement to the development of more environmentally friendly paints. However these waterborne paints still need a certain amount of solvent to improve film formation depending on the nature of the polymer resin. A possible way to further reduce VOCs can be the use of softer polymer resins in order to reduce the amount of cosolvent used in the formulation. With this idea in mind, the soft nature of the fluorinated resin C80 makes it potentially valuable to be used as a component in the formulation that will help in the film formation. In this way, the amount of cosolvent present in the formulation can be reduced or totally replaced.

For this study, three different paints were formulated with no cosolvent. Each paint contained the formulation of the initial Nuplex paint (Table 6.1), but with any cosolvent in the let-down, and with any matting agent, and they contained 16% of the fluorinated polymer resin as in the previous examples. As can be seen in Figure 6.35, the paints with C88 and C100 resins were full of cracks and the quality of the film was extremely bad. For the case of the paint containing the C80 copolymer, the quality of the film was much better due to the soft nature of this material but as can be seen in the point in the left of Figure 6.36, the paint was very soft and also the gloss was relatively high considering that the hardness for the matte reference was around 87 seconds and the gloss at 20º was around 9 and 37 at 60º. In order to improve

hardness and to try to reduce gloss, combinations between the different fluoropolymer resins within the same paint can be done. Specifically, the C80 and C100 resins were incorporated in a 1:1 ratio in a final 16% of the fluorinated resin into the final paint, but the quality of the film was not good and the paint contained cracks although hardness was improved and gloss was reduced (see Figure 6.36, second example). In order to improve film formation in the next step, a mixture of C80 and C100 in a 2:1 ratio was included in the formulation without no cosolvent, and as can be observed in the third case of Figure 6.36, the film formation was improved obtaining a good quality paint but still quite soft and glossy. In order to be able to blend in a 1:1 ratio, to have higher hardness and lower gloss values, a paint with half of the appropriate amount of cosolvent was formulated giving some interesting results. In this case, the hardness was higher and very close to the value of the matte reference and the gloss was very low reaching similar values to the matte reference for both 20º and 60º.

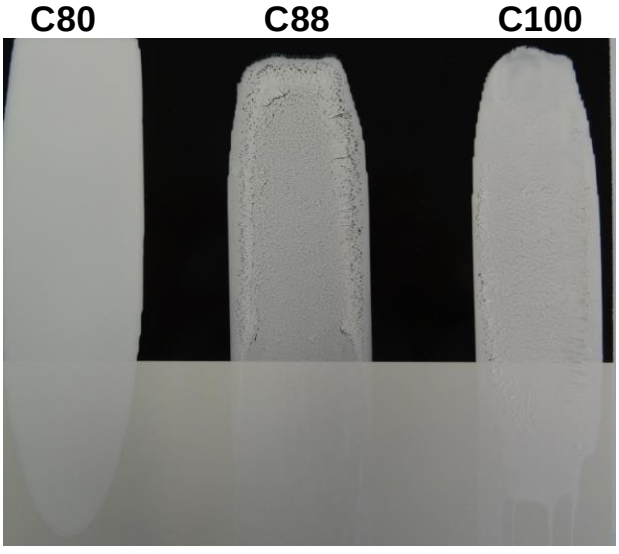

Figure 6.35. Paints containing 16% of fluoropolymer without cosolvent.

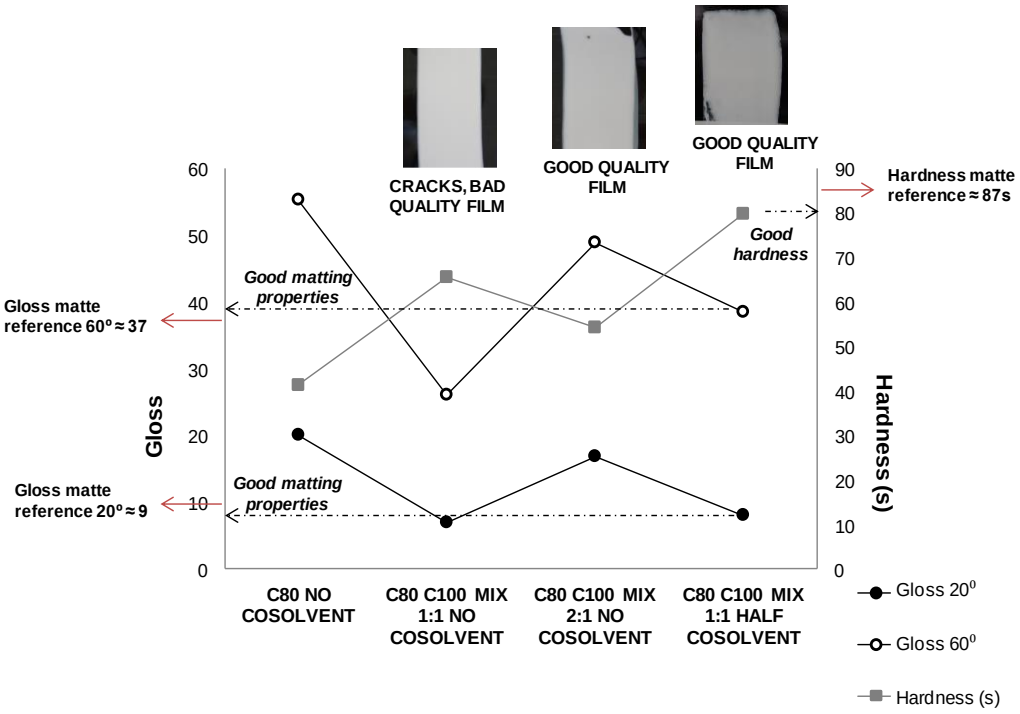

Figure 6.36. Paints with different compositions and cosolvent amounts: evolution of gloss and hardness.

From the SEM micrographs presented in Figure 6.37, it can be observed that in the C80/C100 mixtures, the fluorinated homopolymer particles are present at the top surface of the film. This improved the hardness of the final system and also, increased a little bit the matting efficiency by creating more imperfections in the surface which also had an effect on the contact angle being the last of the combinations the most hydrophobic one.

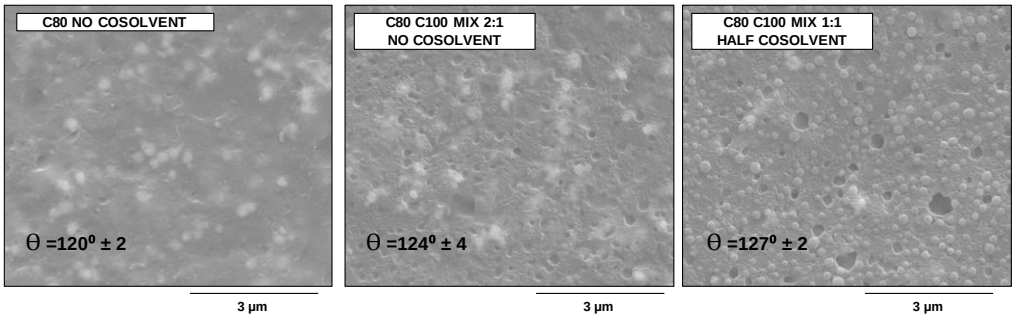

Figure 6.37. Paints with different compositions and cosolvent amounts: microstructure and contact angle.

Water and water vapour resistance were tested for the different paints and also for the references. The procedure followed was the same one as described in the previous section for the blue pigmented paints. In this case the paints were white and they were casted on top of white Q-panels, therefore the observation of the defects created by the water is more complicated. This is the reason why the adhesive tape with the detached paint is presented with every sample. The results for these tests are presented in Figure 6.38 and Figure 6.39.

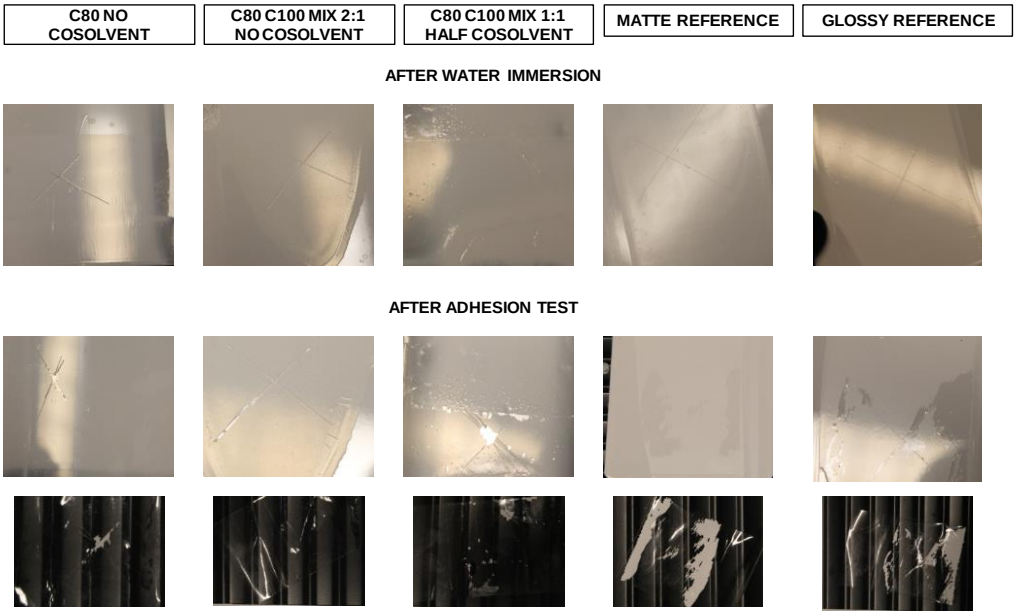

Figure 6.38. Paints after water immersion and adhesion test.

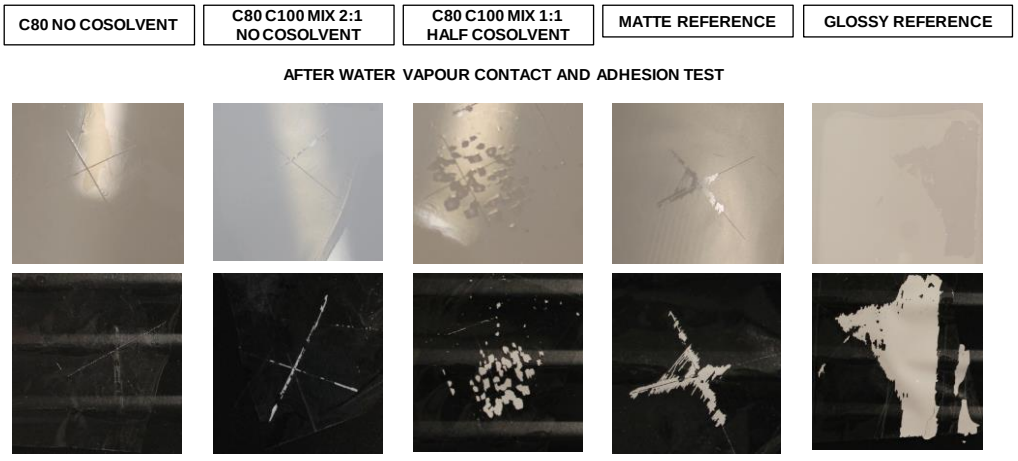

Figure 6.39. Paints after water vapour contact and adhesion test.

As can be observed in Figure 6.38, after the water immersion of the paints for four hours during four days and for two consecutive days, the paints containing fluorinated polymer did not show a big damage, only some blisters appeared in the references. When an adhesive tape was stuck to the cross cut region and detached from the surface it is clear that the references showed the biggest damage. The paints with no cosolvent showed an excellent resistance to water and the surface was much less affected by the contact with water.

The water vapour resistance presented in Figure 6.39 showed similar results and indeed it seems that the paints containing no cosolvent had an excellent resistance to water vapour after the adhesion test. When cosolvent was incorporated to the system, the water vapour resistance got worse and indeed the references suffered a serious damage based on the big residue left on the adhesive tape.

6.4. Conclusions

The synthesis of different fluorinated resins by miniemulsion polymerization using a high pressure homogenizer and their incorporation into commercial paint formulations was addressed in this work. The different resins showed diverse potential applications and improved properties in the different responses of study. The most important aspects of the different resins are exposed below:

Fluorinated homopolymer: C100 was especially good to increment the hardness of the final film and to improve the chemical resistance to different substances. The excellent resistance to ethanol is noteworthy. This fluorinated resin demonstrated low dirt pick up and good easy to clean properties as well as excellent water vapour resistance.

Fluorinated copolymer: C88 showed good matting properties and hardness. The replacement of 2/3 of the matting agent was achieved and the hardness of the system was good reaching similar values as the references. This resin demonstrated as well excellent chemical resistance to water and coffee and water vapour and a satisfactory chemical resistance to ethanol.

Fluorinated copolymer: C80 showed excellent matting properties. The incorporation of this resin into paint formulation was really efficient to replace high amounts of the matting agent, higher that 2/3 of the appropriate amount of the matting agent present in the initial formulation. The resin did not show the same levels of hardness as the references due to the soft nature of this polymer. The resin showed excellent chemical resistance to water, coffee and water vapour and an acceptable chemical resistance to ethanol.

Different combinations of the fluorinated polymer resins C80 and C100 were done within the same paints in order to produce products with optimized properties. Due to the soft nature of the C80 resin, it showed a potential application as plasticizer to produce low VOCs paints contributing to the efficient film formation in the final paint. By the combination of the fluorinated homopolymer C100 and the softer copolymer C80, a paint with high matting appearance, good hardness and excellent hydrophobicity and water resistance was achieved reducing the amount of cosolvent used to the half of the one used in the initial formulation and without using any matting agent.

6.5. References

(1) Paint Quality Institute; Water based vs. Solvent Based. Retrieved from: http://www.paintquality.com/en/understanding-paint/water-based-vs-solvent-based.

(2) Thomas, G. P.; (2013, December 12). Waterborne Coatings - Methods, Benefits and Applications. Retrieved from: http://www.azom.com/article.aspx?ArticleID=8561.

(3) The Effect of Water Resistance on the Durability of Waterborne Coatings. *Paint & Coatings Industry*. **2003**.

(4) Jones, B. Fluoropolymers for Coating Applications. *JCT CoatingsTech Mag.* **2008**.

(5) American Coatings Association. Fluoropolymer Coatings for Architectural Applications. *Coatings Tech*.

(6) Aharoni, S. M. Fluoropolymers and Fluoropolymer Coatings, **1991**.

(7) Iezzi, R. A.; Gaboury, S.; Wood, K. Acrylic-Fluoropolymer Mixtures and Their Use in Coatings. *Prog. Org. Coatings* **2000**, *40*, 55–60.

(8) Toefco Engineerd Coating Systems, INC. (2016, January 14). What is a fluoropolymer coating?. Retrieved from: http://toefco.com/what-is-fluoropolymer-coating/.

(9) The Freedonia Group. (2015, June). Fluoropolymers. Retrieved from: http://www.freedoniagroup.com/industry-study/3278/fluoropolymers.htm.

(10) Hall, D. J.; Giglio, N. M. *Graphic Standards Field Guide to Residential Construction*; **2011**.

(11) ProTect Painters; (2012, July 13). Matte Finish vs. Satin and Gloss: A Guide to Paint Finish Types. Retrieved from: http://www.protectpainters.com/our-blog/2012/july/matte-finish-vs-satin-and-gloss-a-guide-to-paint/.

(12) SpecialChem. Matting Effect Agents: Techno Brief. Retrieved from: http://coatings.specialchem.com/selection-guide/matting-agents-for-coatings.

(13) PQ Corporation. Silica Matting Agents and Flatting Agents for Paints and Coatings. Retrieved from: http://www.pqcorp.com/pc/EMEA/Markets/Surface-Coatings/Silicas-Matting-Agents-and-Flatting-Agents.

(14) Asua, J. M. Miniemulsion Polymerization. *Prog. Polym. Sci.* **2002**, *27*, 1283–1346.

(15) Asua, J. M. Challenges for Industrialization of Miniemulsion Polymerization. *Prog. Polym. Sci.* **2014**, *39*, 1797–1826.

(16) Manea, M.; Chemtob, A.; Paulis, M.; de la Cal, J. C.; Barandiaran, M. J.; Asua, J. M. Miniemulsification in High-Pressure Homogenizers. *AIChe J* **2008**, *54*, 289–297.

(17) López, A.; Chemtob, A.; Milton, J. L.; Manea, M.; Paulis, M.; Barandiaran, M. J.; Theisinger, S.; Landfester, K.; Hergeth, W. D.; Udagama, R.; et al. Miniemulsification of Monomer-Resin Hybrid Systems. *Ind. Eng. Chem. Res.* **2008**, *47*, 6289–6297.

(18) Gao, L.; McCarthy, T. J. How Wenzel and Cassie Were Wrong. *Langmuir* **2007**, *23*, 3762–3765.

(19) Babcock, K. L.; Prater, C. B. *Phase Imaging: Beyond Topography*.

(20) BYK-Gardner. *Introduction to Hardness*.

(21) Q-Lab. Q-panel standard substrates. Retrieved from: http://www.q-lab.com/products/q-panel-standard-substrates/q-panels

(22) Vandezande, G. Improved Dirt Pickup Resistance Critical to Future Coating Innovation. *Paint & Coatings Industry*. **2007**.

(23) Vandezande, G. Improved Dirt Pickup Resistance Critical to Future Coating Innovation. *Paint & Coatings Industry*. **2008**.

(24) Xerox Corporation. *Demystifying Three Key Paper Properties: Whiteness, Brightness and Shade*.

(25) Routh, A. F.; Russel, W. B. Deformation Mechanisms during Latex Film Formation: Experimental Evidence. *Ind. Eng. Chem. Res.* **2001**, *40*, 4302–4308.

(26) Interior Paints. **2009**. Retrieved from: *http://www.consumerreports.org*.

Chapter 7. Conclusions

The purpose of this Thesis was to produce highly hydrophobic (θ > 110º) and superhydrophobic (θ > 150º) cohesive and non-porous coatings applicable to large and irregular surfaces in a cost effective and environmentally friendly manner. The production of water repellent surfaces from water-based polymers is particularly challenging because in order to obtain stable polymer dispersions in water, particles should have a relatively hydrophilic surface. Furthermore, as reviewed in Chapter 2, most of the techniques used to obtain hydrophobic and superhydrophobic surfaces included the use of highly expensive procedures and they could not be applied to large and complex surfaces by the use of conventional coating methods.

In order to achieve this purpose, fluorinated polymers that provide natural hydrophobicity were used. These polymers also provide with a large number of additional benefits to the coatings such as low surface energy, insulating properties, impermeability to gases, high resistance to water, oil, chemicals, corrosion and UV radiation as well as low dirt pick up. As the water contact angle of these polymers is around 110º (the maximum within

polymers), the topography of the surface should be varied to increase the contact angle. Therefore, different methods to fine tune the film surface topography were developed.

Film-forming latexes were produced by miniemulsion copolymerization of the fluorinated monomer 1H, 1H, 2H, 2H-perfluorodecyl acrylate (PFDA) and 2-ethylhexyl acrylate (2EHA) in a 82/18 wt/wt ratio but polymer films from this latex yielded a contact angle of 114º. Formulations richer in PFDA led to higher contact angles, but films of poor quality were obtained at room temperature.

Blending of these latexes with a latex of PFDA homopolymer (which is not film forming at room temperature) did not show any improvement in the case of thick films because the denser PFDA particles sedimented due to the high density of the fluorinated polymer. Sedimentation was reduced by using thinner films and higher contact angles were observed (θ = 123º). In an attempt to take advantage of gravity, films were dried upside down and a contact angle of 130º was achieved because PFDA particles sedimented at the air-film interface. However, this type of drying was difficult to implement in practice. Higher contact angles (θ = 133º) were obtained reducing sedimentation by using a film forming 60 wt% solids content latex of poly(vinylidene chloride) that increased both the viscosity of the blend and the density of the soft polymer. A dual coating strategy which is not limited in terms of density of the polymers and takes advantage of the open time of the waterborne coatings was developed. In this strategy, a film forming dispersion was cast first and during its open time, a latex of hard hydrophobic particles is cast on top of it using spray coating. A contact angle of 137º was obtained using this strategy (Figure 7.1).

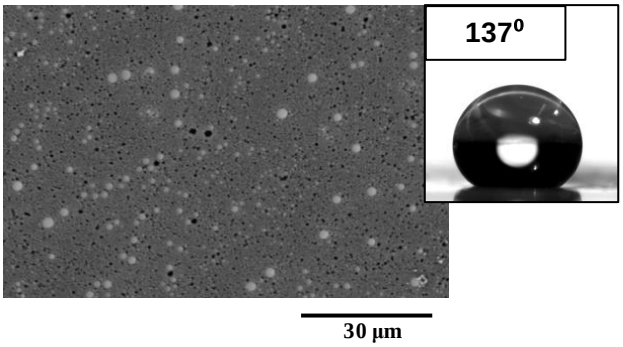

Figure 7.1. SEM image and water contact angle for a film obtained by means of the double coating strategy.

Another approach to increase the contact angle from the 114º obtained from the film forming copolymer PFDA/2EHA of 82/18 composition was to manipulate the film formation process of waterborne dispersions of PFDA/2EHA copolymers with different Tg values. The roughness of the different films cast from these dispersions was enhanced by creating wrinkles, which were naturally formed during film formation when the following conditions were met: 1) the rate of water evaporation was high enough to make the velocity of the receding water front faster than the rate of diffusion of the polymer particles in the wet film, and 2) the rate of coalescence of the particles was similar or faster than the rate of evaporation. Under these conditions, a polymer skin was formed at the film-air interface before the interior of the film becomes dry. The mechanical mismatch between the surface of the film and its interior led to the formation of wrinkles when the film dried. Among the different ways in which these rates could be modified, temperature and hardness of the polymer were chosen to demonstrate the proof of concept. This allowed the formation of transparent films with a wrinkled surface that

had a contact angle of 133º, which is a substantial increase with respect to the film cast under standard conditions (Figure 7.2).

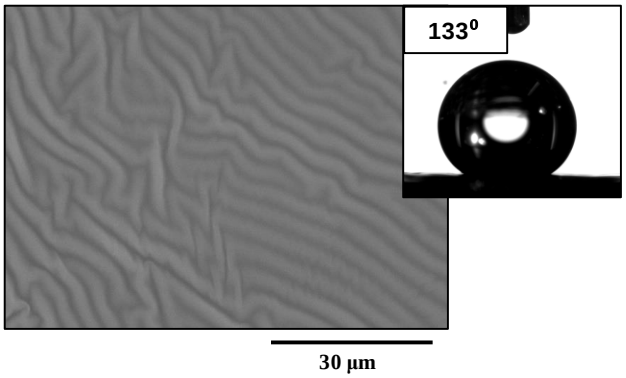

Figure 7.2. SEM image and water contact angle for a film obtained from a 75/25 PFDA/2EHA copolymer showing a wrinkled surface.

In order to reach the superhydrophobic regime (θ > 150º) a rougher topography of the film surface was necessary. A new method that allowed the formation of superhydrophobic coatings with good film forming properties and mechanical strength (Figure 7.3) was presented. The method involves the use of film forming coatings that are cast on the substrate and during the open-time of these films a second dispersion is sprayed on the first film. A key aspect of this development is the use of a fractal dispersion of a hydrophobic hard polymer. A method to synthesize relatively high solids fractal dispersions during the polymerization process is presented. Miniemulsion polymerization of PFDA was used and the surfactant and the initiator systems were used to control the fractal structure. This one step method is advantageous with respect to the previous methods that require two steps and usually achieve low solids contents.

A MMA/BA/MAA high solids film forming latex was used as a first coating. Contact angles > 150º, sliding angles of 7º and contact angle hysteresis ≈ 5º that belong to the superhydrophobic regime were obtained. The film showed oleophobic behaviour giving a contact angle of 120º for olive oil. The films showed good mechanical strength retaining an acceptable hydrophobicity (θ = 140º) after 50 cycles of an aggressive scrub test.

Icephobicity of the sprayed materials was tested and compared with a conventional MMA/BA/MAA coating. Although ice formation and accumulation on top of the surface still occurred for the sprayed systems, they demonstrated potential to reduce ice adhesion strength to the surface as compared to the MMA/BA/MAA film, maintaining their hydrophobic character under water vapour condensation conditions.

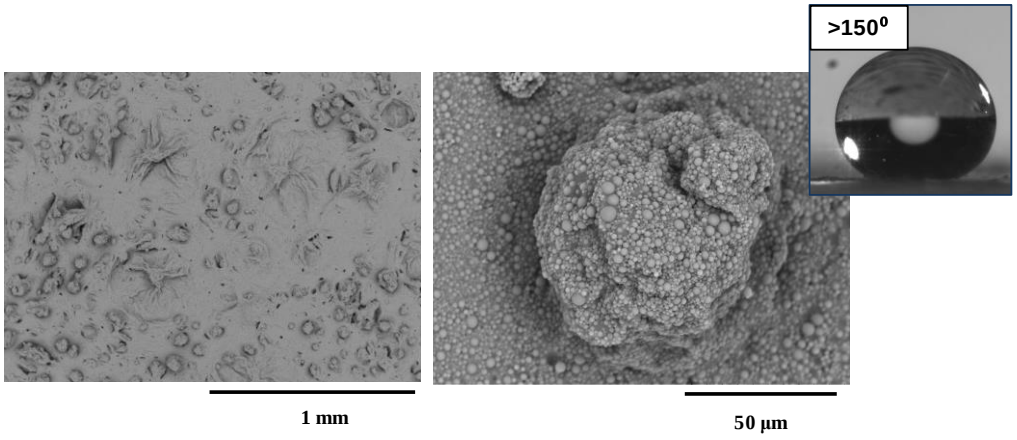

Figure 7.3. SEM micrographs and contact angle for the films produced by spraying a fractal aggregated polymer dispersion on top of a film forming latex.

After analyzing the potential of fluorinated polymers to produce hydrophobic and superhydrophobic coatings, the fluorinated homopolymer and copolymers were incorporated into paint formulations in order to evaluate their performance. Preliminary studies done with some copolymer latexes synthesized in previous stages of the work showed that these polymers provide a matte appearance to the surface. Therefore, the possibility of replacing the commercial matting agent used in the original formulation was also studied. A fluorinated PFDA homopolymer (C100) and two PFDA/2EHA/MAA copolymers in 80.8/17.7/1.5 and 88.6/9.9/1.5 wt/wt/wt ratios respectively abridged as C80 and C88 were analyzed. The most important aspects of the incorporation of each polymer into paint formulation are summarized below:

Fluorinated PFDA homopolymer: C100 was especially good to increment the hardness of the final film and to improve the chemical resistance to different substances. The excellent resistance to ethanol is noteworthy. This fluorinated resin demonstrated low dirt pick up and good easy to clean properties as well as excellent water vapour resistance.

Fluorinated PFDA/2EHA/MAA 88.6/9.9/1.5 copolymer: C88 showed good matting properties and hardness. The replacement of 2/3 of the matting agent originally contained in the formulation was achieved and the hardness of the system was good reaching similar values as the references. This resin demonstrated as well excellent chemical resistance to water and coffee and water vapour and a satisfactory chemical resistance to ethanol.

Fluorinated PFDA/2EHA/MAA 80.8/17.7/1.5 copolymer: C80 showed excellent matting properties. The incorporation of this resin into paint formulation was really efficient to replace high amounts of the matting agent, higher that 2/3 of the appropriate amount of the matting

agent present in the initial formulation. The resin did not show the same levels of hardness as the references due to the soft nature of this polymer. The resin showed excellent chemical resistance to water, coffee and water vapour and an acceptable chemical resistance to ethanol.

Different combinations of the fluorinated polymer resins C80 and C100 were done within the same paints in order to produce products with optimized properties. Due to the soft nature of the C80 resin, it showed a potential application as plasticizer to produce low VOCs paints contributing to the efficient film formation in the final paint. By the combination of the fluorinated homopolymer C100 and the softer copolymer C80, a paint with high matting appearance, good hardness and excellent hydrophobicity and water resistance was achieved reducing the amount of cosolvent used to the half of the one used in the initial formulation and without using any matting agent.

Overall, it can be concluded that hydrophobic and superhydrophobic coatings were successfully produced from waterborne fluoropolymer dispersions showing good film forming properties and mechanical strength.

List of publications and conference presentations

Part of this Thesis have been published or will be published soon. The list of papers that would be issued from this work is as follows (variation in the authors list and/or paper title might be possible).

"**High Highly hydrophobic coatings from waterborne latexes**" Ana B. López, José C. de la Cal, José M. Asua. Submitted to Langmuir (18/03/2016).

"Controlling film topography to form highly hydrophobic waterborne coatings" Ana B. López, José C. de la Cal, José M. Asua. Submitted to Soft Matter (9/05/2016).

"From fractal aggregation to superhydrophobic coatings" Ana B. López, José C. de la Cal, José M. Asua. To be submitted.

"Incorporation of waterborne fluoropolymers in paint formulation" Ana B. López, Silfredo J. Bohórquez, Marcel Meeuwise, Dirk Mestach, José C. de la Cal, José M. Asua. To be submitted.

Parts of this work have been presented in national and International Conferences, as well as in internal meetings from the Industrial Liason Program (ILP).

Oral presentations

"Waterborne fluoropolymer dispersions for hydrophobic coatings", Ana B. López, José C. de la Cal, José M. Asua. JIP-VII Congreso de Jóvenes Investigadores en Polímeros, Menorca, Spain, May 2013.

"Waterborne fluoropolymer dispersions for hydrophobic coatings", Ana B. López, José C. de la Cal, José M. Asua. Career in Polymers VI Workshop, Prague, Czech Republic, July 2014.

"Waterborne fluoropolymer dispersions for hydrophobic coatings", Ana B. López, José C. de la Cal, José M. Asua. 3rd Workshop by the Working Party of Polymer Reaction Engineering, San Sebastian, Spain, September 2014.

"Waterborne fluoropolymer dispersions for hydrophobic coatings", Ana B. López, José C. de la Cal, José M. Asua. Graduate Research Symposium (IPCG Conference), New Hampshire, United States, June 2015.

Poster presentation

"Waterborne fluoropolymer dispersions for hydrophobic coatings", Ana B. López, José C. de la Cal, José M. Asua. Frontiers of Polymer Colloids: from synthesis to macro-scale and nano-scale applications, Prague, Czech Republic, July 2014.

"Waterborne fluoropolymer dispersions for hydrophobic coatings", Ana B. López, José C. de la Cal, José M. Asua. 3rd Workshop by the Working Party of Polymer Reaction Engineering, San Sebastian, Spain, September 2014.

"Waterborne fluoropolymer dispersions for hydrophobic coatings", Ana B. López, José C. de la Cal, José M. Asua. International Polymer Colloids Group Conference, New Hampshire, United States, June-July 2015.

"Scientific Photography Award" in 1st Scientific Photography Contest organized by POLYMAT Institute (March, 2015)

"Award for Poster Communication" during the conference "Frontiers of Polymer Colloids: from synthesis to macro-scale and nano-scale applications" (July, 2014).

"Scientific Photography Award" in 2nd Scientific Photography Contest organized by POLYMAT Institute (March, 2014)

Resumen y conclusiones

El desarrollo de superficies hidrofóbicas y superhidrofóbicas ha despertado gran interés en los últimos años en el campo de los recubrimientos, donde la repelencia al agua supone un gran valor añadido. Estos revestimientos ofrecen múltiples posibilidades en diferentes aplicaciones tales como recubrimientos anticorrosivos, antibacterianos o incluso antihielo.

La hidrofobicidad de los materiales se caracteriza mediante la medida del ángulo que forma la superficie de una gota de agua al entrar en contacto con la superficie de un cierto material. De este modo, si el ángulo de contacto obtenido es superior a 90º la superficie se define como hidrofóbica y si el ángulo de contacto es superior a 150º la superficie se denomina superhidrofóbica. El ángulo de contacto de una superficie depende de la naturaleza del propio material, que puede ser caracterizada midiendo el ángulo de contacto de una superficie plana del mismo, y de la textura de la propia superficie. Las superficies artificiales más hidrofóbicas son aquellas formadas por polímeros fluorados, sin embargo, los ángulos de contacto medidos en superficies planas de dichos materiales generalmente no superan los 110º. Por tanto, para aumentar la hidrofobicidad de una superficie es necesario introducir cierta rugosidad en el sistema.

La mojabilidad de superficies rugosas ha sido ampliamente estudiada por Cassie y Wenzel llegando a la conclusión de que para conseguir superficies superhidrofóbicas, son necesarios perfiles de rugosidad muy pronunciados o incluso rugosidad a diferentes niveles. La naturaleza ofrece ejemplos de este tipo de estructuras tales como la hoja de la Flor de Loto, sobre la cual el agua no se puede depositar debido a que posee una estructura con rugosidad a distintos niveles. En los últimos años ha habido un gran avance en el desarrollo de materiales hidrofóbicos y superhidrofóbicos mediante el uso de diferentes técnicas para generar superficies con estructuras rugosas tales como la litrografía, tratamiento químico de las superficies o uso de moldes. Este tipo de técnicas permiten generar superficies con una microestructura muy controlada, sin embargo, en la mayoría de los casos su uso requiere un gran coste y no son técnicas aplicables para recubrir superficies amplias y complejas.

Los polímeros fluorados son excelentes candidatos para el desarrollo de este tipo de superficies puesto que además de crear superficies naturalmente hidrofóbicas, ofrecen otras múltiples ventajas tales como la resistencia al agua y aceites, a la intemperie, a la corrosión, a la suciedad, etc.

Por otra parte, debido a la normativa cada vez más estricta en cuanto a la emisión de compuestos orgánicos volátiles (VOCs), los fabricantes de pinturas y recubrimientos están transformando muchos de sus procesos basados en disolventes en nuevos procesos basados en agua. De este modo, la obtención de superficies hidrofóbicas y superhidrofóbicas a partir de productos obtenidos en base agua es particularmente interesante pero al mismo tiempo, supone un gran reto debido a que para estabilizar partículas poliméricas en un medio acuoso, estas partículas deben tener una superficie relativamente hidrofílica.

Para preparar dispersiones de materiales fluorados en agua es necesario considerar su naturaleza altamente hidrofóbica. En este caso particular, la polimerización en emulsión convencional no es un método apropiado puesto que es necesario que el monómero difunda a través de la fase acuosa. En el caso de monómeros insolubles en agua tales como los monómeros fluorados, la polimerización en miniemulsion puede ser una buena alternativa. En este tipo de polimerización, la difusión de los monómeros a través de la fase acuosa no es necesaria debido a que la polimerización ocurre en gotas que han sido previamente formadas mediante la aplicación de altas dosis de energía a la mezcla inicial formando una dispersión estable.

En esta tesis se ha investigado tanto la síntesis de dispersiones acuosas como la aplicación de diferentes técnicas para el desarrollo de superficies hidrofóbicas y superhidrofóbicas de polímeros fluorados.

Inicialmente se sintetizaron dispersiones acuosas de homopolímeros y copolímeros de 1H,1H,2H,2H-perfluorodecil acrilato (PFDA) y acrilato de 2-etilhexilo (2EHA) en diferentes proporciones. El copolímero PFDA/2EHA en relación en peso 82/18 permitió la formación de recubrimientos de buena calidad sin embargo, al ser su superficie relativamente plana, los ángulos de contacto con agua no superaban los 114º. La síntesis de copolímeros con contenidos de monómero fluorado mayores permitió incrementar el valor del ángulo de contacto pero en este caso los recubrimientos obtenidos no tenían una buena resistencia mecánica. Con el objetivo de producir recubrimientos más hidrofóbicos de buena calidad se desarrollaron diferentes estrategias que se resumen a continuación:

- **Mezclas físicas de copolímeros y homopolímeros fluorados**

Con el fin de aumentar la hidrofobicidad del sistema manteniendo la calidad de los recubrimientos se hicieron mezclas del copolímero 82/18 y el homopolímero fluorado pero no se observó ninguna mejora en el ángulo de contacto. La razón principal es que para recubrimientos relativamente gruesos (1250 μm de espesor de 'film' o película húmeda) la alta densidad del homopolímero hace que las partículas sedimenten durante el secado sin modificar la superficie del film. Para evitar la sedimentación de las partículas del homopolímero se han utilizado diferentes técnicas:

a) Preparación de recubrimientos más finos

Al preparar recubrimientos más finos del orden de 90 μm de espesor de película húmeda se obtuvieron ángulos de contacto de alrededor de 123º debido a que el secado es más rápido y por tanto la sedimentación no es tan drástica.

b) Secado en posición invertida

La diferencia entre la densidad del homopolímero y el copolímero se aprovecha para favorecer el movimiento de las partículas más densas hacia la superficie del film. Mediante esta técnica, se obtuvieron superficies con ángulos de contacto alrededor de 130º.

c) Utilización de copolímeros de mayor densidad y viscosidad

Para reducir el efecto de la sedimentación se realizaron mezclas con un látex de mayor viscosidad consistente en una dispersión comercial al 60% de contenido en sólidos de un polímero de mayor densidad (policloruro de vinilideno). Se obtuvieron en este caso recubrimientos de buena calidad y ángulos de contacto de 133º.

d) Aprovechamiento del 'tiempo abierto' de las dispersiones ('open time')

Se desarrolló una estrategia en dos etapas aprovechando el denominado 'tiempo abierto' u 'open time' de las dispersiones. Se denomina 'open time' al tiempo tras aplicar la dispersión durante el cual la superficie se puede volver a pintar o corregir sin dejar marcas. Siguiendo esta estrategia, se aplicó inicialmente una primera capa de un látex con buenas propiedades filmógenas y durante su 'open time', se esprayó una segunda dispersión homopolímero fluorado. Mediante la utilización de esta técnica se obtuvieron superficies con ángulos de contacto de 137º.

- **Recubrimientos con arrugas en la superficie**

Otra posibilidad propuesta para la obtención de superficies altamente hidrofóbicas consiste en la manipulación de las condiciones de secado de dispersiones de copolímeros (PFDA/2EHA) con diferentes temperaturas de transición vítrea. Concretamente, se modificó la rugosidad de la superficie del recubrimiento mediante la formación de arrugas que pueden obtenerse cuando la técnica de secado cumple las siguientes condiciones: 1) la velocidad de evaporación del agua es mayor que la velocidad de difusión de las partículas en el seno del

líquido, y 2) la velocidad de coalescencia de las partículas es similar o superior a la velocidad de evaporación del agua. Cuando se dan estas circunstancias, en la superficie del recubrimiento, se forma una capa de polímero ("piel") mientras que todavía contiene agua en su interior. Este fenómeno genera ciertas tensiones que dan lugar a la formación de arrugas durante el secado. Las velocidades de secado y de coalescencia de las partículas se controlaron mediante la variación de la temperatura de secado y de la dureza de los polímeros. Utilizando este procedimiento se obtuvieron recubrimientos de buena calidad y ángulos de contacto de alrededor de 133º.

- **Recubrimientos superhidrofóbicos mediante agregación de partículas**

Para alcanzar el régimen superhidrófóbico definido por ángulos de contacto superiores a 150º es necesaria una gran rugosidad en la superficie. En este trabajo, se desarrolló un nuevo método para la obtención de superficies superhidrofóbicas con buena resistencia mecánica basado de nuevo en el 'open time' de los recubrimientos. En dicho método, se utilizó como polímero base una dispersión acuosa de alto contenido en sólidos de un polímero convencional con buenas propiedades filmógenas (metacrilato de metilo/ acrilato de butilo/ ácido metracrílico (MMA/BA/MAA)). Durante el 'open time' de esta dispersión base, se esprayó una segunda dispersión de polímero fluorado. Esta dispersión de PFDA, se obtuvo por polimerización en miniemulsion modificando las condiciones de síntesis con el fin de obtener agregados coloidales con estructura fractal de gran rugosidad. Tras el secado, se obtuvieron recubrimientos con ángulos de contacto superiores a 150º, ángulos de deslizamiento de alrededor de 7º y valores de histéresis del ángulo de contacto de alrededor de 5º. Además, los

recubrimientos demostraron una buena resistencia a la fricción y resistencia mecánica y también cierto carácter oleofóbico obteniéndose valores de 120º de ángulo de contacto medidos al depositar una gota de aceite de oliva sobre su superficie. La repelencia al hielo de estas superficies fue evaluada demostrando potencial para reducir la adhesión del hielo con respecto a recubrimientos convencionales de MMA/BA/MAA.

Finalmente, una vez analizado el potencial de diferentes dispersiones de fluoropolímeros para la obtención de superficies hidrofóbicas y superhidrofóbicas, dichas dispersiones fueron incorporadas en formulaciones comerciales de pinturas con el objetivo de evaluar su efecto en las propiedades finales. La incorporación de copolímeros fluorados de naturaleza más blanda mostraron un interesante efecto mate con ángulos de contacto muy altos pero con menor dureza que las correspondientes referencias comerciales. Las pinturas en las que se incorporaron dispersiones de fluoropolímeros de naturaleza más dura presentaron valores de dureza iguales o superiores a los de las referencias comerciales mejorando además la resistencia química al etanol, al vapor de agua y a la suciedad.

La incorporación de mezclas de fluoropolímeros de diferentes composiciones permitió reducir a la mitad el contenido de cosolventes disminuyendo notablemente el contenido en compuestos orgánicos volátiles (VOCs). Además la pintura obtenida presentó una apariencia mate similar a las referencias sin necesidad de usar ningún tipo de agente mate además de una buena resistencia al agua y al vapor de agua.

En resumen, este trabajo recoge diferentes técnicas en las que dispersiones acuosas de fluoropolímeros han sido utilizadas para la obtención de recubrimientos hidrofóbicos y superhidrofóbicos de buena calidad y fácil aplicación en todo tipo de superficies.

Acronyms

2EHA	2-ethylhexyl acrylate
AFM	Atomic Force Microscopy
AIBN	2,2-azobisisobutyronitrile
AMBN	2,2'-azodi(2-methylbutyronitrile)
BA	Butyl acrylate
CAH	Contact angle hysteresis
C80	PFDA/2EHA/MAA (80.8/17.7/1.5) copolymer
C88	PFDA/2EHA/MAA (88.6/9.9/1.5) copolymer
C100	PFDA/2EHA (100/0) copolymer
DDI	Double deionized water
DSC	Differential scanning calorimetry
HAP	Hazarous air pollutants
KPS	Potassium persulfate
M.A.	Matting agent
MAA	Methacrylic acid
MFFT	Minimum film formation temperature
MMA	Methyl methacrylate
PFDA	1H, 1H, 2H, 2H-perfluorodecyl acrylate

PFHA	1H, 1H, 2H, 2H-perfluorohexyl acrylate
PIL	Polimeric ionic liquid
(Poly(ViEtIm^{+}Br^{-})	Poly(1-vinyl-3-ethylimidazolium bromide)
p(VDC)	Poly(vinylidene chloride)
SA	Sliding angle
SC	Solids content
SEM	Scanning electron microscopy
TBHP	Tert-butyl hydroperoxide
VOC	Volatile organic compound
WI-CIE	Whiteness index (CIE)

Symbols

g	Gravity force
Tg	Glass transition temperature
Z_i	Height deviation from the mean to the i point (equation 5.1)
m	Mass of the droplet
Pmax	Maximum pressure (Homogenizer equipment)
Tm	Melting temperature
Pmin	Minimum pressure (Homogenizer equipment)
Mw	Molecular weight
N	Number of data points (equation 5.1)
$d_{particle}$	Particle diameter
Xc	Polymer crystalline fraction
RMS (Rq)	Root mean square roughness
r	Roughness factor
S	Spreading coefficient
T	Temperature
w	Width of the droplet

Greek letters

θ_{adv}	Advancing contact angle
θ	Contact angle
θ_r	Contact angle of the rough surface
Φ_S	Fraction of the horizontal surface in contact with the liquid
ΔHf	Heat of fusion
$\emptyset_0$	Initially occupied volume fraction
γ_{LV}	Liquid-vapour interfacial tension
θ_{rec}	Receding contact angle
α	Sliding angle
γ_{SL}	Solid-liquid interfacial tension
γ_{SV}	Solid-vapour interfacial tension